A Low-Cost Genomic Sensor

for Ocean-Observing Systems and Infectious Disease Detection

by

Shufang Ci

A Dissertation Presented in Partial Fulfillment
of the Requirements for the Degree
Doctor of Philosophy

Approved December 2016 by the
Graduate Supervisory Committee:

Deirdre R. Meldrum, Chair
Shih-hui Chao
Susanne Neuer

ARIZONA STATE UNIVERSITY

May 2017

ABSTRACT

Many environmental microorganisms such as marine microbes are un-culturable; hence, they should be analyzed *in situ*. Even though a few *in situ* ocean observing instruments have been available to oceanographers, their applications are limited, because these instruments are expensive and power hungry.

In this dissertation project, an inexpensive, portable, low-energy consuming, and highly quantitative microbiological genomic sensor has been developed for *in situ* ocean-observing systems. A novel real-time colorimetric loop-mediated isothermal amplification (LAMP) technology has been developed for quantitative detection of microbial nucleic acids. This technology was implemented on a chip-level device with an embedded inexpensive imaging device and temperature controller to achieve quantitative detection within one hour. A bubble-free liquid handling approach was introduced to avoid bubble trapping during liquid loading, a common problem in microfluidic devices. An algorithm was developed to reject the effect of bubbles generated during the reaction process, to enable more accurate nucleic acid analysis. This genomic sensor has been validated at gene and gene expression levels using *Synechocystis* sp. PCC 6803 genomic DNA and total RNA. Results suggest that the detection limits reached 10 copies/μL and 100 fg/μL, respectively. This approach was highly quantitative, with linear standard curves down to 10^3 copies/μL and 1 pg/μL, respectively. In addition to environmental microbe characterization, this genomic sensor has been employed for viral RNA quantification during an infectious disease outbreak. As the Zika fever was spreading in America, a quantitative detection of Zika virus has been performed. The results show that

the genomic sensor is highly quantitative from 10 copies/μL to 10^5 copies/μL. This suggests that the novel nucleic acid quantification technology is sensitive, quantitative, and robust. It is a promising candidate for rapid microbe detection and quantification in routine laboratories.

In the future, this genomic sensor will be implemented in *in situ* platforms as a core analytical module with minor modifications, and could be easily accessible by oceanographers. Deployment of this microbial genomic sensor in the field will enable new scientific advances in oceanography and provide a possible solution for infectious disease detection.

ACKNOWLEDGMENTS

The Ph.D. study is like an adventure in my life. I still remember how excited I was when I arrived at the States for the first time in 2013, and started a whole new life in this country. During the past three years, I felt so grateful to have met so many kind people, who shared the exciting moments with me, and encouraged me while I came across obstacles.

First of all, I would like to thank my supervisory committee. My advisor, Dr. Deirdre Meldrum, guides me to explore the amazing research topics, provides me the best research environment, and supports me throughout my Ph.D. study. I feel so honorable to have been working with such a distinguished scientist. Her personality and her insight set a great example to me, and lead me to become an independent researcher. Dr. Shih-hui Chao is a great mentor that advises me wholeheartedly every day. I was depressed during a period of time that my experiment did not work, but Dr. Chao kept encouraging me—"this is research", he said—and worked with me together in the lab to find out the solutions. It is so fortunate for me to have him as my mentor, not only for research, but also for the attitude to life. I sincerely thank Dr. Susanne Neuer for willing to serve on my committee. I could not feel more impressed when she revised my written report word by word, and gave me a lot of insightful suggestions for my project. I really appreciate her carefulness and considerate. Without the help from my committee, I could never imagine how my Ph.D. study looks like.

Additionally, I would like to express my gratitude to the staffs in Biodesign's Center for Biosignatures Discovery Automation (CBDA): Dr. Rhett Martineau and Dr.

Weimin Gao for working as a group, and discussing interesting ideas; Dr. Liqiang Zhang, Dr. Xiangxing Kong, Dr. Fengyu Su, Dr. Yanqing Tian, and Dr. Hong Wang, for their help in both research projects and daily life; Carol Glaub, Christine Willett, and Kristen Lee for administrative supports. Thanks to Dr. Juan Maldonado Ortiz from Biodesign's Swette Center for Environmental Biotechnology for his assistance in DNA sequencing.

Special thanks to Dr. Antonio Garcia and Laura Hawes from the Biological Design Graduate Program for their academic guidance. Thanks to my classmates and friends for the companion during the past three years: Dr. Kuo-Chen Wang, Ganquan Song, Dr. Bin Cao, Dr. Jordan Yaron, Dr. Saeed Merza, Dr. Xu Shi, Dr. Jia Zeng, Dr. Bo Wang, Dr. Jieying Wu, Dr. Hansa Done, Jing Chen, Mateusz Szczerba, Steven Hart, Dr. Rachel Yoho, Dr. Bradley Lusk. Heartfelt thanks to Dr. Yanan Zhao for unceasing advice and endless support along the way.

Finally, I would like to thank the NEPTUNE project and Biological Design Graduate Program from Arizona State University to fund my research and study over the years.

TABLE OF CONTENTS

Page

CHAPTER Page

LIST OF TABLES

Table Page

LIST OF FIGURES

Figure Page

Figure Page

1. OBJECTIVES AND CONTRIBUTION

1.1 Objectives

The ocean is a unique ecosystem that contributes to a large portion of the global primary production, and regulates the climate of the earth. However, most of the ocean remains unexplored. In the past few decades, researchers began to realize that bacteria played dominant roles in maintaining the abundance and diversity of marine ecosystems, while most of the bacteria are not cultivable in lab conditions. With the successful implementation of ocean-observing systems, especially *in situ* genomic sensors, ocean-related research has achieved significant progress. Unfortunately, *in situ* genomic sensors are in their infancy, and only available to small groups of scientists for very limited marine microbiology studies.

In my dissertation project, a low cost and low energy-consuming, chip-level device has been developed to serve as a core analytical unit for future *in situ* instruments. The objectives of this project are as follows:

(1) For the first time, a real-time colorimetric nucleic acid quantification method has been developed for LAMP reactions. Image acquisition, processing, and data modeling tools have been built to automate the data analysis process. The colorimetric quantification method, whose signals can be easily picked up by the naked eye and cameras, is promising to become competitive to traditional fluorescence-based quantifications.

(2) A hardware platform has been designed and built with a heating element and chip-level device to be compatible with real-time colorimetric detection and

quantification for the LAMP reaction. The goal of this objective is that the hardware platform design must be simple and portable for future *in situ* implementation. The platform should use low-cost and easily accessible materials and elements, so that it can be used in both academia and industry.

(3) The performance of the platform has been validated by environmental microbe (*Synechocystis* sp. PCC 6803) detection at both gene and gene expression levels. The LAMP reaction protocols have been optimized to achieve a good performance, and been compatible with the chip-level device.

(4) The platform has been applied in viral RNA detection and quantification, targeting the Zika crisis in America. This is an external application and further validation of the colorimetric quantification platform. This platform proves its broad applications not only in the area of environmental observations but also in the region of infectious disease diagnostics. This objective seeks the potential application of the genomic sensor to benefit other research communities.

(5) The bacterial community in the Biosphere 2 Ocean has been characterized. The microbiota information will become available for researchers, serving as a foundation for future *in situ* device validation.

The ultimate goal of this project is to build a low-cost and portable ocean-observing system that is accessible to most oceanographers. This ocean-observing system should contain multiple modules and units, for example, the sampling and sample processing module, the nucleic acid analytical module and power system, etc. This dissertation mainly focuses on the core nucleic acid analytical module development. The analytical

module that is constructed in this dissertation project will be available to perform the detection for multiple purposes with minor modifications. **Figure 1** shows the pipeline of the device design process.

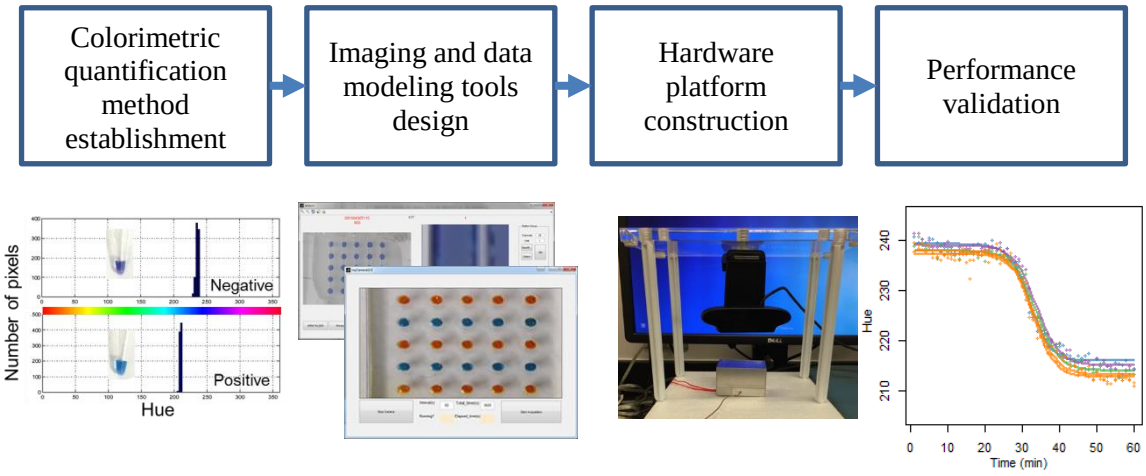

Figure 1. Device development and validation pipeline

1.2 Scientific contributions

All of the objectives have been achieved, based on the results of my dissertation projects. The scientific contributions of my dissertation project are as follows:

(1) A real-time colorimetric LAMP quantification method has been established. The results indicated that hue is a reliable and robust parameter to quantify the color shift, which is the most important indicator of the LAMP amplicons. The reasons for choosing hue are: (i) it is independent to the room lighting intensity, which decreased the requirements to optical setups. (ii) It simplified the device and reduced the cost. A generalized data analysis pipeline and related supporting platform have been built. This whole process is fully automated to perform image acquisition, image processing, and data analysis. A bubble and background rejection algorithm has been implemented in this pipeline, solving the bubble issue that frequently occurred in microfluidic devices.

Compared with the traditional fluorescence-based quantifications, this colorimetric quantification method has high tolerance on the effects of bubble generated during the heating and incubation process. The completion of this part of the project opened a new path for rapid nucleic acid quantification.

(2) A low-cost chip-level device, as well as the supporting hardware setup, has been established. The chip-level device was fabricated with easily accessible plastics. The results showed that the chip-level device was suitable to perform colorimetric LAMP quantifications within one hour. The hardware platform, including a temperature controlling unit, and a digital camera, has been constructed. Each individual part in the hardware platform can be easily accessed in conventional laboratories or in remote areas.

(3) The performance of the colorimetric LAMP platform has been validated. The results suggested that the platform was highly specific, quantitative, and sensitive to the target nucleic acid sequence. Compared with qPCR, this platform achieved comparable sensitivity, while detection was rapid, and eradicated the requirement of thermal cycling. A rapid isothermal amplification reduced the need of power supplies, and potentially elongated the endurance of the genomic sensor when deployed *in situ*.

(4) The colorimetric LAMP platform has been applied to Zika viral RNA detection and quantification. The results indicated that the Zika viral RNA can be quantitatively detected by the colorimetric LAMP platform within 40 minutes, while other similar viral RNA (dengue, chikungunya, West Nile) did not cross-react. This suggested the colorimetric LAMP platform can be a promising technology for infectious disease diagnostics. It will be especially useful in remote areas, where healthcare infrastructure is

minimal. This part of the project offered an unprecedented opportunity for rapid and quantitative virus diagnostics, and will cut down the infectious disease diagnostics associated health care expenditures.

(5) A practical application of this platform is to test it in the Biosphere 2 Ocean. The bacterial community structure in the Biosphere 2 Ocean has been identified. The Biosphere 2 Ocean is an ideal location for ocean-observing instrumentation validation. This part of project provided bacterial community information from the Biosphere 2 Ocean, as well as interesting detection targets for developing *in situ* genomic sensors in the future. This work served as a foundation for future instrument development.

The colorimetric quantification method and the related platform have been developed and validated. Besides environmental observation and health care applications, this platform will be useful for multiple purposes with minor modifications. The results of this PhD study and research have culminated in one patent applications, one conference publication, one submitted journal manuscript and three manuscripts that are under preparation for submission.

1. Ci, S., Martineau, R., Chao, S. H., Gao, W., Wang, H., & Meldrum, D. R. On-chip quantitative colorimetric loop mediated isothermal amplification, *in preparation.*

2. Ci, S., *et al*. Quantitative detection and analysis of Zika using colorimetric loop mediated isothermal amplification, *in preparation*.

3. Ci, S., *et al*. Bacterial community structure analysis in Biosphere 2 Ocean, *in preparation*.

4. Martineau, R., Murray, S. A., Ci, S., Gao, W., Chao, S. H., & Meldrum, D. R. Improved performance of loop-mediated isothermal amplification assays via Swarm priming. *Anal Chem, Accepted*.

5. Martineau, R., Houkal, J., Chao, S. H., Gao, W., Ci, S., & Meldrum, D. (2016). *U.S. Patent No. 20,160,114,323*. Washington, DC: U.S. Patent and Trademark Office.

6. Martineau, R. L., Ci, S., Houkal, J., Gao, W., Chao, S. H., & Meldrum, D. R. (2014). DEEP-well microfluidics for arrayed colorimetric LAMP analysis. In *18th International Conference on Miniaturized Systems for Chemistry and Life Sciences, MicroTAS 2014.* (pp. 1009-1011). Chemical and Biological Microsystems Society.

2. INTRODUCTION

The effect of marine microbes on the global ecosystem is tremendous. Marine microbes account for more than 90% of the ocean biomass (Whitman *et al*., 1998). They perform most of the primary production in the oceans, accounting for half of the global primary production (Field *et al*., 1998; Rivkin and Legendre, 2001). They also control the biogeochemical dynamics in the ocean (Stocker, 2012). In recent years, studies regarding ocean acidification, carbon cycling, and climate change require increased understanding of microbial populations (Bardgett *et al*., 2008; Follows *et al*., 2007; Liu *et al*., 2010). Despite the progress achieved in ocean microbial research, the behavior of many mysterious bacterial communities remain undiscovered (DeLong, 2006), and around 91% of the species in the ocean are still waiting to be discovered and described (Mora *et al*., 2011).

A typical and conventional approach to study the microbial community is culture-based. In brief, bacterial species from a sample were filtrated, plated and incubated for a period of time. The bacteria was expected to grow into colonies (Abbaszadegan, 2004). The bacterial colonies can be counted, followed by molecular methods for species identification (Laiz *et al*., 2003). However, because of the unculturability of a major (> 98%) environmental microorganisms (Wade, 2002) in lab conditions, more and more researchers realized that the conventional culture-based microbial community analysis is inadequate for marine microbial research (Rusch *et al*., 2007; Streit and Schmitz, 2004; Wagner *et al*., 1993).

There are some explanations for the unculturability. For example, even though some microbes remain alive in laboratory conditions, they could not proliferate, because some specific nutrients required for their growth was not present in the culture medium (Roszak and Colwell, 1987). On the other side, inappropriate cultivation conditions (e.g. toxins in the culture medium, temperature, pH, and oxygen concentration) inhibit the growth of the specific microbe (Vartoukian *et al*., 2010). Besides, some microbes collaborate and depend on each other to form a complex community (e.g. biofilms) (Mulcahy *et al*., 2008). When microorganisms are separated from their communities, they fail to grow *in vitro*. In addition, *in vitro* cultivation is likely to disrupt the cytokine networks of the microbes. The cytokine networks play an important role in bacterial signaling and are responsible for extracellular matrix construction (Kell and Young, 2000; Wade, 2002). The disruption of the cytokine networks may contribute to the unculturability of microorganisms (Wade, 2002).

Thus, to study the marine microbes more efficiently, *in situ* analysis instruments are desired. Below is a summary of the currently available *in situ* ocean-observing technologies.

2.1 *In situ* ocean-observation instruments

In the past few decades, with the successful implementation of genomic sensors and ocean-observing systems (Griffiths, 2010), researchers began to realize that bacteria played dominant roles in maintaining the abundance and diversity of marine ecosystems, and the ocean-related studies were accelerated. There are a few technologies that are currently available for *in situ* microbe observation. A lot of progress has been achieved

recently in developing *in situ* ocean-observing systems. Unfortunately, today's reality is that *in situ* genomic sensors are still in their infancy (Paul *et al*., 2007), and only available to small groups of scientists for very limited marine microbiology studies. Some of the most important reasons are that instruments are too expensive, too cumbersome, too complex, and too power-hungry. Therefore, there is a need to develop inexpensive *in situ* genomic sensors for ocean-observation.

2.1.1 Environmental Sample Processor (ESP)

ESP (Greenfield *et al*., 2006), and the second generation ESP (2G-ESP) were developed by the Monterey Bay Aquarium Research Institute (MBARI). As a remote ocean-observing instrument, ESP and 2G-ESP have been deployed in multiple locations to perform *in situ* cell-free molecular analysis for microbe identification and algal toxin detection (Greenfield *et al*., 2008; Scholin *et al*., 2009).

The ESP consists of multiple modules: a sampling module, a core ESP, and an analytical module (Scholin *et al*., 2006). The sampling module is for pressurizing seawater to the instrument, and introducing the filtered particulates to the core ESP (Scholin *et al*., 2006). The core ESP is for concentrating particulates and performing chemical assays. In the first generation ESP, a low-density microarray was implemented, and hybridized with the ribosomal RNA (rRNA) from the sample (Goffredi *et al*., 2006). As the concentration of the target molecules increased, the fluorescence intensity became stronger. This microarray technology is capable of multiple target analysis (Doucette *et al*., 2009; Jones *et al*., 2008). Unfortunately, its quantification capability is limited at low copy numbers (e.g. $< 2.5 \times 10^4$ cells/L) (Greenfield et al., 2006).

For better quantification and performance, in 2G-ESP, PCR-based microbe detection has been implemented in the analytical module (Preston *et al*., 2011). The DNA from the collected biomass was purified, concentrated, and introduced to the PCR module. If a target gene presents in the sample, it would be amplified, and would generate stronger fluorescence signals. For deep sea exploration, 2G-ESP has been upgraded to a deep-sea version (D-ESP) as well (Ussler *et al*., 2013). These instruments have been successfully deployed in multiple locations, and identified target species (Aylward *et al*., 2015; Ottesen *et al*., 2014).

However, even in 2G-ESP, it seems the multi-target capability is not significantly improved. Additionally, as multiple thermal cycling steps are required in qPCR, the automated system has to provide more power supply (Hatch *et al*., 2014), and the endurance of the system could be potentially decreased.

2.1.2 Integrated In-Situ Analyzer-Gene (IISA-Gene)

IISA-Gene (Fukuba and Fujii, 2012; Fukuba *et al*., 2011) was developed by the Japan Agency for Marine-Earth Science and Technology. Similar to 2G ESP, IISA-Gene performs qPCR based analysis as well. The IISA-Gene system contains a control unit and an analysis unit. It collects the biomass from the ocean, lyses the cells, and purifies the DNA for PCR amplification. In the analysis unit, there is a microfluidic device for flow-through PCR. The device is a PDMS-glass hybrid chip with three pieces of heating elements to generate temperature gradients. The fluorescence signals of the PCR reactions were measured by a photomultiplier tube (PMT) and monitored by a PC. IISA-Gene was mounted on an ROV named HYPER-DOLPHIN, and tested *in situ*. Even

though it successfully amplified 16S rRNA close to the hydrothermal site, it seems its performance was not stable. During the field operation, the PCR reaction was occasionally interrupted, either due to a malfunctioned solenoid actuated valve, or power shortage (Fukuba *et al*., 2011). In addition, this device required relatively complicated fluidic design.

2.1.3 Autonomous Microbial Genosensor (AMG)

AMG was developed by a research group in University of South Florida. So far, AMG has been deployed for *in situ* gene expression level characterization (e.g. *rbc*L gene mRNA), and red tide monitoring. AMG was able to perform sample collection and filtration, RNA extraction, and RNA amplification. AMG applied Nucleic Acid Sequence Based Amplification (NASBA) for gene expression measurement. NASBA is a sensitive and quantitative technology (Cook, 2003; Leone *et al*., 1998). The major drawback of this technology is that it is limited to RNA amplifications (Sooknanan and Malek, 1995).

There are some critical limitations of current *in situ* observation instruments. This reminds us some important design criteria in building such systems (Paul *et al*., 2007). First, the detection approach should be rapid and consume less energy, so that the experiment can be performed more frequently, and the device can have a longer working period. Second, the detection technology should be simple, without multiple sample manipulation steps. This reduces the need of complicated electrical elements, and decreases the load of the instrument. Third, the detection method should have sufficient analytical capability. The instrument should be able to perform analysis at both DNA and RNA levels, based on the research topic. Fourth, in many situations, a quantitative

measurement is desired, for example, to analyze the abundance of a microbial species, and to characterize the structure of a microbial community. Thus, the detection approach should be highly sensitive and quantitative.

2.2 Culture-independent microbial analysis methods

As conventional cultivation-based microbial detection technologies are labor intensive, time-consuming, and not able to analyze uncultivable microorganisms. Thus, for *in situ* analysis purpose, instead of cultivation-based approaches, culture-independent methods should be applied. There are three types of culture-independent microbial detection technologies available that could be potentially useful for *in situ* analysis.

2.2.1 Sequencing-based microbial community analysis

Three main types of DNA sequencing technologies have been developed and widely used for biological research: basis DNA sequencing (Sanger sequencing, Maxim-Gilbert sequencing), advanced DNA sequencing (short-gun sequencing), next-generation sequencing (or high-throughput sequencing), and third-generation sequencing (single-molecule sequencing).

Compared with basis DNA sequencing and advanced DNA sequencing, next-generation sequencing reduced the cost from around $1000 to less than $1 per 1 million bases. Major commercialized next-generation sequencing platforms include (1) 454 pyrosequencing (GS FLX+ system from Roche), (2) Illumina sequencing platforms (e.g. MiSeq, NextSeq, HiSeq), (3) Ion Torrent from ThermoFisher Scientific, (4) SOLiD from Life Technologies, and (5) Single-molecule real-time sequencing (Pacific Biosciences).

Next-generation sequencing has been widely used for microbiome studies. One of the most popular topics in microbiology is the human microbiome. It has been reported that human metabolism and energy balance are associated with the gut microbiome (Le Chatelier *et al*., 2013; Turnbaugh and Gordon, 2009). The human microbiome may substantially contribute to a wide range of diseases; for example, Alzheimer's disease (Shoemark and Allen, 2015), inflammatory bowel diseases (Morgan *et al*., 2012), diabetes (Pflughoeft and Versalovic, 2012), and obesity (Turnbaugh *et al*., 2006). Similarly, in the ocean, the marine microbiome caught researchers' attentions also. Sunagawa *et al.* studied the global ocean microbiome by investigating the microbial community structures in seawater samples collected from 68 *Tara* Oceans sampling stations, and reported that the microbial community composition was mainly affected by temperature (Sunagawa *et al*., 2015). Interestingly, even though the ocean and human gut are two ecosystems with different physicochemical properties, they found more than 73% of the abundance in the ocean microbiome was overlapped with the human gut microbiome (Sunagawa *et al*., 2015).

Even though next-generation sequencing has brought about a revolution in biological and medical research, the technologies have some limitations. For example, the accuracy and read length is not comparable with Sanger sequencing (Shendure and Ji, 2008). To address these problems, new technologies (third-generation sequencing) are currently being developed. Third-generation sequencing includes nanopore sequencing (Branton *et al*., 2008), electron microscopy (Bell *et al*., 2012), sequencing by tip-enhanced Raman scattering (Yeo *et al*., 2009), etc. Among the approaches, nanopore

technology seems to be most promising regarding high throughput, high accuracy, long read length, and low cost (Wang *et al*., 2015). Commercial sequencing platforms (e.g. MinION from Oxford Nanopore Technologies) have become available for nanopore sequencing since 2015. Besides being useful for DNA and RNA (Biswas et al., 2016), this technology has been applied to amino acids and peptides identification (Im et al., 2016; Lindsay et al., 2013; Zhao et al., 2013, 2014) This is inspiring as there are no PCR-type approaches for peptide amplifications. Hence, peptide sequencing cannot be achieved by amplification based next-generation sequencing technologies. This technology is promising to integrate genomic, transcriptomic, and proteomic data simultaneously for a deeper level microbial community analysis.

While sequencing technologies have achieved remarkable progress, they still require great effort to be miniaturized and the processing time shortened for reliable *in situ* device development.

2.2.2 Immunoassay-based microbial analysis

Enzyme-linked immunosorbent assay (ELISA) was developed and used in many areas (e.g. molecular biology, microbiology, and immunology) in the past few decades (Crowther, 2008). It identifies a specific substrate by antigen-antibody interactions and color change.

There are two ELISA detection strategies: direct and indirect. In ELISA, the antibodies are immobilized on the plate surface and the target antigens are captured. In direct detection, the labeled primary antibody is directly immobilized on the plate surface, and interacts with the antigens (Beier *et al*., 1988; Czerkinsky *et al*., 1983). In indirect

detections, a labeled secondary antibody is conjugated with the primary antibody. The secondary antibody captures the target antigens (Russell *et al*., 1984). Indirect ELISA has a higher sensitivity than direct ELISA (Friguet *et al*., 1985). Labeling the primary antibody in direct ELISA is costly and time-consuming, while labeling the secondary antibody in indirect ELISA increases the rate of non-specific binding (Gan and Patel, 2013).

Even though various substrates, conjugates, and buffers have been commercially available, the principles of these ELISAs are the same. ELISAs have been well developed for low cost microbial detections. They need multiple washing and incubation steps, which is labor-intensive, and difficult to be implemented for automatic *in situ* analysis (Huet *et al*., 2010).

2.2.3 Microbial biosensors

Microbial biosensors are devices that implement microbial analytical units with physical transducers to produce quantitative signals, which can be monitored mechanically, electronically, electrochemically, or optically (Kelbauskas et al., 2017; Song et al., 2013; Su et al., 2011).

Biosensors are promising candidates for precise and rapid microbial analysis. Park *et al*. reported a DNA array detection approach with gold nanoparticles by recording the conductivity changes during DNA hybridization (Park *et al*., 2002). Tront *et al*. built microbial fuel cells and cultivated bacterial biofilms on the electrode. They reported that the current values were linearly correlated with acetate concentrations, which was an indicator of the respiration rate of *Geobacter sulfurreducens* (Tront *et al*., 2008).

Fiorentino *et al*. designed a whole-cell bacterial biosensor to monitor the aromatic aldehydes concentration. They engineered *E. coli* with alcohol dehydrogenase inducible promoter, which controlled the expression of green fluorescent protein (GFP). The fluorescence from GFP was detected by optical sensors (Fiorentino *et al*., 2008).

So far, a few microbial biosensors have been commercialized. However, there are some problems of microbial biosensors that still need to be overcome. Usually, microbial biosensors have relatively poor specificities, and the response is slow (Su *et al*., 2011).

2.2.4 Nucleic acid amplification based microbial analysis

Nucleic acid amplification approaches have a wide range of applications, from analyzing environmental samples, to monitoring food safety and detecting infectious diseases. These approaches are usually precise, accurate, and provide quantitative results. Depending on the requirement of thermal cycling steps, nucleic acid amplification approaches can be divided into two groups: PCR-based methods, and isothermal amplification methods.

2.2.4.1 PCR-based methods

PCR stands for polymerase chain reaction. It amplifies the target sequence by repeating three steps: a denaturation step at high temperature (94-98 °C), a primer annealing step at low temperature (50-65 °C), and an elongation step (usually at 72 °C). During the reaction, the amplicons accumulates exponentially. A traditional way to visualize the PCR products is by agarose gel electrophoresis. Depending on research purposes, a few variations of PCR have been developed.

Multiplex PCR: Multiplex PCR is a complex version of PCR, and the multiplex PCR system contains multiple primer sets in one reaction, targeting different DNA sequences. For example, Cebula *et al.* evaluated Mismatch Amplification Mutation Assay-Multiplex PCR (MAMA-multiplex PCR) with *E. coli* O157:H7 (Cebula *et al*., 1995). Primers used in MAMA-multiplex PCR targeted three genes: *SLT-I, SLT-II,* and *uidA*. *SLT-I* and *SLT-II* are Shiga-like toxins (SLTs) encoding genes (Strockbine *et al*., 1988). SLTs are enterotoxins produced by *E.coli* O157:H7. However, some non-O157:H7 *E.coli* produces SLTs also. Including *uidA* gene discriminated SLT-producing *E.coli* from *E. coli* O157:H7 (Feng and Lampel, 1994). Oliveira *et al.* reported using multiplex PCR for methicillin-resistant *Staphylococcus aureus* identification (Oliveira and Lencastre, 2002). They designed PCR primers targeting eight loci to characterize the *mec* element, which is related to drug resistance. The results showed this approach was able to identify 18 MRSA strains from an outbreak in Barcelona, Spain.

Quantitative PCR (qPCR): PCR amplicons can be real-time quantified by incorporating fluorescent compounds to the reactions. There are two types of fluorescent compounds: TaqMan probe, and SYBR Green DNA intercalating dye (Burgos *et al*., 2002). The TaqMan probe is an oligonucleotide that has a fluorophore and a quencher labeled at both two ends, and can anneal to the target DNA sequence. By taking advantage of the 5’ to 3’ exonuclease activity of the Taq polymerase, the TaqMan probe is designed such that the Taq polymerase can degrade the probe during the PCR elongation step. Thus, the fluorophore and the quencher can be separated, and release fluorescent signals. Compared with TaqMan probes, SYBR Green dye is more

straightforward to use. SYBR Green dye has high affinity to double stranded DNA. During the amplification, it is incorporated in the double stranded DNA, and generates fluorescence. In qPCR, DNA was quantified by calculating the number of cycles that the increase of fluorescence exceeded the threshold cycle (C_t) (Kuboniwa *et al*., 2004). Both absolute and relative quantification (Klein, 2002) can be achieved in qPCR. Absolute quantification means calculating target gene concentrations or copy numbers given a standard curve plotted by C_t values (Yu *et al*., 2005), while relative quantification means the fold change (or ratio) of concentrations comparing the C_t values of target gene and reference gene (Lehmann and Kreipe, 2001; Livak and Schmittgen, 2001). Using qPCR, Kuboniwa *et al*. (Kuboniwa *et al*., 2004) detected and quantified six bacteria as well as their species richness from both tooth and tongue debris specimens.

Quantitative reverse transcription PCR (RT-qPCR): RT-qPCR is a sensitive and specific approach to quantify the gene expression changes at mRNA levels. Quantification methods used in qPCR can also be used for RT-qPCR. RT-qPCR is relatively fast and a less labor-intensive approach for gene expression measurements than other alternative approaches (Gao *et al*., 2011), such as fluorescence *in situ* hybridization (FISH) (Franks *et al*., 1998), and flow cytometry (Strovas and Lidstrom, 2009). Matsuda *et al*. performed an rRNA-targeted RT-qPCR method to identify bacterial populations in feces and blood samples (Matsuda *et al*., 2007). This method was able to identify 10^3 *Pseudomonas aeruginosa* cells per gram of feces (Matsuda *et al*., 2007). In addition, RT-qPCR is particularly suited to single cell gene expression analysis. Shi *et al*. developed a single-cell RT-qPCR analysis pipeline (Shi *et al*., 2011), and applied this method to

quantitatively measure the gene expression of *Thalassiosira pseudonana* at the single-cell level (Shi *et al*., 2013). Their single-cell RT-qPCR results revealed the heterogeneity in cell-to-cell gene expression levels.

Generally, PCR-based methods are sensitive and specific to the targets. However, the thermal cycling steps in PCR usually require complex fluidic design. The heating and cooling steps consume a lot of energy.

2.2.4.2 Isothermal amplifications

Due to the requirement of multiple thermal cycling steps, PCR is not an appropriate technology for *in situ* device development. Instead, isothermal amplifications can be performed at a constant temperature, and do not require cycle heating and cooling steps. This could reduce the complexity of the instruments and save a lot of energy.

Nucleic Acid Sequence Based Amplification (NASBA): NASBA is an isothermal amplification method (Compton, 1991) that can be performed with simple fluidic devices and low energy consumption. In NASBA, three types of enzymes are added: reverse transcriptase, RNAase H, and T7 RNA polymerase. One primer anneals to the complementary sequence at the 3' side of the RNA target. With the presence of reverse transcriptase, a complementary DNA strand is synthesized, and the amplification is initialized. Next, the RNA template is hydrolyzed by RNAase H, leaving a single DNA strand. The second primer anneals to the DNA strand, elongates with reverse transcriptase, and forms a double strand DNA. The first primer has been specifically designed, so that a T7 RNA polymerase promoter site is coded when a double strand DNA is synthesized. Hence, T7 RNA polymerase binds to its promotor site, and

synthesizes RNA with the DNA template. This cycle is repeated until a large amount of amplicons can be accumulated at 41 °C within 2 hours (Compton, 1991). NASBA has been widely employed in microbiological labs for pathogen detection, such as West Nile, St. Louis encephalitis viruses (Lanciotti and Kerst, 2001), *Mycoplasma pneumoniae* (Templeton *et al*., 2003), Aspergillus fumigatus (Loeffler *et al*., 2001), and dengue viral RNA (Wu *et al*., 2001). Schneider *et al*. reported that real-time NASBA has a comparable sensitivity with qPCR, as both of the technologies have the sensitivity of detecting 20 *Plasmodium falciparum* per milliliter of blood (Schneider *et al*., 2005). Even though it is highly sensitive and quantitative in RNA targets detection, its DNA amplification capability is limited because DNA amplification can only occur when the RNA target is absent, and its amplification efficiency is low (Deiman *et al*., 2002).

Strand displacement amplification (SDA): SDA is able to amplify both DNA and RNA targets (Walker *et al*., 1992). In a two-primer SDA system, the primer with a restriction endonuclease recognition site at the 5' end anneals to the target sequence, and starts to elongate by the DNA polymerase. The restriction endonuclease nicks the primer at the recognition site. The DNA can be synthesized from the nicking site, and displace the previous synthesized DNA sequence. The nicking, extension, and displacement repeat, resulting in the accumulation of DNA products. Instead of using two primers, a four-primer SDA system has been reported to enhance the sensitivity (Walker *et al*., 1994). SDA has been applied in pathogenic bacteria and virus detection, such as *Mycobacterium tuberculosis* (Walker *et al*., 1996) and *Neisseria gonorrhoeae* (Akduman *et al*., 2002). Drawbacks of this technique include: (1) the primers cannot bind with the target sequence

specifically, and (2) the amplification is not efficient for long target sequences (Yan *et al*., 2014).

Loop-mediated isothermal amplification (LAMP): In a basic LAMP system, there are four primers recognizing six regions on the target sequence. The forward inner primer FIP anneals to the F2c region on the target sequence, and initiates the elongation. As the DNA polymerase in LAMP reaction has strand-displacement activity, the template sequence was replaced by the newly synthesized DNA strand. The forward outer primer F3 anneals to the F3c region, and initiates DNA synthesis. It replaces the strand synthesized by FIP. This single-stranded DNA contains two complementary sequences (F1 and F1c regions), which can form a loop structure at one end. The loop structure serves as a template for the FIP primer. At the backward side, backward inner primer BIP and outer primer B3 initiate the same reaction. The reaction is cycled by primer hybridization, elongation, strand displacement, and loop structure formation. The final products are cauliflower-like structures containing repeats of the target sequence connected by the loops (Notomi *et al*., 2000). In addition, loop primers LF and LB can be added in the solution to increase the sensitivity of the LAMP reaction (Nagamine *et al*., 2002). The loop primers are designed to hybridize at the loop structures (Mori and Notomi, 2009; Nagamine *et al*., 2002). Since LAMP uses four to six primers for amplification, it has higher specificity than NASBA and SDA (Notomi *et al*., 2000). Moreover, LAMP is able to amplify a few copies of target sequences up to 10^9 copies within one hour (Notomi *et al*., 2000). It is more robust to inhibitors than PCR (Kaneko *et al*., 2007). Therefore, it has become a powerful approach for molecular detection and

disease diagnostics. So far, LAMP has been applied for rapid detection of microbes, including *E. coli* O157 (Zhao *et al*., 2009), *Bacillus anthracis* (Qiao *et al*., 2007), *Vibrio cholerae* (Yamazaki *et al*., 2008), *Yersinia pseudotuberculosis* (Horisaka *et al*., 2004), dengue virus (Parida *et al*., 2005), chikungunya virus (Parida *et al*., 2007), pseudorabies virus (En *et al*., 2008), white spot syndrome virus (Jaroenram *et al*., 2009), orf virus (Tsai *et al*., 2009), H1N1 virus (Kubo *et al*., 2010), etc.

There are a few more isothermal amplification technologies published, for example, helicase-dependent amplification (HDA) (Vincent *et al*., 2004), rolling circle amplification (RCA) (Lizardi *et al*., 1998), signal mediated amplification of RNA technology (SMART) (Wharam *et al*., 2001), and recombinase polymerase amplification (RPA) (Piepenburg *et al*., 2006). These technologies are not as popular as LAMP because they require stringent conditions such as complicated buffer systems (Yan *et al*., 2014).

2.3 Miniaturized microfluidic devices for microbial analysis

Micro-Electro-Mechanical Systems (MEMS) (Ho and Tai, 1998) are extremely useful for microbial analysis. A combination of microactuators, microsensors, and microelectronics enable the analysis of microbes by their physical, chemical, and/or optical properties (Thielicke and Obermeier, 2000). As the analysis is performed in micro- or nanoscale structures, these devices usually require tiny amount of samples and fluids (Squires and Quake, 2005). Therefore, these devices are called microfluidics (Whitesides, 2006). Microfluidic devices usually yield high sensitivity, as the small volume increases the local concentration of a specific target (Wu and Dekker, 2016). There are multiple approaches (e.g. photolithography, soft lithography, electron-beam

lithography) to fabricate micro- and nanoscale features (Wu and Dekker, 2016). Based on the need, the surface of the features can be modified, before or after assembly of the MEMS device. The applications of MEMS devices include bacteria filtration, separation, sorting, on-chip cultivation, detection, etc. (Bridle *et al*., 2014). Wu *et al*. reported a high-throughput microfluidic device to separate *E. coli* from human blood cells by taking advantage of the soft inertial force on the fluid (Wu *et al*., 2009). Balagaddé *et al*. fabricated a microfluidic bioreactor to cultivate programmed *E.coli* cells, and monitor their behavior at the single-cell level over long time periods (Balagaddé *et al*., 2005). Koh *et al*. integrated PCR amplification and gel electrophoresis on a plastic MEMS device, and successfully identified *E. coli* O157 and *Salmonella typhimurium* (Koh *et al*., 2003). Their PCR reaction volume can be as low as 29 μL (Koh *et al*., 2003).

Considering the accuracy, cost, power consumption, and time duration of the aforementioned microbial detection technologies, a simple LAMP-based nucleic acid detection and quantification approach has been developed in this dissertation project. This technology was implemented with a chip-level device for miniaturized analysis. This platform will serve as a core analytical module in the future ocean-observing system.

3. REAL-TIME COLORIMETRIC QUANTIFICATION METHOD

3.1 Introduction

Loop mediated isothermal amplification (LAMP) is a rapid and sensitive gene amplification method (Notomi *et al*., 2000). LAMP reactions are conducted at a single temperature (between 60-65 °C) and the results are usually obtained within one hour. The technique is based on a polymerase with strand displacement activity and three pairs of primers. LAMP is generally considered to be highly specific because the three pairs of primers recognize six distinct regions in the target DNA. LAMP products—and thus the presence of an analytical target of interest in an unknown sample—can be assessed through a wide variety of detection chemistries (Fischbach et al., 2015; Martineau et al., 2017). Turbidity measurement (Mori *et al*., 2004), bioluminescence (Gandelman *et al*., 2010), fluorescence via intercalating dyes (Nagamine *et al*., 2002; Notomi *et al*., 2000) , and even fluorescence by removal of fluorophore quenchers (Tanner *et al*., 2015) are among the most commonly used real-time detection methods to date. Drawbacks to these methods include poor signal-to-noise ratio and high susceptibility to measurement artifacts (turbidity), increased rates of false positives (intercalating dyes) (Njiru, 2011), and high cost of reagents, detectors, or both (bioluminescence, fluorophore quenching, and intercalating dyes). Colorimetric reagents, including metal ion indicators such as hydroxyl naphthol blue (HNB) (Goto et al., 2009; Martineau et al., 2014) and pH indicators such as cresol red (Tanner *et al*., 2015) may offer the best performance to cost values. For both reagents, fast differentiation between positive and negative reactions has been reported (Goto *et al*., 2009; Tanner *et al*., 2015). However, real-time quantitative

results have not been achieved using either colorimetric method. Of the two colorimetric approaches, indicators based on metal ion concentrations may be best suited for environmental applications since these reactions are robust in pH-buffered master mixes, as opposed to pH-based indicator methods which rely on pH changes in weak or non-buffered masters.

To achieve real-time quantification using the colorimetric method, a novel real-time quantitative colorimetric LAMP reaction is proposed. Compared with conventional fluorescence-based nucleic acid quantification, this proposed colorimetric method is independent of the ambient lighting. This technology could be used in room lighting conditions, not affected by lighting intensity. Therefore, an additional light control element is not required.

3.2 Experiments

3.2.1 Colorimetric detection

To represent color changes during LAMP, it is desired that a color space is applied in which any color is a single value that is independent from brightness and illumination. HSV (Hue, Saturation, Value) (Solomon and Breckon, 2011) is a color space for describing color properties. It uses a hexone model in the H, S, and V axes in a cylindrical coordinate system to represent colors (Smith, 1978). The hue value is the azimuth, defined from red at 0°, yellow (60°), green (120°), blue (240°), and back to red again at 360°. The hue value can be used as a single quantity for tracking color changes as LAMP reactions precede.

To obtain real-time hue information, color images of the LAMP reaction are captured every one minute. Colorimetric detection begins by estimating the radius of a reaction chamber on real-time images. Based on the radius of the reaction chamber shown on the image, a square Region of Interest (ROI) is defined which can be fitted into the reaction chamber area. To reduce the variations, the same side length is applied to all of the ROIs in one experiment. Once an ROI of a specific reaction chamber was defined, its location and area are not changed until the whole stack of images is processed. The RGB (Red, Green, Blue) values of all of the pixels in each ROI are extracted. The RGB values from each pixel are transformed into HSV color space (Wang *et al*., 2011). The HSV values of each ROI are obtained by calculating the mean H, S, and V of all the pixels that passed the bubble and background rejection algorithm. The mean H, S, and V of each ROI are used to represent the color information of the corresponding reaction chamber.

3.2.2 Bubble and background rejection algorithm

Air bubbles are a common issue in microfluidic devices (Kang *et al*., 2008). During the chip fabrication process (Chapter 4), the following approaches were employed to reduce bubble trapping during the on-chip liquid loading process: (1) attached a piece of hydrophobic filter membrane beneath the reaction chamber, and (2) hydrophilic treatment of the channel and chamber surface by PEG. However, these approaches did not completely prevent the generation of small bubbles caused from degassing during the heating process. These air bubbles presented along the edge of the reaction chambers and reflected ambient illumination. Compared with the areas containing LAMP mixtures, air

bubbles and background areas tend to exhibit low saturation, which provided the basis to reject bubbles during image processing. Saturation S is the radial coordinate in HSV color space that shows the purity of a color. I set a threshold on the saturation of S = 0.1. When the S of a pixel was below the threshold, our algorithm rejected the pixel. All pixels that passed the bubble and background rejection algorithm were used to compute the average hue.

3.2.3 Curve fitting algorithm

The record of hue changes as a function of time represents the LAMP amplification curve. Similar to qPCR, this amplification reaction is best characterized as a sigmoid function (Cobbs, 2012; Spiess *et al*., 2008). The real time hue data is fitbased on the sigmoid function shown in Eq. (1):

$$h = H_{\max} + S_1 t + \frac{H_{\min} - H_{\max}}{1 + 10^{S_2(T_t - t)}} \quad (1)$$

where h is the hue value of the reaction as a function of reaction time t. H_{max} and H_{min} are the maximum and minimum asymptotes, respectively. Similar to the threshold cycle (C_t) value in qPCR, T_t, the threshold time of the reaction, represents the time when the hue value approaches the inflection point. T_t is also the time when the derivative of the curve displays a maximal absolute value and the time the amplification has the highest rate. S_1 and S_2 are slope factors. Five parameters, H_{max}, H_{min}, T_t, S_1 and S_2, were estimated by nonlinear least-squares.

3.3 Results

The end point color of the LAMP reactions is shown in **Figure 2**. The image was captured after a 60 min reaction. The positive LAMP reaction (**Figure 2B**, template DNA:

Synechocystis sp. PCC 6803 genomic DNA) was sky blue, while the negative control (**Figure 2A**, template DNA was replaced by ddH_2O) was purple. The color difference can be seen with the naked eye.

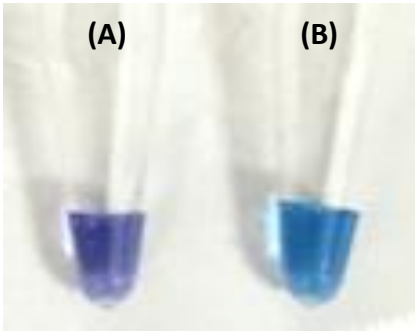

Figure 2. End point colorimetric negative (A) and positive (B) LAMP reactions

To analyze the color changes, three positive and one negative LAMP reactions in PCR tubes were recorded (one frame per minute). For each reaction, the color information was extracted. **Figure 3** shows how hue, saturation, and value shift in LAMP reactions as a function of time. While all of the three parameters showed significant change as the reaction preceded, saturation and value were more dependent on the actual room lighting conditions. As the room lighting intensity changed, both saturation and value shifted immediately. Compared with saturation and value, hue was robust and not affected by the change of room lighting intensity. Additionally, hue showed appealing results in representing the color change in both positive reactions and negative controls. This suggested that hue could be used as a feature to characterize the LAMP reaction.

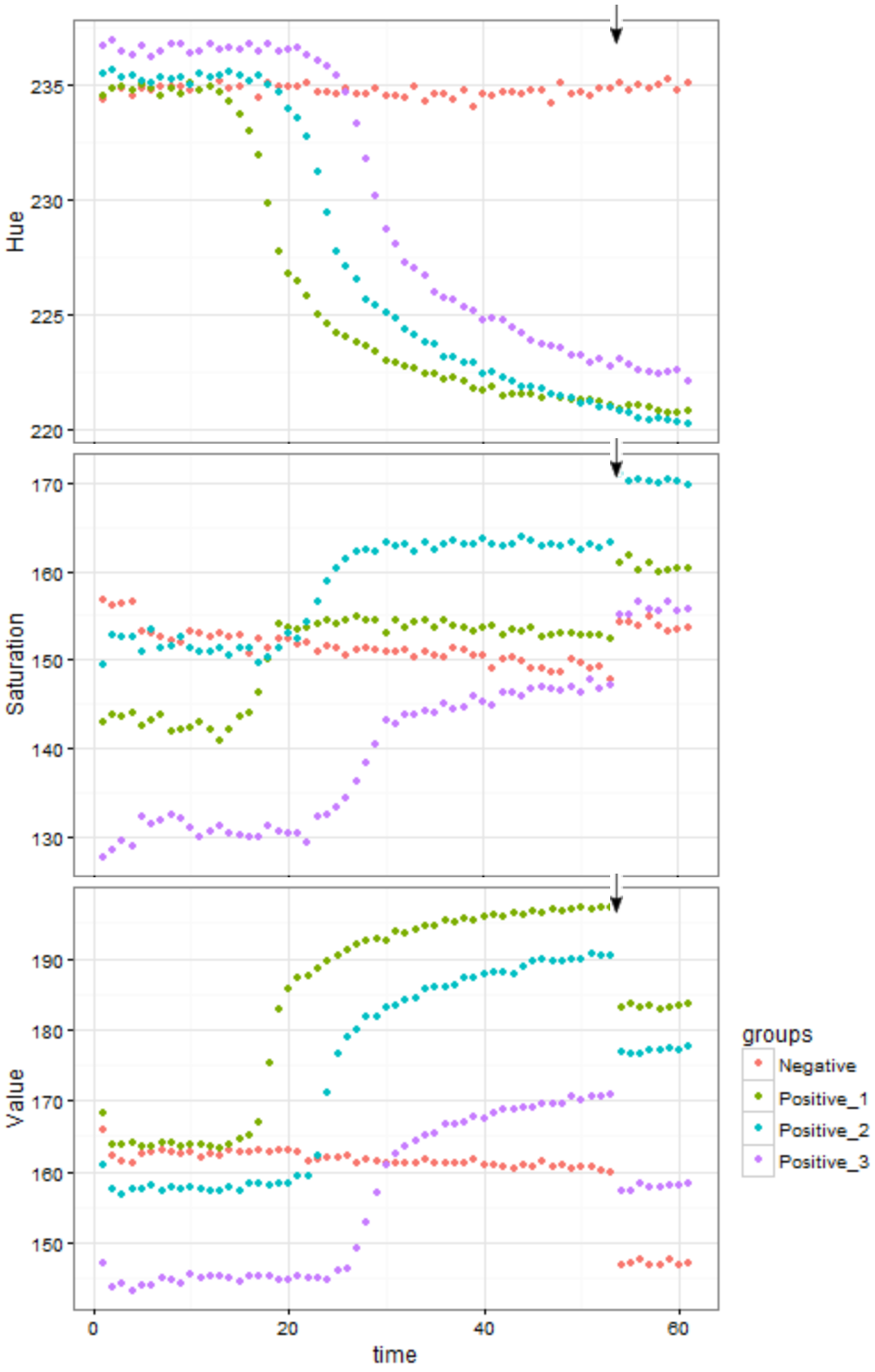

Figure 3. Hue, saturation, and value shift in negative and positive LAMP reactions.

(Arrow: time point that the room light intensity decreased.)

To validate the effectiveness of the bubble and background rejection algorithm, real-time LAMP reactions were selected to evaluate the performance of the bubble and background rejection algorithm. The results were plotted in **Figure 4**, where triplicate reactions were analyzed by both of the two methods (**A** and **D**, **B** and **E**, **C** and **F**). **Figure 4A** shows that without the rejection algorithm, the raw hue values from replicate 1 cannot be fit with the sigmodal function, while using the algorithm, the trend of the hue can be captured. The results from three replicate experiments indicated that the bubbles and background area potentially affected the hue calculation, and lead to inaccurate curve fitting. The bubble and background rejection algorithm reduced the effects of the bubbles and background areas in the images, resulting in more constant T_t values.

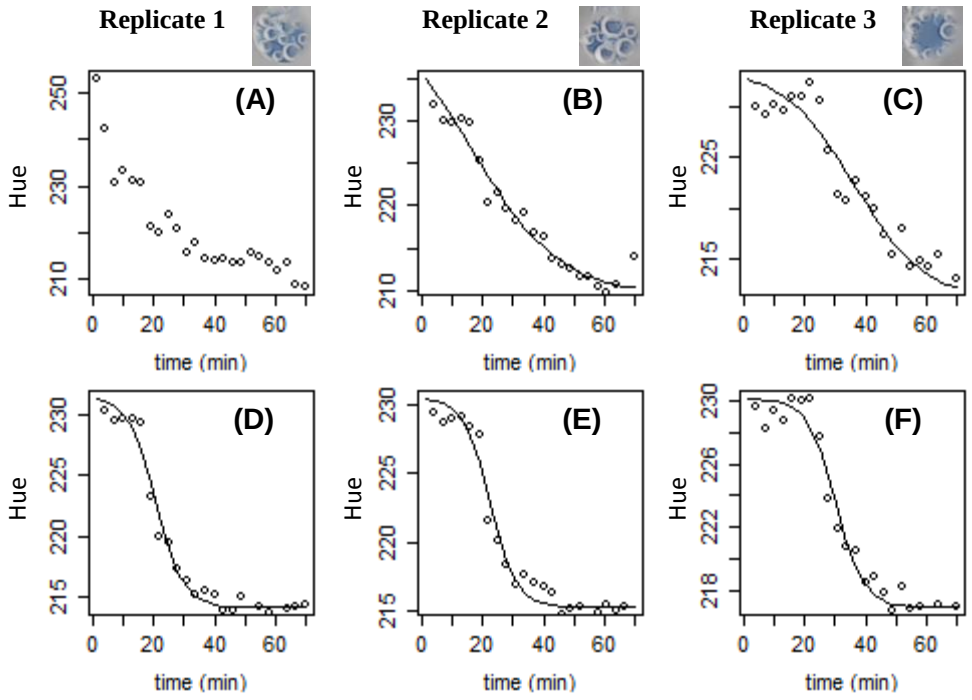

Figure 4. Real-time hue shift in triplicated colorimetric LAMP reactions without (A, B, C) and with (D, E, F) applying the bubble and background rejection algorithm.

(Dots: raw hue values, lines: fitted amplification curves. DNA template concentration: 10^6 copies/μL.)

3.4 Discussion

The following targets have been achieved in this chapter: (1) hue has been applied as a major feature to characterize the color shift of a LAMP reaction, (2) saturation has been selected as an auxiliary feature to control the quality of the pixels, (3) a regression model has been defined to represent real-time hue change, and (4) rapid image acquisition, processing, and data analysis tools have become available for future experiments.

In many situations, such as in the field, the ambient lighting intensity is largely affected by the weather. For many field-operable devices, an individual light control unit

is built to regulate lighting during signal detection. This is an effective approach; however, adding these elements into the system usually increase the size and cost of the device. The robustness of hue in this research suggested that the LAMP reaction could be performed in a platform without the need of additional components for controlling the ambient lighting conditions, which means the size and weight of the hardware platform could be reduced.

4. HARDWARE FABRICATION

4.1 Introduction

A miniaturized nucleic acid detection component is required to be implemented in an *in situ* device and deployed widely in the field (Auroux *et al*., 2004). Miniaturization accelerates chemical reactions, reduces the volume of assays, and decreases the need of sample amount (Ahmad and Hashsham, 2012).

In the past few years, significant progress has been achieved by integrating LAMP into lab-on-a-chip technologies. The availability of various LAMP product detection approaches, including turbidity (Fang *et al*., 2012; Mori *et al*., 2001), fluorescence (Ahmad and Hashsham, 2012; Wu *et al*., 2011), and colorimetric-based methods (Safavieh *et al*., 2014; Tanner *et al*., 2015) have further advanced the development. Fang *et al*. (Fang *et al*., 2010) reported a real-time quantitative μLAMP system by measuring turbidity on a polydimethylsiloxane (PDMS)-glass hybrid microfluidic chip. Hsieh *et al*. (Hsieh *et al*., 2012) reported a quantitative LAMP platform by adding DNA-binding methylene blue redox reporter molecules in the amplification step. Electrochemical monitoring of the redox current, which decreases during DNA synthesis, enables quantitative detection. However, it required a network of integrated microelectrodes in the microfluidic channels to measure the current, thus drastically increasing the cost and complication of the device.

The goal of this chapter is to validate the fundamental concept of a microfluidic LAMP device, and provide a benchtop prototype device that can be modified and integrated into the *in situ* genomic profiler in the future. All of the components in this

proposed handheld platform can be acquired easily. Therefore, this platform dramatically reduces the cost.

4.2 Experiments

4.2.1 Chip design and fabrication

To validate the use of qLAMP on chip level devices, a stamp-sized plastic chip was designed and fabricated. The chip had five isolated columns and each column had five reaction chambers (**Figure 5A**). This arrangement was used to perform qLAMP with multiple template concentrations and to characterize the performance with an amplification standard curve.

The chip is a 25.4 mm by 25.4 mm square with five layers (**Figure 5B, 5C**). The chip fabrication process includes forming liquid loading channels on the first layer by hot-embossing, creating reaction chambers as well as liquid loading inlets and outlets on the first two layers by mechanical drilling, cutting an oil chamber on the fourth layer by laser-ablation, and assembling the chip by thermal bonding. The surface structures on the first layer were formed using an aluminum master mold and hot embossing. The hot embossing process was performed in a heat press (Tetrahedron Associates, San Diego, CA) for 7 min at a temperature of 141 °C and pressure of 220 psi. Since the master mold had positive channel shaped patterns, after hot embossing, the patterns were replicated to the first layer. Each channel was 380 μm wide and 250 μm deep. The second layer consisted of an array of reaction chambers. Each chamber was 2 mm deep, with a volume of 2.5 μl. The third layer was a piece of hydrophobic polypropylene filter membrane (pore size: 0.22 μm, Sterlitech, Kent, WA). The top three layers were thermally bonded at

a temperature of 135 °C and pressure of 220 psi for 7 min. To create an oil chamber, a 0.05 mm thick pressure sensitive adhesive polyethylene terephthalate (PET) frame (layer 4) was attached between the filter membrane and the bottom layer (layer 5). Layers 1, 2, and 5 in the chip were made from cyclic olefin polymers (Zeon Chemicals, Louisville, KY).

All chip layers were completely rinsed with 1M EDTA and ddH_2O to remove potential contaminants. To increase surface hydrophilicity, the channel and reaction chamber were exposed to air plasma (PDC-32G, Harrick Plasma, Ithaca, NY) for 10 min. These layers were rinsed in 50 mg/mL EDC and 5 mg/mL NHS (Sigma-Aldrich, St. Louis, MO) solution for 10 min. Then, the layers were incubated in 0.2 M carbonate buffer (pH: 9.0) with 10 μM NH2-PEG-OH (Sigma-Aldrich, St. Louis, MO) for 1 hour.

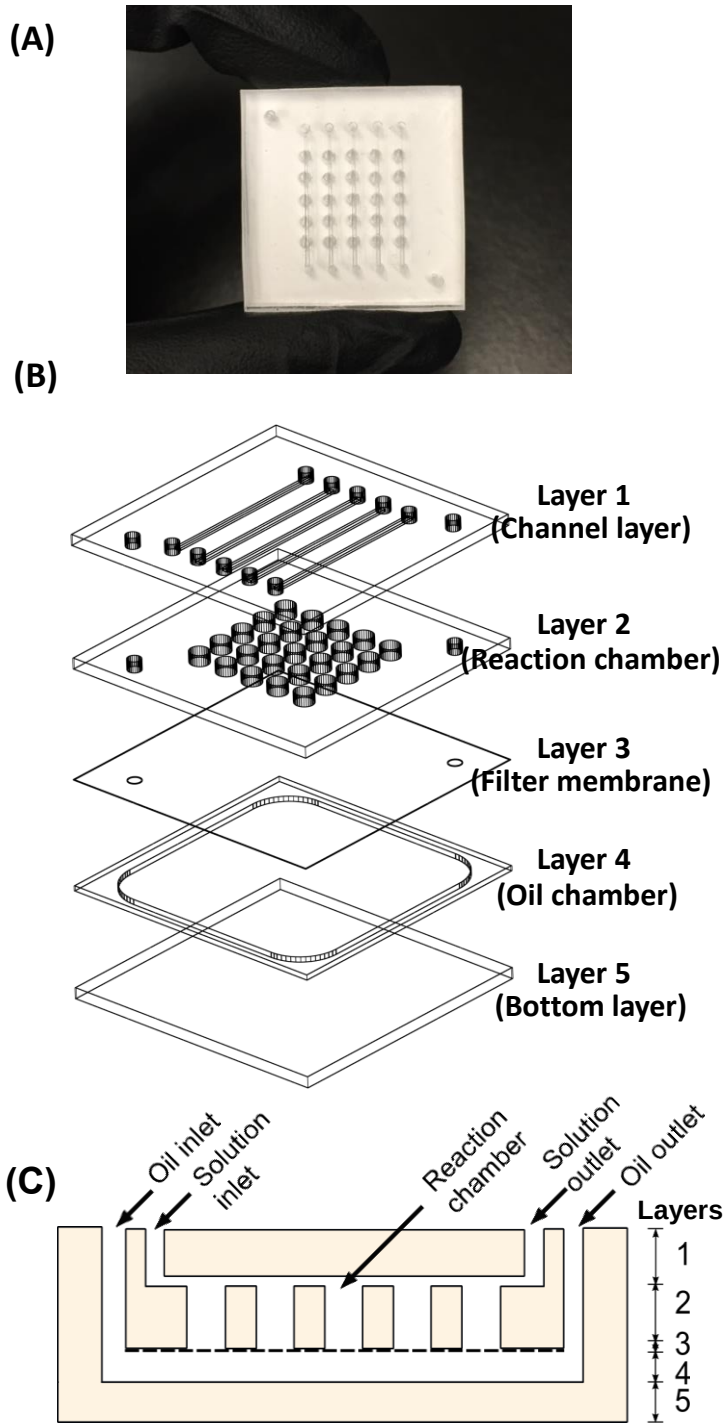

Figure 5. Structure of qLAMP chip

(A) Top view of the assembled chip, (B) Schematic of the chip layers, (C) Cross-section view of the chip (not to scale)

4.2.2 Liquid loading

A critical step for visualizing the color of the on-chip LAMP reaction was to manufacture deep reaction chambers with a high aspect ratio (depth / diameter of the reaction chamber). However, when the chambers have only one inlet, the high aspect ratio geometry results in dead volumes that trap bubbles during liquid loading. To solve this problem, a hydrophobic polypropylene filter membrane (PP022005, Sterlitech, Kent, WA) was added underneath the reaction chambers (**Figure 6A**). Air would easily vent through the porous filter membrane and the liquid stopped once it touched the hydrophobic surface (**Figure 6B**). In addition, channels and reaction chambers were treated to be hydrophilic to prevent bubbles trapping or attached to the surface of either the channels or inner walls of the reaction chambers. After the liquid loading was done, the liquid inlets and outlets were sealed. Silicone oil was loaded to the backside of the filter membrane to ensure that the pores on the filter membrane were sealed by oil. With the chip inlets and outlets sealed, conduction of the LAMP reaction at an elevated temperature resulted in increased reaction pressures which prevented bubble formation via outgassing (**Figure 6C**).

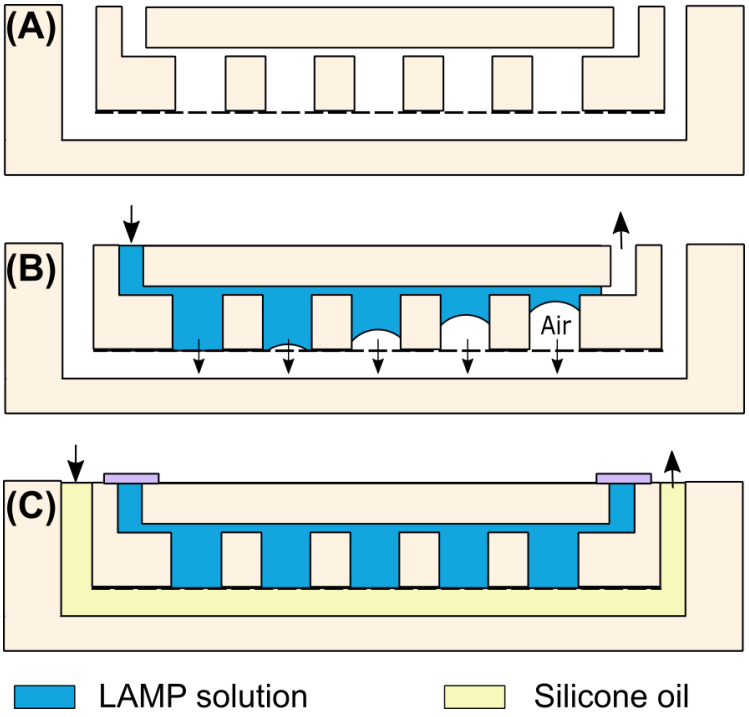

Figure 6. Image sequence of liquid loading into chambers

4.2.3 Heater design

A key advantage of colorimetric LAMP is that the system architecture is relatively simple. **Figure 7** shows the three major components of a general LAMP system: a chip with multiple reaction chambers, a color camera and white light illumination, and a heater that maintains the reaction temperature at a constant 65 °C during amplification.

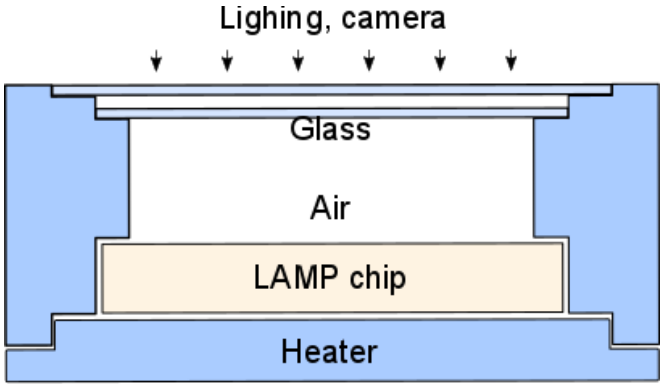

Figure 7. Heater structure

4.3 Results

4.3.1 Bubble reduction during liquid loading

As indicated previously, the chip design included a hydrophobic filter membrane to vent air in the deep reaction chambers. The filter membrane allowed bubbles to pass through yet retains the liquid in the wells. The design was evaluated by compareingthe formation of bubbles by loading food coloring into the chips with and without the filter membrane layer. The structure of the chip with the filter membrane was identical to that illustrated in **Figure 5**, while the one without the filter did not have layers 3 and 4 in **Figure 5B**. **Figure 8B** showed that without the filter membrane, large bubbles formed at the base of all chambers. When the filter layer was added (**Figure 8A**), the trapped air vented through the filters so no bubbles formed in the chambers.

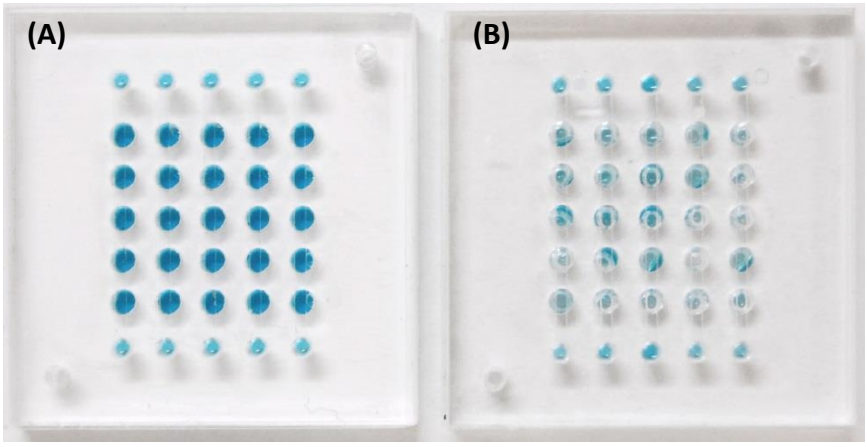

Figure 8. Liquid loading with (A) and without (B) a hydrophobic membrane at the bottom of the wells

4.3.2 Chip temperature validation

To validate the heating capability, the temperature of the heater and the chip was monitored every 30 seconds (**Figure 9**). The chip requires 13 minutes to reach 65 °C. Then, the temperature remains constant at 65 °C.

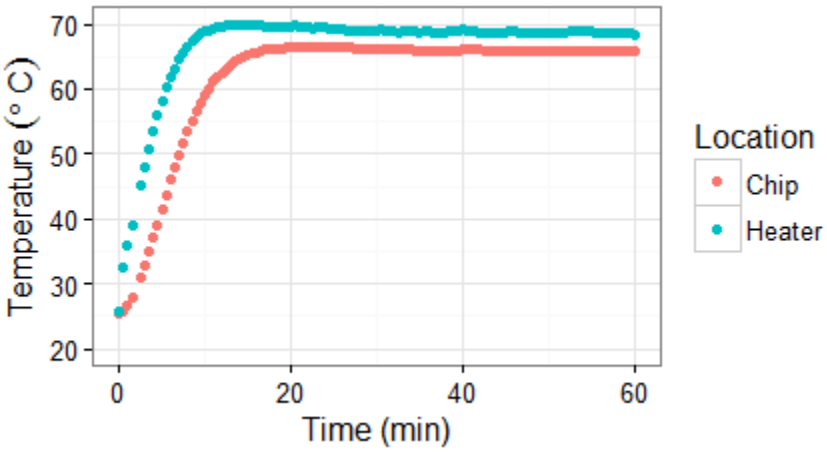

Figure 9. Heater and chip temperature

4.4 Discussion

In summary, the hardware platform is ready to use for colorimetric LAMP reactions. In this part of the project, a chip level device has been designed and assembled to perform colorimetric LAMP reactions. The implementation of the hydrophobic filter member enabled bubble-free reaction solution loading. A temperature controller was designed and built for the chip to maintain isothermal conditions at 65 °C.

The cost of the chip material was negligible. Moreover, the fabrication process of the chip can be easily scaled up for mass production, which reduced the cost further.

5. ON-CHIP REAL-TIME COLORIMETRIC LAMP

5.1 Introduction

Many genomic analytical applications require quantitative measurements under resource-limited conditions (Nolan and Bustin, 2013; Thomson and Cooper, 2013). Examples include point-of-care diagnosis devices (Punter-Villagrasa *et al*., 2015), portable field-operable devices (Nakamura, 2012), and automated in situ instruments (Kotiaho, 1996). Such devices benefit from techniques and subsystems which enable low energy consumption, a small footprint, and robust operation to achieve long operational duration and easy deployment (Wang *et al*., 2016).

In situ monitoring of environmental microbial communities is an important application potentially addressed by portable nucleic acid analyzers (Buffle and Horvai, 2000). The predominant analytical methods for this purpose are fluorescence-based nucleic acid amplification methods such as polymerase chain reaction (PCR) because they are highly sensitive and quantitative (Shi *et al*., 2011, 2013). Quantitative PCR (qPCR) is particularly useful to quantitatively analyze the constituency of the microbial communities (Fredricks, 2011). Although qPCR is a routine technology and is widely adopted in molecular biology laboratories, it has intrinsic limitations for portable instruments. The requirement for repetitive thermal cycling and high temperatures for DNA melting consumes large amounts of energy, and fluorescence-based detection requires more complicated, expensive optical setups (Kokkinos *et al*., 2013). Instrument developers have made progress on reducing the thermal load by reducing reagent volume

using microfluidics (Curtis Saunders *et al*., 2013), but the final products are still less than ideal for portable operations.

In this chapter, the on-chip, real-time quantitative LAMP with colorimetric hydroxy naphthol blue (HNB) detection is presented. Images are captured by an inexpensive digital color camera, and the color changes are correlated to the concentration of the template quantitatively by assessing the time required to produce colorimetric changes. This appears to be the first demonstration of real-time colorimetric and quantitative LAMP (qLAMP) on a microfluidic device. In addition, colorimetric LAMP allows for a simple and inexpensive system architecture. The feasibility of on-chip qLAMP will encourage further development of easily accessible, miniature, quantitative *in situ* biological instruments.

5.2 Experiments

5.2.1 Experimental apparatus

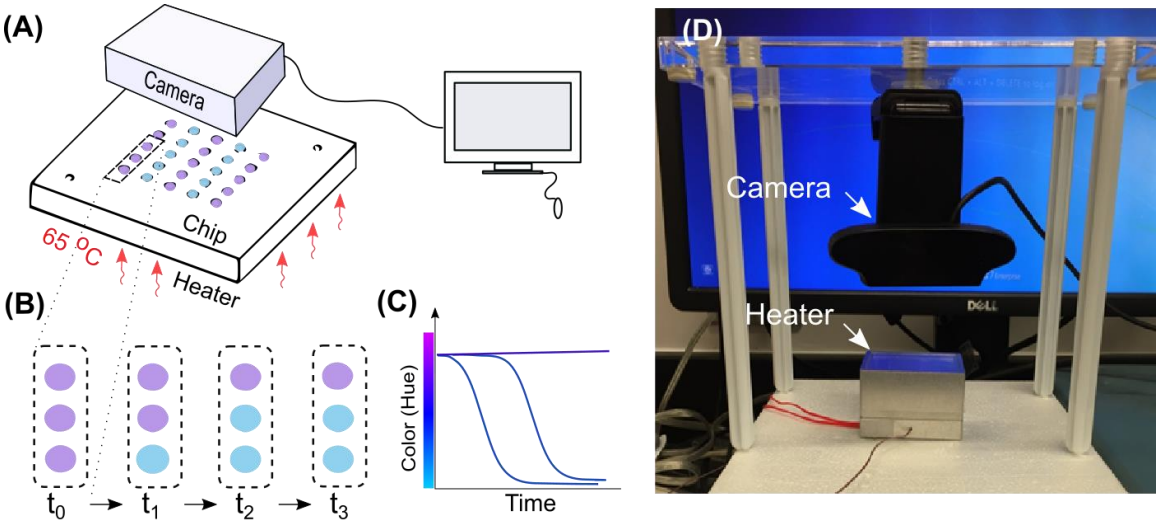

Figure 10. Experimental setup

A key advantage of colorimetric qLAMP is its relatively simple system architecture. **Figure 10A** shows the three major components of the qLAMP system: 1) a chip with multiple reaction chambers, 2) a color camera, and 3) a heater that maintains the reaction temperature at a constant 65 °C during amplification. A photograph of the experimental setup is shown in **Figure 10D**. The basic approach to on-chip, colorimetric LAMP analysis relies on the color change that occurs as the amplicon accumulates during a LAMP reaction. The experimental setup tracks the colors of each LAMP reaction over time to follow reaction progression. **Figures 10B** and **10C** show the principle of the colorimetric qLAMP measurement. The disks in **Figure 10B** represent the LAMP reaction chambers. At the beginning of the LAMP reaction (**Figure 10B**, t_0), the solutions in the LAMP reaction chambers are purple. As reactions proceed (**Figure 10B**, from t_0 to t_3), the colors of positive reactions shift from purple to sky blue, while the negative controls remain purple. The computer converts the color of the digital image from the RGB (Red, Green, Blue) space into the HSV (Hue, Saturation, Value) space. The color of the LAMP reactions are plotted as amplification curves (**Figure 10C**). The time period of the color change during amplification can be used to infer the concentration of the target template in the sample in a manner similar to the determination of the threshold cycle 'C_t' (Muller *et al*., 2002) value of qPCR.

5.2.2 Bacterial cultivation and genomic DNA preparation

Synechocystis 6803 has been cultivated in BG11 medium at 30 ^{o}C under a light intensity of 35 μE/m^2/s (Rippka *et al*., 1979). *Synechocystis* cells were harvested, and their genomic DNA was extracted and purified. LAMP primers are designed to target the *rbcL*

gene. *rbcL* is an important carbon dioxide fixation gene (Huang *et al*., 2002). It allows *Synechocystis* to grow in a range of carbon dioxide concentrations with the presence of light. Genome copy number was calculated using the following equation:

$$CopyNumber = \frac{m_{\mathrm{DNA}} * N_{\mathrm{A}}}{l_{\mathrm{DNA}} * w_{\mathrm{basepair}}},$$

where *CopyNumber* is the number of copies of the genome in a specific amount of genomic DNA, m_{DNA} is the amount of DNA, N_{A} is Avogadro's number, l_{DNA} is the length of the DNA (in bp), and w_{basepair} is the average weight of a base pair.

5.2.3 Reaction mixture for LAMP

The LAMP amplification procedure was modified based on the previous work described by Tomita *et al.* (Tomita *et al*., 2008) and Goto *et al*. (Goto *et al*., 2009). Three pairs of primers were designed by the online LAMP primer design tool PrimerExplorer V4 (http://primerexplorer.jp/elamp4.0.0/index.html), and synthesized by Invitrogen (Life Technologies, Grand Island, NY). LAMP primers were designed to target the *rbcL* gene of *Synechocystis* sp. PCC 6803 genome. Primer sequences are as follows.

Table 1. Primer sequences for *Synechocystis* sp. PCC 6803 qLAMP

Primer	**Sequence (5' - 3')**
FIP	AAGTCCAAACCACCCCGGAGAAACTTGGTCTGTCCGCCA
BIP	ATCAACTCCCAGCCCTTCATGCGCTTTTTCGATCGCCTCTTG
LF	AACAGCCCGACCGTAGTTCT
LB	GCGCGATCGTTTCCTCTTCG
F3	GTCCTCTGCTTGGTTGTACC
B3	TCGTTGGTCTCAGCCTGG

The LAMP reaction mixture contained: 20 mM Tris-HCl, 10 mM $(NH_4)_2SO_4$, 10 mM KCl, 6 mM $MgSO_4$, 800 μM dNTP, 180 μM HNB (Sigma-Aldrich, St. Louis, MO), 800U/mL Bst 2.0 warmstart polymerase (New England Biolabs, Ipswich, MA), 1.6 μM FIP, 1.6 μM BIP, 0.8 μM LF, 0.8 μM LB, 0.2 μM F3, 0.2 μM B3, and *Synechocystis* sp. PCC 6803 genomic DNA. The genomic DNA was quantified by a Nanodrop spectrophotometer (Thermo Scientific, Wilmington, DE). For acquiring the standard curve, the DNA template was 10-fold serial diluted. DNA was replaced by DEPC-treated water (Thermo Fisher Scientific, Cat No. AM9916) in negative controls. The LAMP reaction was incubated in 65 °C for 1 h.

5.2.4 Experimental procedures

The LAMP reaction mixture was prepared following the protocol mentioned above. A serial dilution of *Synechocystis* sp. PCC 6803 genomic DNA was added and completely mixed in each reaction. All of the procedures were performed in a biosafety cabinet.

After assembly, LAMP reaction solutions were loaded into the microfluidic chip through the liquid inlets with one template concentration in each channel. Driven by both capillary action and positive pressure, the liquid flowed through the channels and filled the entire reaction chambers. This microfluidic chip enables five reactions to be performed simultaneously, including four positive LAMP reactions plus a negative control group. When the reaction chambers and channels were filled, both of the liquid loading inlets and outlets were sealed to create an airtight reaction condition. Then a vacuum was applied on the oil outlet to introduce the hot silicone oil (65 °C) to the oil chamber. In this way, the filter membrane was immersed in silicone oil as well.

Therefore, all of the pores in the filter membrane were sealed. Silicone oil prevented the reaction liquid from evaporating. Finally, the whole chip was placed on the pre-heated heater, and incubated at 65 °C for 1 h. The webcam (HD Pro Webcam C910, Logitech, Newark, CA) was placed right above the reaction chamber, and the images were taken every 1 min. The images were batch-processed to extract hue information for each single reaction chamber. The hue data was exported for curve fitting and T_t value calculation.

5.3 Results

5.3.1 Colorimetric quantification

To validate the HNB-based colorimetric measurement and to evaluate the range of sensitivity, the template concentration was serially diluted with a factor of 100, from 10^7 copies/μL to 10 copies/μL. **Figure 11A** shows the webcam image captured right after loading the LAMP mixture, where the first column from the right is the negative control. The colors of all chambers were uniform. **Figure 11B** is the image after 70 minutes of LAMP reaction. All chambers with concentrations higher than 10^3 copies/μL showed significant color changes, indicating positive LAMP reactions. All five chambers for the negative control became purple, indicating negative LAMP reactions. Only one chamber for the 10 copies/μL concentration had a positive reaction. The result showed that the LAMP platform was sufficiently sensitive for concentrations higher than 10^3 copies/μL. In addition, **Figures 11A** and **11B** can be easily perceived with the naked eye or a cell phone camera.

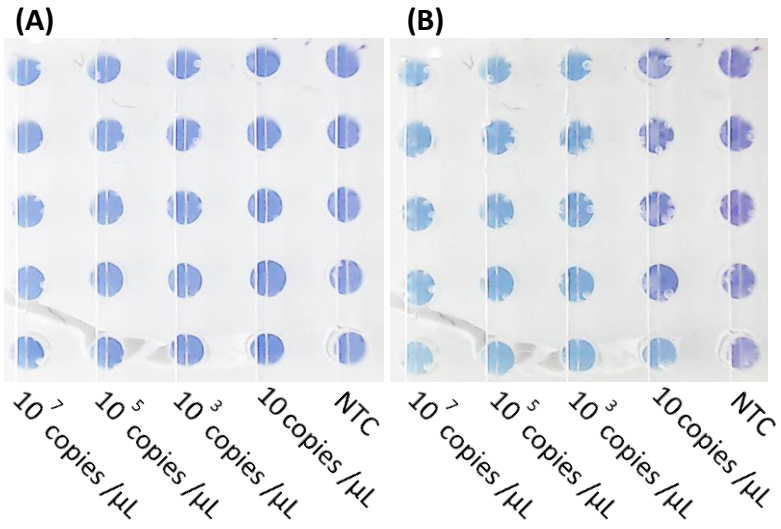

Figure 11. The images of the qLAMP array at (A) the beginning and (B) 70 minutes after the start of *Synechocystis* sp. PCC 6803 qLAMP reaction

In addition to recording the images at the beginning and the end of the experiment, a PC was programmed to record images through the webcam every minute with LabVIEW (National Instruments, Austin, TX), and the hue, saturation, and intensity values were extracted for each reaction chamber at every time point with Matlab (MathWorks, Natick, MA). **Figure 12 (A-E)** shows the quantitative hue changes of the same chip for **Figure 11**. Each color indicates the color of a reaction chamber, where each dot represents the measured hue value at that time point. The solid curves are the curve-fit results using Eq. (1). The results show that although the hue of different chambers had offsets and the rate of color changes differed, the curve-fit algorithm captured the amplification process. At higher DNA concentrations (from 10^3 copies/μL to 10^7 copies/μL), a decreased hue from dark blue (hue 225) to sky blue (hue 210) took

place within 60 min. In negative control groups, hue drifted upward and the color transformed from dark blue (hue 225) to violet (hue 240).

The reactions for concentrations higher than 10^3 copies/μL were fast. The reactions were completed in 35 minutes, and the significant color swing occurred within 10 minutes (**Figure 12A-C**). The amplification of the only positive reaction for 10 copies/μL had a much lower reaction rate (**Figure 12D**).

The standard curves in **Figure 12F** show the average T_t with the error bars as the standard errors among the five reaction chambers with the same template concentration. The relation between the average T_t and the template concentration is highly linear. The T_t of the same concentration has small variations for concentrations >10^3 copies/μL. Higher concentrations had smaller variations.

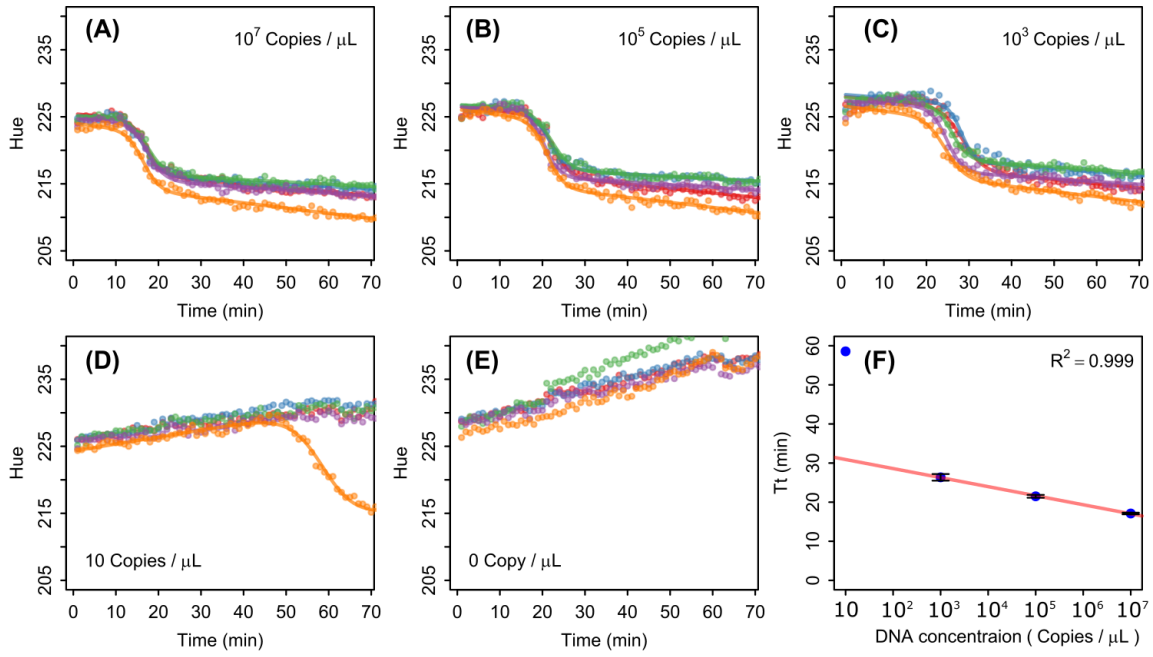

Figure 12. Amplification curves and standard curves of *Synechocystis* sp. PCC 6803 qLAMP

A continuously decreasing trend was observed in positive LAMP reactions after the threshold time. This phenomenon happened slowly, which is very similar to the "fluorescence drift" (Rutledge and Stewart, 2008) phenomenon that occurs in qPCR. To interpret the hue drift in colorimetric LAMP reactions, a linear term $S_1 t$ was added into the proposed model. A slightly increasing trend of the hue was observed in non-reacting wells. Because non-reacting wells were not counted for T_t value calculations, this trend does not affect the quantification results. Therefore, investigating the reasons that led to this phenomenon is beyond the scope of this study.

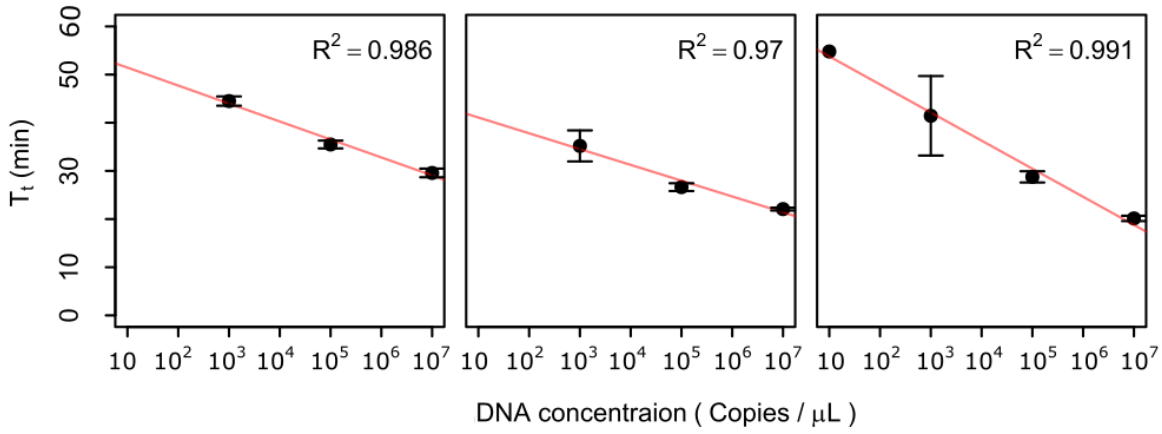

Figure 13. Repeatability of the chip-based qLAMP reactions with *Synechocystis* sp. PCC 6803

Beyond the experiment shown in **Figure 12**, additional chip-based LAMP reactions were performed and the standard curves are plotted in **Figure 13**. The standard curves showed that the chip-based LAMP reactions were highly quantitative and repeatable. The quantitative range was from 10^3 copies/µL to 10^7 copies/µL. Around 20% of the reactions in the 10 copies/µL group showed up positive, indicating that this concentration was not a good candidate for quantification, but the sensitivity of the

LAMP reaction reached 10 copies/µL. Similar to qPCR, due to different experimental setups and different batches of reagents, it was noticed that the slope of the standard curves varied in chip-based LAMP reactions.

It was initially expected that the color of the same column would be uniform at the end of a 60-minute experiment because the chambers of the same column are connected by channels; however, the results showed that this is not the case. It is interesting to see that, in **Figure 11**, only one out of five reaction chambers had a positive reaction. Even though the reaction chambers were connected by a main channel, it seems the reaction in one reaction chamber does not affect the reaction in its adjacent reaction chamber within the timeframe of these experiments. It was also evident that even though the reaction chambers were connected, the T_t values showed heterogeneity. The variations of the T_t values tend to be larger at a lower template DNA concentration. This evidence suggested that diffusion might not affect the reactions among different reaction chambers, perhaps contrary to expectations. It appears that the rates needed for amplified products and HNB or $Mg^{2+}$to migrate to the neighboring chambers were much lower than the rate of LAMP amplification, thus reducing the crosstalk between neighboring chambers as long as the duration is less than 60 minutes. The 0 copy/µL negative control results also showed that the reaction system was stable and reliable during the measuring time period, without production of false positive results. Future device designers should exploit this feature to simplify their microfluidic platforms with architectures that do not require full liquid isolation with qLAMP.

5.3.2 Primer specificity test

The specificity of the reaction has been evaluated by replacing the DNA template with other non-target DNA. Non-target DNA used in this study include the genomic DNA extracted from the following species: (1) *E. coli*, (2) *Bacillus* sp., (3) *Thaiassiosira pseudonana*, and (4) human cell line FLO-1. The end point measurement showed the proposed *Synechocystis* primers only target *Synechocystis*, and do not generate cross-reactions with the above non-target DNA. This indicates high primer specificity.

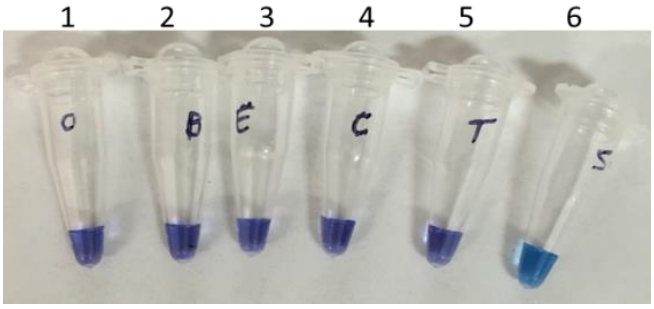

Figure 14. Specificity test of *Synechocystis* sp. PCC 6803 primers

(1) Negative control (H_2O), (2) *Bacillus* sp. DNA, (3) *E. coli* DNA, (4) Human cell line FLO1 DNA, (5) *Thalassiosira pseudonana* DNA, (6) Positive control (*Synechocystis* sp. PCC 6803 DNA)

5.4 Discussion

This study reports a low-cost system for real-time quantitative LAMP reactions by colorimetric measurement that was easy to build and user-friendly. In this system, the LAMP reactions were loaded into the microfluidic chips and then incubated at 65 °C. Instead of using optical fibers and fluorescence detectors, this device can be placed in ambient light, and only requires a webcam for monitoring the reactions. The application of a webcam as the imaging tool eliminated the need for delicate electrical elements. The

chip fabrication process is simple, which can be scaled up for mass-production, and the cost of the materials in the chip is negligible; thus, manufacturing this plastic microfluidic chip is inexpensive. Additionally, heaters (or ovens) and webcams can be easily accessed, even in remote areas. This system is a handy platform for performing quantitative DNA analysis without expensive instruments. The simple imaging method also reduces the time and resources for operator training.

To date, the microfluidic chip in this system enables the simultaneous detection of up to five DNA targets. To increase the throughput of the chip, the arrangement of the reaction chambers can be modified to be denser.

This detection system could be applied to a wide range of applications, including microbial community monitoring, food and water quality control, and infectious disease diagnostics. This low-cost, portable system for LAMP analyses shows promise for reducing the expense associated with high-performance, DNA-based analyses.

6. ON-CHIP COLORIMETRIC RT-LAMP WITH BACTERIAL RNA

6.1 Introduction

It has been reported that gene expression level change can be used to predict the consequence of the ocean change, as gene expression alters the physiological function of marine species (Evans and Hofmann, 2012). Monitoring gene expression becomes an important goal of ocean conservation (Evans and Hofmann, 2012). Thus, an ocean-observing device having gene expression level quantification capability could advance ocean studies significantly.

Real-time reverse transcription loop-mediated isothermal amplification (RT-LAMP) is a rapid and sensitive RNA quantification technology. In RT-LAMP, reverse transcriptase synthesizes cDNA via RNA templates. The amplification initiates by primer annealing, and continues by forming dumbbell structures and strand displacement. The reaction results in rapid accumulation of amplicons within one hour. As Bst polymerase has strand displacement activity, RT-LAMP reaction eradicates the need of thermal cycling. In one step RT-LAMP, by adding reverse transcriptase and Bst polymerase to the reaction, cDNA synthesis and LAMP reactions can be performed simultaneously in one tube. Similar to LAMP, one step RT-LAMP products can be detected using routine molecular biology laboratory techniques in molecular biological laboratories. End point HNB measurement is one of the commonly used techniques. However, no real-time colorimetric and quantitative RT-LAMP methods have been reported so far.

Cyanobacteria are some of the major players of nitrogen fixation (Falcón *et al*., 2004) and photosynthesis (Falkowski *et al*., 1998) in the natural environment. Among

cyanobacteria, *Synechocystis* is one of the most common genera (Kaneko and Tabata, 1997). They are widely distributed, not only in freshwater, but also in the ocean (Falcón *et al*., 2004). Because of their essential role in oxygenic photosynthesis, *Synechocystis* sp. Strain PCC 6803 has become an interesting target of researchers (Wang *et al*., 2012), and is a commonly used model for photosynthesis studies (Kaneko and Tabata, 1997).

In this study, the real-time colorimetric quantification approach to RT-LAMP was applied for the first time by using *Synechocystis* 6803 total RNA.

6.2 Experiments

6.2.1 Reverse transcriptase selection

In one-step RT-qLAMP, chemical components remain the same with qLAMP, except the template and enzymes (Lee *et al*., 2011). Because the Bst 2.0 DNA polymerase in qLAMP reactions does not have reverse transcript activity, additional reverse transcriptase needs to be added in the reaction solution. Three types of reverse transcriptase have been evaluated based on their performance: (1) WarmStart RTx, (2) AMV reverse transcriptase, and (3) Bst 3.0 (a DNA polymerase with reverse transcriptase activity). Among these types of reverse transcriptase, WarmStart RTx generated the best RT-qLAMP results, regarding sensitivity, specificity, and quantitative capability. Therefore, WarmStart RTx was used for future one step RT-qLAMP reactions.

6.2.2 Reaction mixture for *Synechocystis* RT-qLAMP

The primer sequences used in RT-qLAMP reactions are listed in **Table 2**. All of the primers were synthesized by Integrated DNA Technologies (Coralville, Iowa, USA). RT-qLAMP reaction mixture contains 1x ThermoPol DF buffer (New England Biolabs,

Ipswich, MA), 1.6 μM inner primers, 0.8 μM loop primers, 0.2 μM outer primers, 180 μM HNB, 6 mM $MgSO_4$, 800 μM dNTP, 800U/mL Bst2.0 WarmStart polymerase (New England Biolabs, Ipswich, MA), 300U/mL WarmStart RTx Reverse Transcriptase (New England Biolabs, Ipswich, MA), and *Synechocystis* sp. PCC 6803 total RNA. In negative control group, the RNA template was replaced by DEPC-treated water. The total RNA was extracted by ZR Fungal/Bacterial RNA kits (Zymo Research, Irvine, CA, USA), and quantified by Nanodrop 1000 spectrophotometer (Thermo Scientific, Waltham, MA, USA).

Table 2. Primer sequences for *Synechocystis* sp. PCC 6803 RT-qLAMP

Primer	**Sequence (5' - 3')**
FIP	AAGTCCAAACCACCCCGGAGAAACTTGGTCTGTCCGCCA
BIP	ATCAACTCCCAGCCCTTCATGCGCTTTTTCGATCGCCTCTTG
LF	AACAGCCCGACCGTAGTTCT
LB	GCGCGATCGTTTCCTCTTCG
F3	GTCCTCTGCTTGGTTGTACC
B3	TCGTTGGTCTCAGCCTGG

6.2.3 Experimental procedures

To demonstrate that this colorimetric RT-qLAMP approach can be robust even in small volume reactions, amplifications were performed in a homemade 24-well optical plate. The plate was a piece of acrylic with an array of 2.2 mm deep, 1.4 mm diameter wells cut by a CO_2 laser. RT-qLAMP reactions of 3 μL were loaded into each well and covered by silicone oil to prevent evaporation. To maintain the reaction temperature, the plate was

placed on a 65 °C heating element. All of the reactions were recorded by a webcam, which captured time-lapse images every minute. The images were analyzed and hue values of the reactions were extracted. The trend of the hue values was fit with a sigmoidal function to obtain a faithful representation of the chemical reactions. The exponent parameter of the sigmoidal function was represented as threshold time (T_t) to characterize reaction dynamics. The T_t values were plotted to construct a standard curves.

6.3 Results

Three types of reverse transcriptases were compared. The RT-qLAMP reaction with WarmStart RTx reverse transcriptase shows the highest sensitivity, specificity, and quantitative capability. However, Bst 3.0 generated non-specific amplifications. Even though AMV reverse transcriptase did not generate false positives, its quantification capability is not as decent as WarmStart RTx.

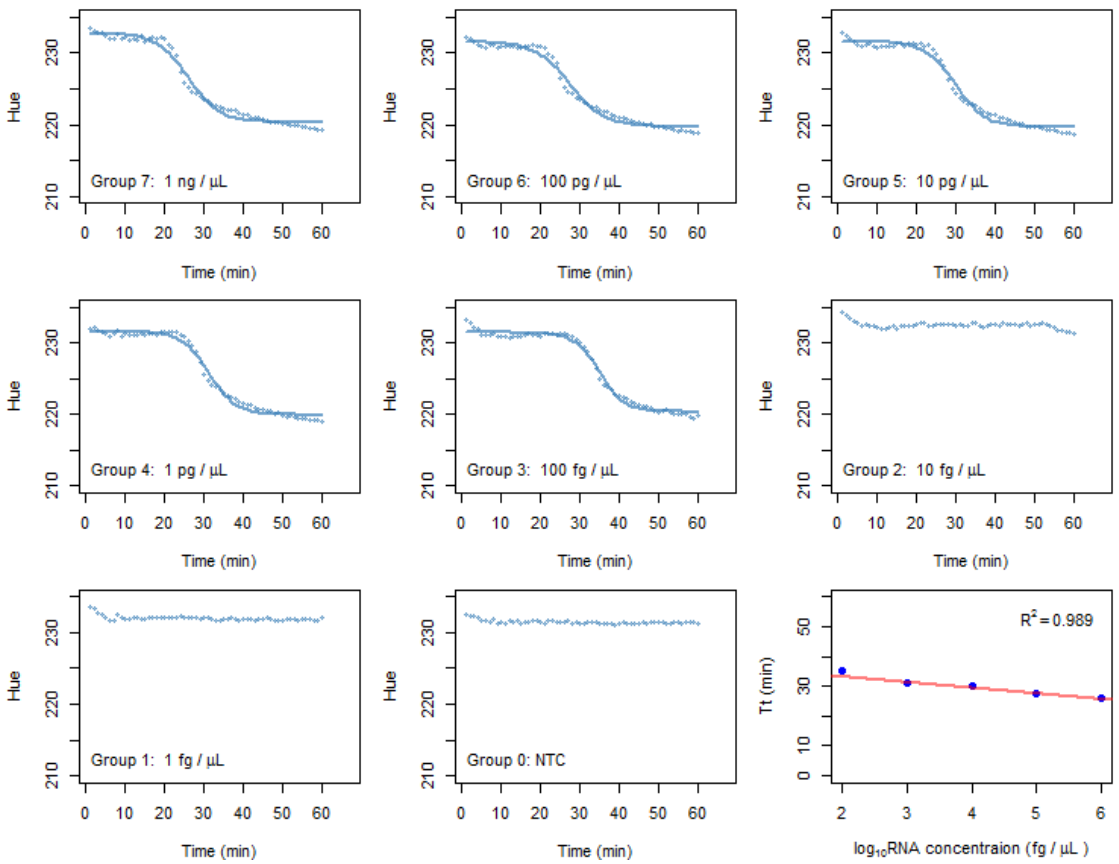

Figure 15. RT-qLAMP standard curves and amplification curves with Warmstart RTx reverse transcriptase

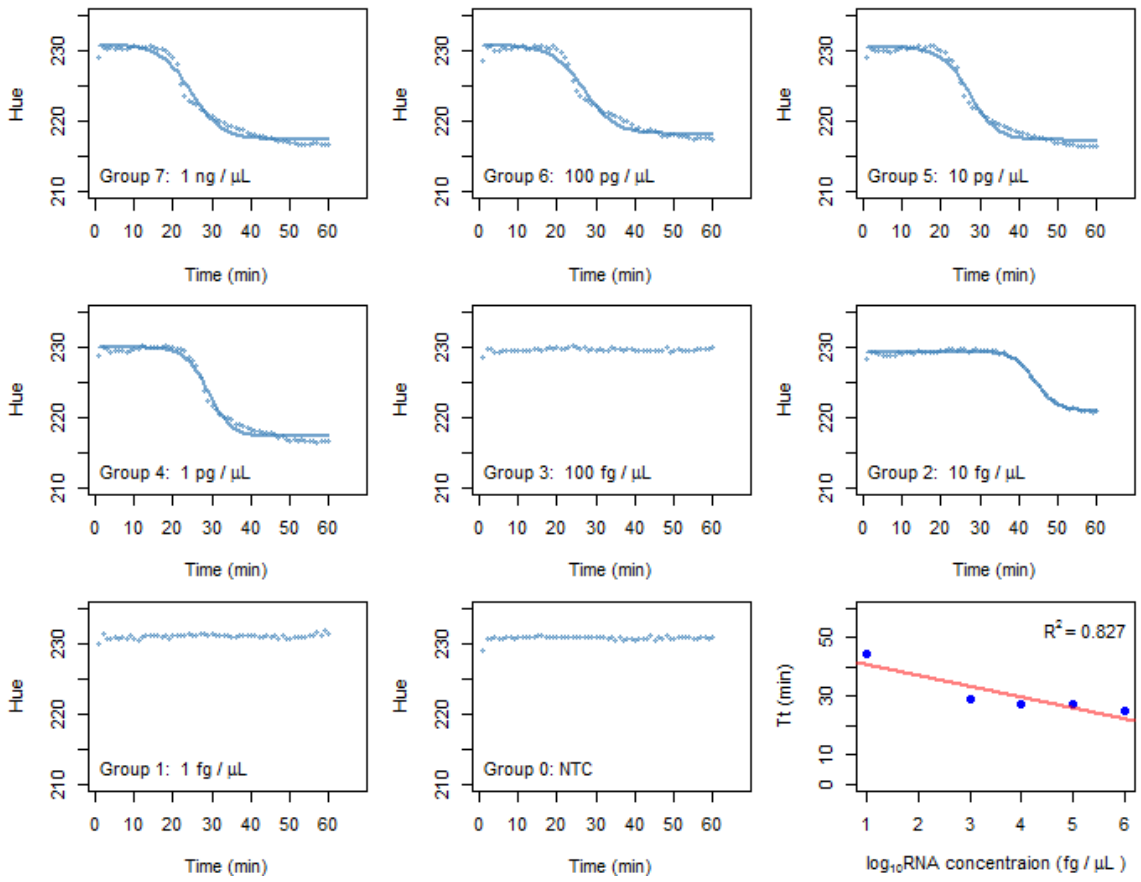

Figure 16. RT-qLAMP standard curves and amplification curves with AMV reverse transcriptase

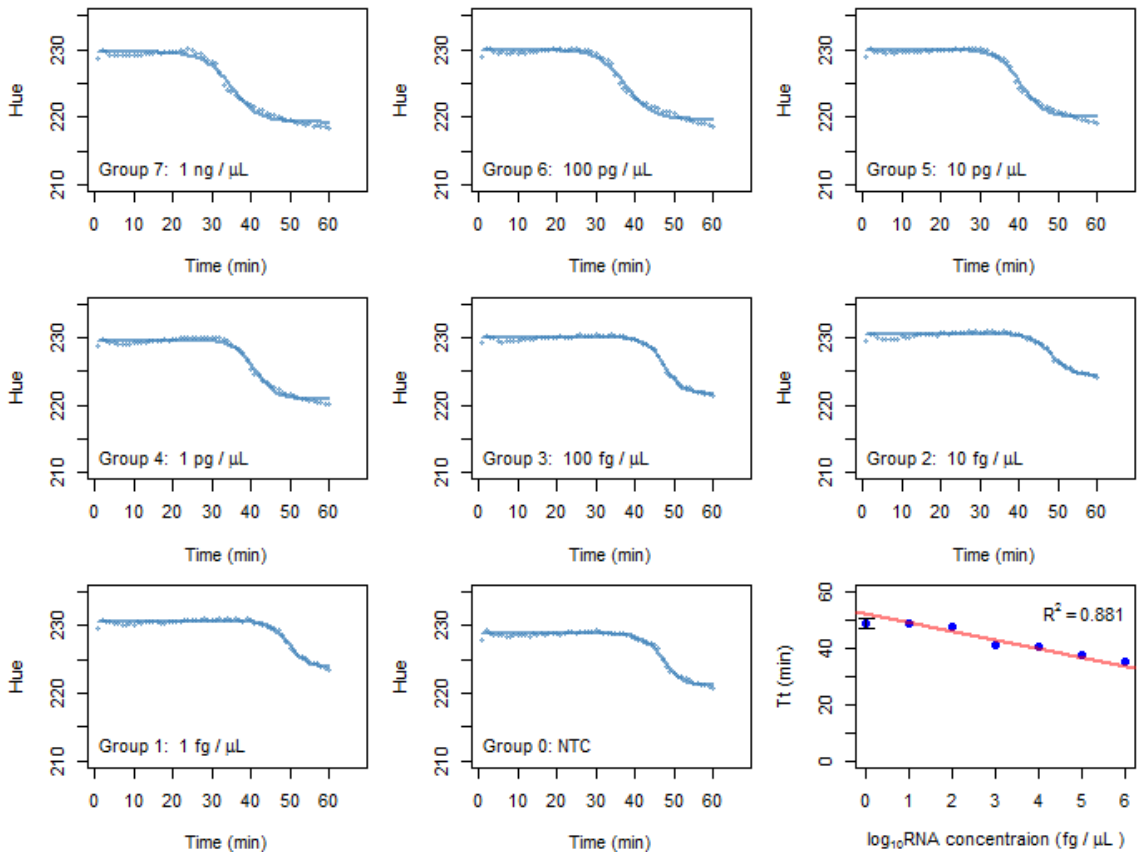

Figure 17. RT-qLAMP standard curves and amplification curves with Bst 3.0 DNA polymerase

The sensitivity and quantitative range of RT-qLAMP were evaluated by performing RT-qLAMP with 10-fold series diluted RNA templates. In positive RT-qLAMP reactions, the hue values exhibited significantly decreasing trend within one hour (**Figure 18**). The color of the reactions shifted from violet to sky blue. However, no decreasing trend of the hue values was observed in negative controls. 33% of the wells reacted when the RNA concentration is 100 fg/µL, suggesting that the sensitivity of the reaction reached 100 fg RNA/µL. The quantitative range of the RT-qLAMP reaction was from 1 pg RNA/µL to 1 ng RNA/µL (R^2 = 0.9915).

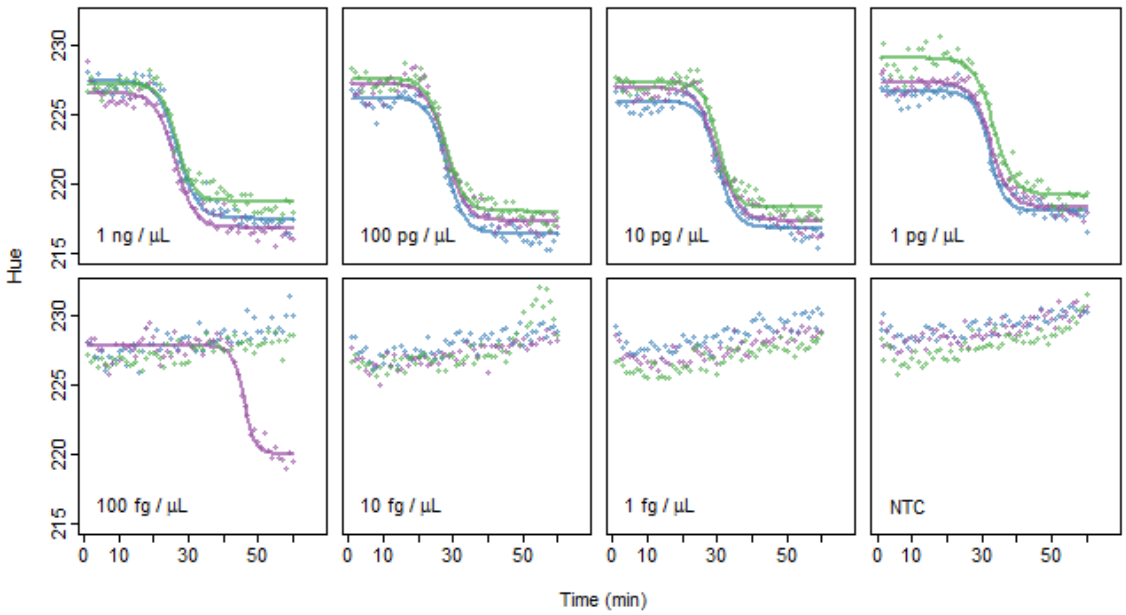

Figure 18. Colorimetric RT-qLAMP Amplification curves (template: *Synechocystis* sp. PCC 6803 total RNA)

The specificity of the assay was validated by replacing the RNA template with non-target RNAs. In this study, total RNA from *Bacillus* sp., *E. coli*, *Thalassiosira pseudonana*, and human cell line FLO-1 have been evaluated as control experiments. The results showed that none of the control experiments was amplified. This means the *Synechocystis* rbcL primers in this study was highly specific and did not generate cross-reactions from other non-targeted RNAs.

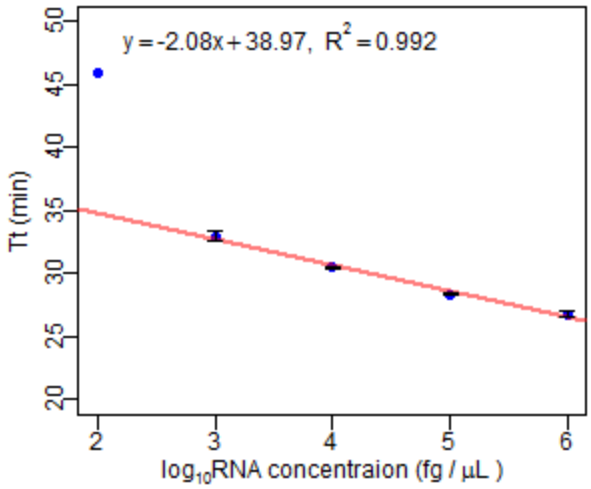

Figure 19. Colorimetric RT-qLAMP Standard curve (template: *Synechocystis* sp. PCC 6803 total RNA)

6.4 Discussion

This study presents what is believe to be the first report on hue-based real-time quantitative RT-qLAMP reaction. The reaction was specifically targeting *Synechocystis* sp. PCC6803 rbcL RNA, and was sensitive with a detection limit 100 fg/µL. This approach required only a heating element and a simple optical setup to produce highly quantitative gene expression results. Compared with other fluorescence based RNA quantification methods, this approach eliminated the demand of expensive thermocyclers and signal detectors to achieve rapid and low cost quantification by applying computational methods. This quantitative RT-qLAMP approach is also compatible with multiple reaction platforms. In this study, the reactions performed in custom-made microplates and PCR tubes are reported. The reactions can be performed in other commercial optical plates based on specific volume requirements. This novel RT-

qLAMP quantification approach is promising as a tool for gene expression characterization, field research, and rapid medical diagnosis in front line clinics.

7. ON-CHIP COLORIMETRIC RT-LAMP WITH ZIKA VIRAL RNA

7.1 Introduction

The Zika crisis is growing and affecting public health in the Americas. Six years after the first reported Zika outbreak in Yap State in 2007 (Duffy *et al*., 2009), the Zika fever became a larger epidemic in French Polynesia in 2013 (Cao-Lormeau *et al*., 2014). Since then, the Zika fever was actively circulating in the Pacific islands. During 2015-2016, the Zika fever arrived and was spreading rapidly in the Americas (Musso and Gubler, 2016; Musso *et al*., 2014). As of August 31, 2016, it was actively transmitting in more than 50 countries and territories throughout the world (CDC). The ongoing Zika crisis is caused by the Zika virus (ZIKV). ZIKV is a species from the flavivirus genus, and is usually transmitted by mosquitoes (Dick *et al*., 1952). It is an enveloped virus with approximately 10,676 bases single-stranded positive-sense RNA genome (Cunha *et al*., 2016; Sirohi *et al*., 2016). ZIKV has been reported to be highly associated with a neurological disorder called Guillain-Barré syndrome in adults (Oehler *et al*., 2014), and recently confirmed to cause Microcephaly in neonates (Rasmussen *et al*., 2016). So far, as there is no vaccine available for ZIKV, and no medications available for Zika infection treatments, it is crucial to control the spread of ZIKV.

Effective, rapid Zika detection methods are urgently needed, but the development to detect this emerging infectious disease is in its infancy. Various groups have demonstrated the detection of ZIKV from a variety of clinical samples. However, since the clinical presentation of the Zika fever is similar to those of chikungunya and dengue fever, the Zika fever can be misclassified as other diseases, increasing the difficulty for

ZIKV infection diagnosis (Musso *et al*., 2015). Currently, to diagnose ZIKV, there are two main types of methods routinely used in laboratory conditions, RT-PCR based (Faye *et al*., 2008; Gourinat *et al*., 2015; Calvet *et al*., 2016) molecular tests and ELISA based (Lanciotti *et al*., 2008) serological tests. The FDA has published a list of Zika diagnostic kits under Emergency Use Authorizations (e.g. LightMix® Zika rRT-PCR Test from Roche). Even though these technologies identified a large amount of Zika cases, false positives and cross-reactions with other flaviviruses (e.g. DENV) occur frequently (Musso and Gubler, 2016; Shan *et al*., 2016). In addition, RT-PCR based detection methods require multiple thermal cycling stages, forming a bottleneck to assess the pandemic situation.

In addition to diagnosis, there is also a need for a quantitative tool to measure the viral burden of ZIKV. Not only qualitative detection at the end point, but also quantitative measurement of ZIKV RNA is desired when developing ZIKV diagnosis platforms. For developing vaccines, medications, or treatments for ZIKV infections, researchers can quantitatively measure ZIKV RNA loads to evaluate pathogen reduction efficacy (Epstein and Vostal, 2003). An effective treatment should be able to reduce pathogen load by 6 to 10 log copies/mL in a blood product (Epstein and Vostal, 2003). In addition, for point-of-care usage, the diagnostics technology should be inexpensive and rapid. Pardee *et al.* (Pardee *et al*., 2016) reported the performance of a low cost diagnosis device using a combination of NASBA and the CRISPR/Cas9 technology. This technology is sensitive and robust, but to achieve quantitative measurements, more expensive electrical elements are required. In addition, it takes around 3 hours for

diagnostics. Song *et al.* (Song *et al*., 2016) reported a portable microfluidic cassette for Zika diagnosis in the field using the end point colorimetric RT-LAMP technology. LAMP is a sensitive, selective, and rapid (~ 1 hour) gene amplification method that is performed in isothermal conditions (65 ^{o}C – 70 ^{o}C) (Notomi *et al*., 2000). Adding the colorimetric dyes in the reaction solution gives qualitative measurement of a specific nucleic acid target. The platform was reported (Song *et al*., 2016) with a high sensitivity for ZIKV detection. However, no real-time ZIKV RNA quantification has been achieved using colorimetric RT-LAMP.

A simple platform for ZIKV RNA detection and quantification using a real time colorimetric RT-qLAMP technology is presented. This is believed to be the first real-time quantitative and colorimetric viral RNA detection on a chip-level device. The feasibility of this novel real-time colorimetric RT-qLAMP technology is demonstrated using an inexpensive digital camera and heater. All analyses were performed on a mass-production compatible, stamp-size plastic microwell chip. The combination of inexpensive components, small volume reaction and robust analysis is particularly suited to resource-limited developing countries, where large numbers of ZIKV infections were reported. When mass produced, the cost of running colorimetric RT-qLAMP detections on the microwell chip can be significantly lower than conventional PCR approach. In addition, the device is small and consumes low energy, and allows for rapid analysis. These features enable point-of-care diagnosis/analysis in remote areas. Professionals, or people without specific knowledge, would be able to make their own microwell chip.

7.2 Experiments

RT-LAMP primers were designed to target the ZIKV RNA. There are some conserved regions on the ZIKV genome that are highly diverse among other flaviviruses. These conserved regions include the envelope protein coding region (Faye *et al*., 2008) and NS5 coding sequence (Fulop *et al*., 1993; Maher-Sturgess *et al*., 2008). In order to test the sensitivity, quantification capability, and specificity of the RT-qLAMP reaction, six primers were designed to target the ZIKV envelope protein coding region (position 1279-1497 bp). The primers were optimized and analyzed *in silico* to reduce the formation of secondary structures, including self-dimers and cross-dimers. The targeted sequence of the primers was compared with the genomes of other common flavivirus to ensure that the target sequence shared high homology in ZIKV and low identity in other viruses. The primer sequences are listed in **Table 3**.

Table 3. Primer sequences for Zika virus RT-qLAMP

Primer	Sequence
FIP	5’- CCGGTTGAATGCTCTTCCCGGGCAAAGGGAGCTTGGTGAC -3’
BIP	5’- GCTATCAGTGCATGGCTCCCAGGCGTAACCTCGACTTTCG -3’
LF	5’- AACACGTAAACTTGGCACAT -3’
LB	5’- AGCGGGATGATTGGATATGAA -3’
F3	5’- GGGAAACGGTTGTGGACTT -3’
B3	5’- GCTTCCGCTCTTGGTGAAT -3’

The RT-qLAMP reaction was performed using 300 units/mL Warmstart RTx reverse transcriptase and 800 units/mL Bst 2.0 Warmstart DNA polymerase in 1x ThermolPol DF buffer (New England Biolabs, Ipswich, MA). The reaction solution also contains primer mix (Integrated DNA Technologies, Coralville, Iowa) with concentrations indicated in **Table 1**, 180 μM HNB (Sigma-Aldrich, St. Louis, MO), 6 mM MgSO4, and 800 μM dNTP. A serial 10-fold dilution of viral RNA was added as reaction templates. In negative control, ddH_2O was used to replace the viral RNA.

For proof-of-concept, the performance of the colorimetric quantification method was evaluated using ZIKV genomic RNA (VR-1838DQ™, ATCC, Manassas, VA). This RNA was obtained from the ZIKV strain MR 766. The specificity of the Zika RT-qLAMP primers was tested by the human cell line FLO-1 RNA, dengue virus (DENV) RNA (ATCC® VR-3228SD™, ATCC, Manassas, VA), chikungunya (CHIKV) RNA (ATCC® VR-3246SD™, ATCC, Manassas, VA), and West Nile Virus (WNV) RNA (ATCC® VR-3198SD™, ATCC, Manassas, VA).

Real time colorimetric quantification was performed on an acrylic microwell chip that contains a 5 × 5 array of wells (**Figure 20**). The geometry of each well is a step cylinder: the top 2 mm depth has a diameter of 2.5 mm and the bottom 2 mm has a diameter of 1.3 mm. The microwell chip was rinsed by 0.1% micro90 (Sigma-Aldrich, St. Louis, MO), followed by ddH_2O, to remove potential contaminants.

In this study, acrylic was used for microwell chip fabrication, but other types of plastics, for example, cyclic olefin polymers, polypropylene, polystyrene, could be

suitable for colorimetric LAMP reactions as well. Instead of laser-cutting, the reaction chambers could be produced by other existing plastic forming methods.

The amplification was recorded by obtaining the real-time images of the microwell chip. In a colorimetric RT-qLAMP measurement, the hues of the wells in the image were analzyed to track the color shift. Here, hue is a parameter in HSV (Hue, Saturation, Value) color space that quantifies color. The hue from each pixel was calculated. The average hue in the reaction well area represented the color of a specific reaction.

In conventional real-time PCR, the abundance of templates is described by C_t (cycle threshold), the number of cycles which the fluorescent signal crosses an arbitrary threshold (usually defined as a background signal level). This method is not practical for colorimetric RT-qLAMP measurements because the absolute hue values vary significantly for different reactions. Instead, the historical change of hue was characterized by a four-parameter sigmoid function:

$$h = H_{\max} + \frac{H_{\min} - H_{\max}}{1 + 10^{S(T_t - t)}},$$

where the hue of a reaction h can be represented by a function of time t. H_{max} and H_{min} are two asymptotes. S is a slope factor. T_t stands for the threshold time that hue reached the inflection point. I used T_t to describe the reaction rate.

The RT-qLAMP reaction solution was prepared using the aforementioned protocol. Silicone oil (Fisher Scientific, Pittsburgh, PA) was loaded to the reaction chambers before the reaction solution to prevent the cross contaminations from the loading process. Reaction solutions of 3 µL were loaded into each reaction chamber in

the microwell chip. The chip was placed in a custom-made heater to maintain a constant reaction temperature at 65 ^{o}C for one hour. A webcam (HD Pro Webcam C910, Logitech, Newark, CA) was placed above the chip to monitor the reaction. Color images were captured and recorded every one minute. In this experiment, the color is easily visible and captured by cameras under regular room lighting and white background. The color shift of the reaction was characterized by real-time hue change. The image analysis pipeline introduced in Section 3.2 was followed, the real time raw hue data was fit by a sigmoid function, and the parameter T_t from the function was used to represent the reaction rate.

7.3 Results

End point colorimetric RT-LAMP reaction has been widely used for qualitative virus RNA detection (Ma *et al*., 2010; Zhang *et al*., 2013). The color difference between negative and positive reactions can be easily seen with naked eyes. **Figure 20** shows an overview of the microwell chip with colorimetric RT-qLAMP reactions at the end point. Five groups of reactions were performed simultaneously on the microwell chip. For each group, five replicate experiments can be performed in five isolated reaction chambers. **Figure 20A** is an end point image demonstrating the detection limit of the colorimetric RT-qLAMP reaction. All reactions with template ZIKV RNA concentration higher than 10 copies/μL turned to sky blue at the end of the reaction, while all of the negative controls were purple. Four out of five reactions turned positive in 10 copies/μL group, indicating that the detection limit was close to single copies of target ZIKV RNA. Developing Zika detection methods is a critical step to monitor the transmission of Zika fever. ZIKV can be detected from a variety of clinical samples. For example, the ZIKV

RNA loads can be as high as 2.2 x 10^8 copies/mL in urine (Gourinat *et al*., 2015), 2.1 x 10^6 copies/mL in breast milk (Besnard *et al*., 2014), and 7.3 x 10^5 copies/mL in serum (Lanciotti *et al*., 2008). This suggests that the colorimetric RT-qLAMP technology should be sensitive enough to detect the ZIKV RNA from clinical samples. The specificity of the ZIKV primers was tested (**Figure 20B**). No cross reactivity has been observed between the ZIKV primers and the non-target RNAs. Only the positive control with ZIKV RNA showed sky blue, while the reactions with human cell line RNA, DENV RNA, CHIKV RNA, and WNV RNA remained purple. This results confirmed that the ZIKV primers were specific to Zika viral RNA.

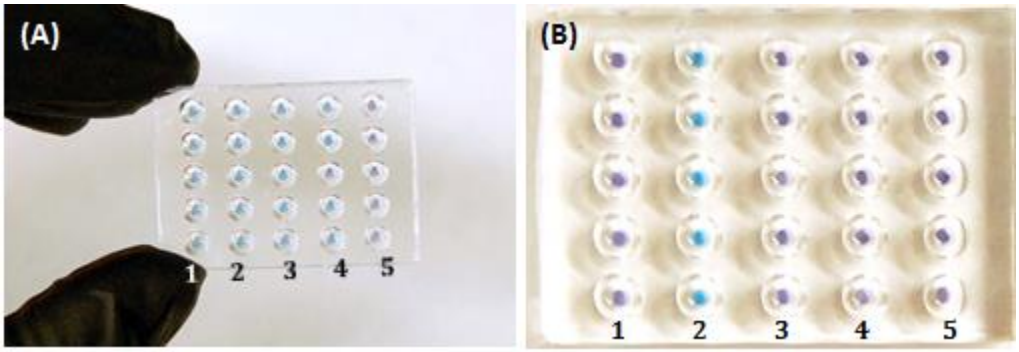

Figure 20. Overview of the chip at the end point

(A) Sensitivity test of the colorimetric RT-qLAMP. Five reaction chambers in one column represent five replicates. (ZIKV RNA template concentration: 1: 10^4 copies/µL, 2: 10^3 copies/µL, 3: 10^2 copies/µL, 4: 10 copies/µL, 5: 0 copies/µL) (B) Primer specificity test with multiple template RNAs (1: human FLO-1 cell line RNA, 2: ZIKV RNA, 3: DENV RNA, 4: CHIKV RNA, 5: WNV RNA)

Real-time quantitation using colorimetric RT-qLAMP was also achieved in this research. **Figure 20A** shows how hue shifts in negative and positive RT-qLAMP

reactions. The data was taken from the same experiment as the one shown in **Figure 20A**. The real time raw hue values were plotted as dots and the values were fitted by the sigmoid function using solid curves. Each color represents a replicate within the same template concentration group. Hue values decreased from around 240 to around 210 in most positive RT-qLAMP reactions (from 10 copies/μL to 10^4 copies/μL), while remained constant at around 240 in negative controls.

The T_t values of positive RT-qLAMP reactions were calculated and plotted in **Figure 21 (F)**. In this experiment, the color shift of all positive reactions was achieved within 40 minutes. There is a strong linear trend between the T_t values and $\log_{10}$RNA concentrations. As RT-qLAMP precedes rapidly, a 10-fold difference in template RNA results in an approximately 3 min ΔT_t in this specific experiment. Even though this ΔT_t is small, the error bars on the standard curve were small also, suggesting that there was not much variations among the T_t values with the same template RNA concentration. Using this standard curve, one can easily tell the template RNA concentration in a reaction based on a T_t value. This result indicates that real-time colorimetric RT- qLAMP can be a promising candidate for characterizing the viral RNA loads in routine practice.

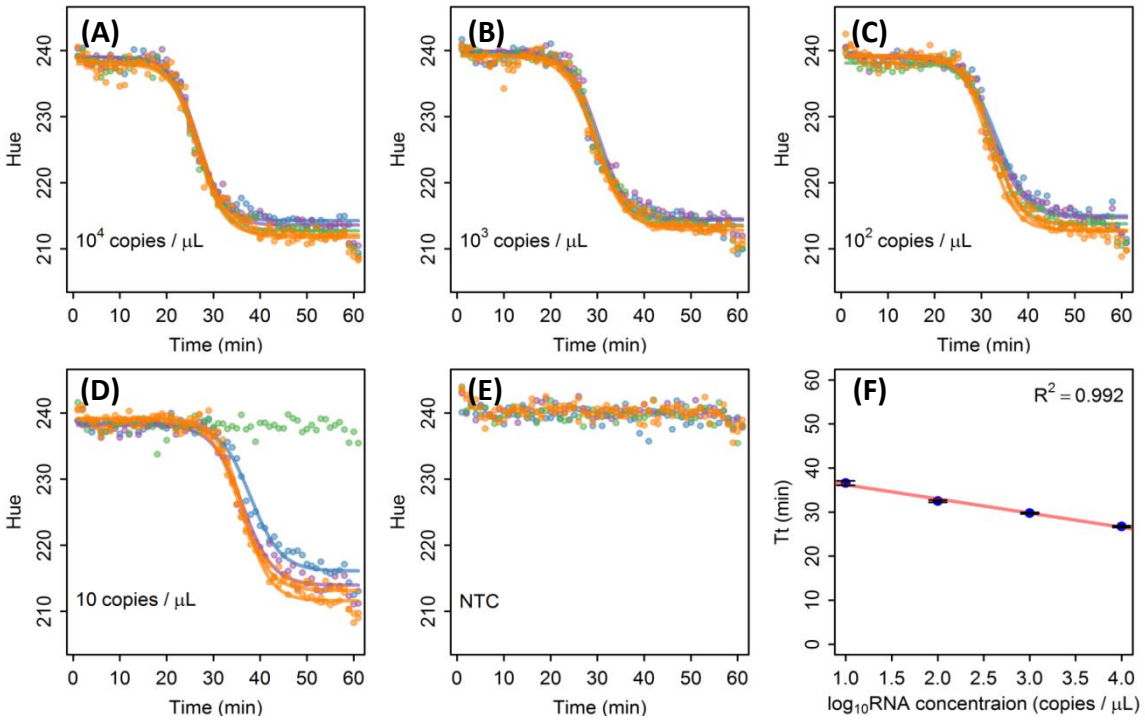

Figure 21. Amplification curves (A-E) and standard curve (F) of real-time colorimetric RT-qLAMP with ZIKV RNA

7.4 Discussion

This reported colorimetric detection approach was rapid, and can be completed within 40 minutes. The results suggest that this technology can specifically identify ZIKV RNA with no cross-reactivity with other common viral RNAs. These characteristics suggest the real-time colorimetric ZIKV RNA detection platform is suitable for both rapid point-of-care diagnostics and front-line Zika monitoring. The highly quantitative feature of this technology indicates the platform can be used for rapid viral load tests for vaccine and therapy development purposes. The colorimetric RT-qLAMP chemical reaction is robust to multiple materials of the reaction vessels. The protocol is portable to different labware

formats, from tubes, microplates, and microwell chips (as presented in this work) to future microfluidic cassettes.

Currently available Zika detection technologies must be performed in a laboratory setting and require a long detection time. They are limited for field operations in resource-limited areas. In the real-time colorimetric ZIKV RNA quantification technology presented here, the amplification can be monitored by a ubiquitous color camera or webcam. In one scenario, health workers can perform the RT-qLAMP on a heating plate or in an oven at 65 ^{o}C and monitor the color changes using a cell phone. The results can be analyzed on the phone or on a cloud server. This approach does not require new technology or infrastructure, but allows rapid outbreak assessment from personal to societal levels.

8. MICROBIOTA ANALYSIS OF THE BIOSPHERE 2 OCEAN

8.1 Introduction

Biosphere 2 is a 3.14-acre ecological system located in Oracle, Arizona. It was built by Apace Biosphere Ventures from 1987 (Allen and Nelson, 1999), and was taken over by Columbia University on January 1, 1996. Since July 2011, Biosphere 2 was operated by the University of Arizona as a teaching, outreach, and research facility. The facility includes an ocean, a mangrove estuary (Finn, 1996), a tropical rainforest (Leigh *et al*., 1999), a savannah grassland, and a desert. The ocean in Biosphere 2 is a 2650 m^3 saltwater tank with algae, microbes, animals, and coral reef (Atkinson *et al*., 1999). There are water pumps to circulate water, aerators to simulate ocean waves, and filtration systems to maintain the water quality. The water chemistry is constantly monitored and stabilized (Atkinson *et al*., 1999).

Due to its proximity to ASU and complementarily simulated environment, Biosphere 2 Ocean habitat is an excellent place for us to validate ocean-observing technologies. In the future, after packaging the molecular detection device with hardware subsystems, the prototype of the genomic sensor will be placed in the Biosphere 2 Ocean for performance characterization. One reason is that compared with real oceans, the Biosphere 2 Ocean is a well-controlled ecosystem (Allen and Nelson, 1999). Additionally, since the Biosphere 2 Ocean is designed to simulate real oceans, its microbial communities have a high degree of complexity (Atkinson *et al*., 1999). Investigating the microbial community structures in the Biosphere 2 Ocean is a critical step towards *in situ* genomic sensor development.

8.2 Experiments

8.2.1 Sampling and sample processing

Samples of the Biosphere 2 Ocean were collected once a month (from September, 2015 to August, 2016) from the location labelled in **Figure 22**. Three liters of Biosphere 2 seawater were collected from the surface, and filtered using EMD Millipore Stericup™ Sterile Vacuum Filter Units (Fisher Scientific, Asheville, NC) with pore size 0.22 μM. This process took approximately 10 mins, after which the filter membranes with biomass were temporarily stored on dry ice, while the filtrate was discarded. After shipping the samples back to the laboratory, the filter membranes with the samples were removed from the filter unit, transferred to sterilized Petri dishes, and stored in -80 ^{o}C freezers.

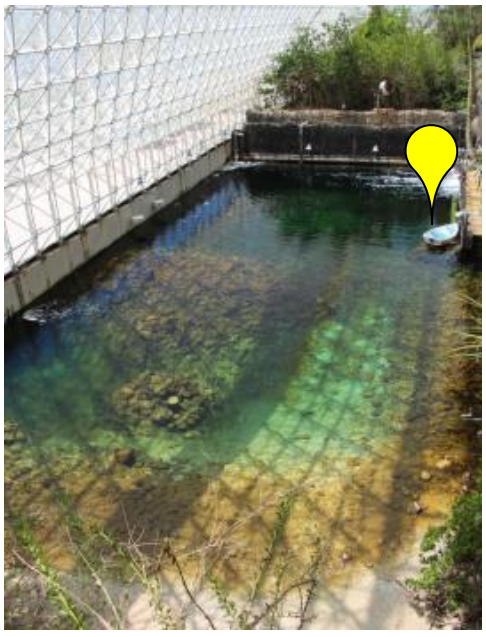

Figure 22. Sampling site (yellow marker) in the Biosphere 2 Ocean

During sample processing, the filter membranes were cut into pieces and the genomic DNA was purified from the biomass. To reduce the bias that could be introduced in the DNA extraction stage, the performance of multiple DNA purification

kits with different cell lysis methods was compared. Three DNA extraction kits were evaluated: the Zymo Quick-gDNA kit, the ZR Fungal/Bacterial DNA kit, and the ZR Soil Microbe DNA kit (Zymo Research, Irvine, CA). A best kit was selected for sample preparations based on the species richness and phylogenetic diversity it provides. Three replicates from the same samples were prepared and the DNA replicates were pooled to reduce the potential bias generated by the individual DNA purification process (Pinto and Raskin, 2012). To ensure the 16S sequencing quality, the purified genomic DNA was quantified by a Nanodrop spectrophotometer (Thermo Scientific, Wilmington, DE).

8.2.2 16S rDNA sequencing

The bacterial community from the Biosphere 2 Ocean was analyzed on the MiSeq platform from Illumina. 16S rDNA sequencing was performed at the Microbiome Analysis Laboratory (http://krajmalnik.environmentalbiotechnology.org/microbiome-lab.html) at Arizona State University (Tempe, AZ). In this project, the V4 region of the 16S rDNA was amplified and sequenced. The amplification was performed using the barcoded primer set 515f/806r designed by Caporaso *et al*. (Caporaso *et al*., 2012), and the library was prepared following the protocol from the Earth Microbiome Project (EMP) (http://www.earthmicrobiome.org/emp-standard-protocols/). For each sample, the PCR amplification was performed in triplicate, then pooled and quantified using Quant-iT™ PicoGreen® dsDNA Assay Kit (Invitrogen, Grand Island, NY). DNA of 240 ng per sample were pooled and then cleaned using QIA quick PCR purification kit (QIAGEN, Valencia, CA). The PCR pool was quantified by the Illumina library Quantification Kit ABI Prism® (Kapa Biosystems, Wilmington, MA). The DNA pool was determined and

diluted to a final concentration of 4 nM then denatured and diluted to a final concentration of 4 pM with a 30% of PhiX. Finally, the DNA library was loaded in the MiSeq Illumina sequencer using the chemistry version 2 (2 × 150 paired-end) and following the manufacturer's protocol.

8.2.3 Data analysis

The 16S rDNA sequence reads were merged to assemble paired-end reads. The reads were clustered to generate operational taxonomic units (OTUs) using the Cluster Database at High Identity with Tolerance (CD-HIT) clustering method (Li and Godzik, 2006). In each OTU, the sequence identity was defined higher than 97%. Representative sequences were selected from each OTU, while other redundant sequences were removed to reduce the computational efforts. All the representative sequences were aligned with the Python Nearest Alignment Space Termination tool (PyNAST) (Caporaso et al., 2010). RDP classifier (Wang et al., 2007) with confidence threshold 80% was used to assign taxonomy information to the representative sequences.

According to the endosymbiosis theory, eukaryotes took up alpha-proteobacteria, which became the organelle called mitochondria in eukaryotes (Giezen, 2011). Similarly, the chloroplasts in eukaryotes were bacteria origin as well (Giezen, 2011). Neither chloroplast nor mitochondria was functional in bacteria. Moreover, the primers in the 16S sequencing should target bacteria, instead of archaea and eukaryotes. In addition, even though the chloroplast in the datasets could partly reflect the dynamic of some photosynthesis algae, the information it conveyed was incomplete, and could not

represent the whole photosynthesis community. Therefore, a quality control step was performed to remove the archaea, chloroplast, and mitochondria from the datasets.

With taxonomy information assigned to the representative bacterial sequences, a phylogenetic tree was built to visualize the evolutionary relationships among the bacterial community. The phylogenetic tree was constructed by the FastTree method (Price et al., 2009). As the sequence read numbers varied among samples, the reads were subsampled and normalized, so that the samples can be compared directly. The minimum count of the 12 samples was calculated and used as a subsampling depth. Species richness, Shannon Index, Simpson's Diversity, and phylogenetic diversity were calculated for each normalized samples. The bacterial community composition was summarized at multiple taxonomic levels.

8.2.4 Comparison between the Biosphere 2 Ocean and real oceans

After analyzing the bacterial community composition within one year's period, the structure of the Biosphere 2 Ocean community was compared with the communities from real oceans. In this part of the project, time series marine microbiome sequencing data from public databases have been incorporated and analyzed. The first database was from the Hawaii Ocean Time-series (HOT) station ALOHA. Scientists from HOT program conducted cruises approximately once each month to ALOHA, and performed 16S sequencing to investigate the bacteria information from the Pacific Ocean's surface ($22^{o}45$'N 158^{o}W) (DeLong, 2006). The sequencing reads from Feb 1, 2013 to May 5, 2013 were downloaded for this project. The second database contained the sampling results from the TARA Ocean project. From 2009 to 2012, 243 samples from 68

locations were collected from the global ocean (Sunagawa et al., 2015). Among them, 17 samples were selected for this project. In sum, the 16S rRNA gene sequencing data of the microbial communities used in this study was collected from the North Pacific Ocean (source: ALOHA station ALOHA130201–ALOHA130503, TARA Ocean NPO137–140), South Pacific Ocean (source: TARA Ocean SPO94–98), Atlantic Ocean (source: TARA Ocean NAO145–148, SAO68–72), Indian Ocean (source: TARA Ocean IO56–62), and the Southern Ocean (source: TARA Ocean SO84–85). The same data processing procedure was carried out as described in the previous sections. The sequencing reads were subsampled to reach the same number of OTUs as the Biosphere 2 Ocean dataset.

8.3 Results

8.3.1 Performance of three DNA purification kits

In this part of project, the aim was to evaluate the performance of commercially available DNA extraction kits. The biomass collected in September 2015 was selected to assess the extraction methods and the chloroplast and mitochondria related sequencing reads were intentionally not removed. To directly compare different DNA purification methods, subsampling was performed on the sequencing data with a subsampling depth of 21667. Both the ZR Fungal/Bacterial DNA kit and the ZR Soil Microbe DNA kit (**Figure 23**) generated a high percentage of gram-positive bacteria (and bacteria with multilayer cell wall structures) DNA. The ZR Soil Microbe DNA kit was considered to have the best performance regarding the species richness and phylogenetic diversity. Using the ZR Soil Microbe DNA kit, 2669 taxa were observed among 21667 total reads, and the phylogenetic diversity was 132.9 (**Table 4**), while the ZR Fungal/Bacterial DNA kit and

ZR gDNA kit yielded a significantly reduced amount of taxa. **Figure 23** shows that the ZR Soil Microbe DNA kit had a high yield of gram-positive bacteria. For example, the ZR Soil Microbe DNA kit yields 4.7% of Actinobacteria, a phylum of gram-positive bacteria, while the ZR Fungal/Bacterial DNA kit and ZR gDNA kit generated 1.5% and 0.1% Actinobacteria, respectively. In terms of the sequencing results, the ZR Soil Microbe kit was selected for subsequent DNA sample preparations.

Table 4. DNA extraction efficiency comparison

	gDNA	**Fungal Bacterial**	**Soil Microbe**
Cell lysis method	Lysis buffer	Lysis buffer Bead beating	Lysis buffer Bead beating
Inhibitor removal	No	No	Yes
Species richness	1624	2026	2669
Phylogenetic diversity	78.2	104.2	132.9

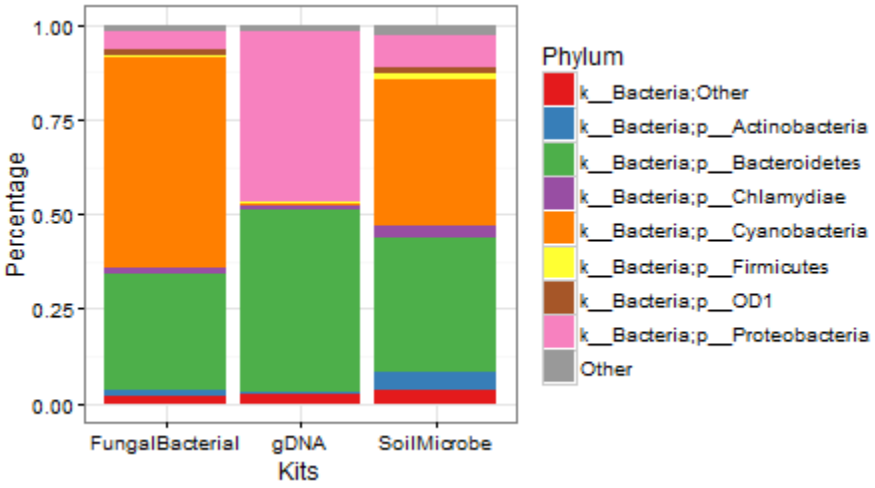

Figure 23. Comparison of three genomic DNA purification kits

8.3.2 Bacterial community composition

Among 35,434 OTUs, a total of 55 distinct bacterial phyla were found in the Biosphere 2 Ocean, suggesting that the bacterial communities in the Biosphere 2 Ocean were highly diverse. However, the community was dominated by a few taxa. Four phyla accounts for an average of 93% of the bacterial community (**Figure 24**): Bacteroidetes (48%), Proteobacteria (38%), Cyanobacteria (5%), and Actinobacteria (2%). In **Figures 24**, **25**, **26**, and **27**, identified taxa that exceeded 0.1% of the total community were plotted. Taxa that have a percentage less than 0.1% in all of the samples or not identified were classified as "Other" in the plots. The seasons were grouped as winter (January – March), spring (April – June), summer (July - September), fall (October - December).

In the surface water of the Biosphere 2 Ocean, the two most abundant phyla were Bacteroidetes and Proteobacteria. During winter and early spring (January to April), the dominant phylum in the Biosphere 2 Ocean was Proteobacteria, while during the remaining months of the year, the phylum with highest abundance was Bacteroidetes. The relative abundance of Bacteroidetes exhibited a seasonal pattern. The percentages of Bacteroidetes during fall (October, November, and December) and spring (April, May, and Jun) are significantly higher than other seasons ($p < 0.05$, *t* test). In contrast, Proteobacteria showed an opposite trend. The percentages during fall (October, November, and December) and spring (April, May, and Jun) are significantly lower than winter and summer ($p < 0.05$, *t* test).

In the Biosphere 2 Ocean, there were 132 distinct classes identified. In Bacteroidetes, the dominant class was Flavobacteriia. The percentage of the class

Flavobacteriia reached a peak value (66%) in October. A minimum percentage (31%) of Flavobacteriia showed up in April. Two dominant classes were found in Proteobacteria: Alphaproteobacteria and Gammaproteobacteria. Alphaproteobacteria reached a peak in July, accounting for 24% of the analyzed OTUs. The number dropped to 7% in August and September. The peak (39%) of Gammaproteobacteria showed up in March, while the lowest relative abundance (6%) of Gammaproteobacteria appeared in June. It is interesting to note that the abundance of the class Rhodothermi from Bacteroidetes experienced an obvious increase during May (5%), June (1%), and July (4%), whereas in the remaining time its abundance was less than 0.2%. In phylum Cyanobacteria, the most abundant class was Oscillatoriophycideae. It peaked during December (25%) and April (25%).

There were 194 orders and 260 families identified, respectively. Flavobacteriales had the highest relative abundance, and accounted for more than 31% of the bacterial community. It was the dominant order in Bacteroidetes in the Biosphere 2 Ocean. Flavobacteriales showed a high percentage during October (66%), November (61%), and December (60%). Rhodobacterales was the dominant order in Alphaproteobacteria. Its percentage fluctuated around 11%, with a maximum 22% in July and minimum 3% in September. The dominant order in Gammaproteobacteria was not identified. In the Biosphere 2 Ocean, Cryomorphaceae played a key role in maintaining the composition of the bacterial community. It was the most abundant family in the samples. Cryomorphaceae was a member of Flavobacteriales. It accounted for 60% of the taxa in

October. Even in April, when it presented a smallest proportion, it still constituted 22% of the taxa.

Three more samples were collected during October, November, and December 2016 to compare the bacterial community structure between 2015 and 2016. The average of the proportion from the three samples was calculated and compared with the three months' average in 2015 (Oct, Nov, and Dec). Bacteroidetes experienced a 27.7% decrease in 2016. Flavobacteriia was the major player that resulted in the shrinkage of the Bacteroidetes community. Compared with 2015, Flavobacteriia decreased 28.6% during the fall. The percentage of Proteobacteria decreased by 20.7%, most of which was contributed by Gammaproteobacteria (increased by 18.7%). Actinobacteria increased by 5.4%. The percentage of other phyla remained stable. The dominant phyla remain the same within two years. Even though certain fluctuations have been found in the Biosphere 2 Ocean bacterial communities, no significant change of major taxa was observed at class, order, and family levels.

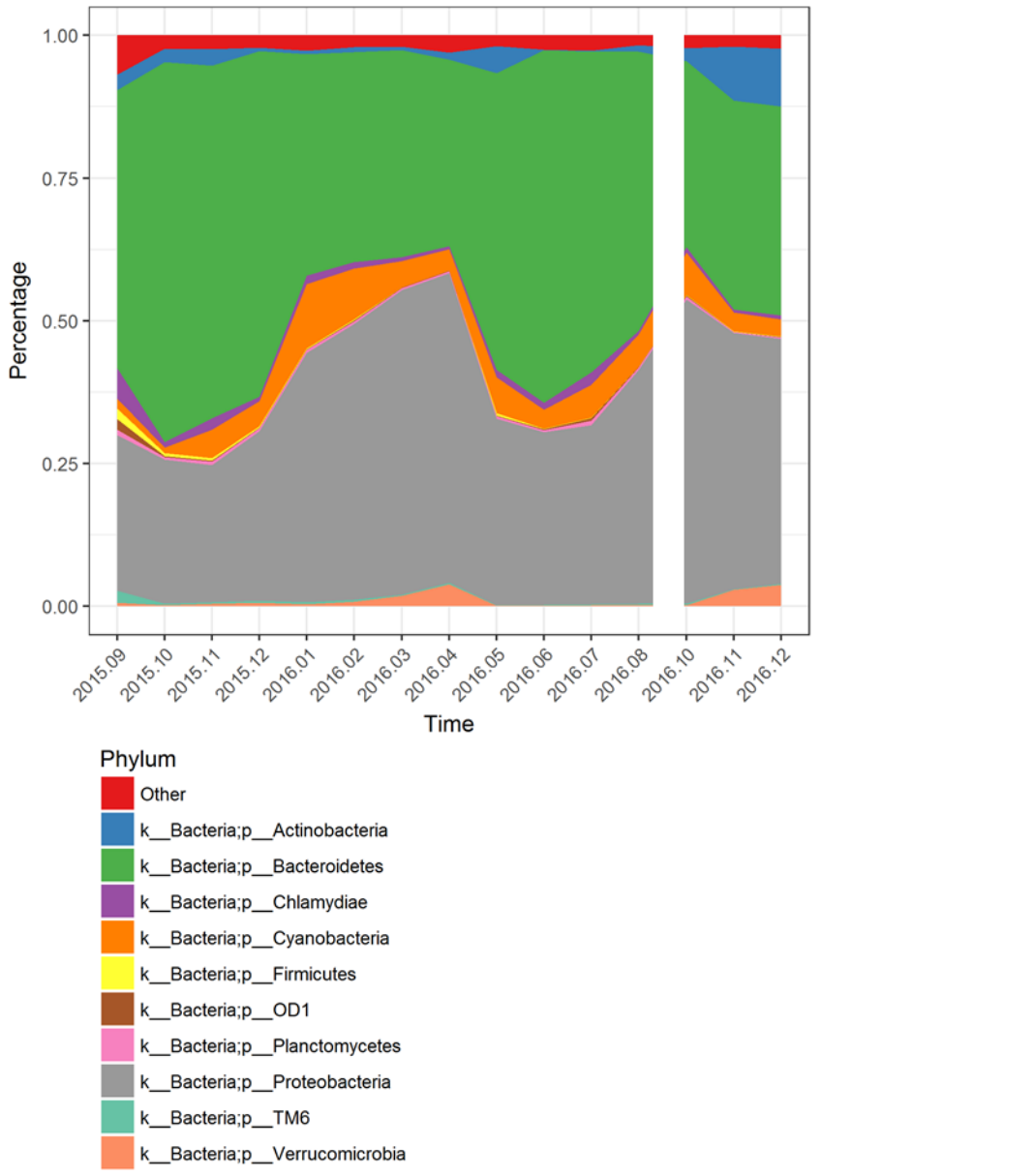

Figure 24. Phylum-level taxonomy of bacterial community in the Biosphere 2 Ocean.

("k__": kingdom, "p__": phylum)

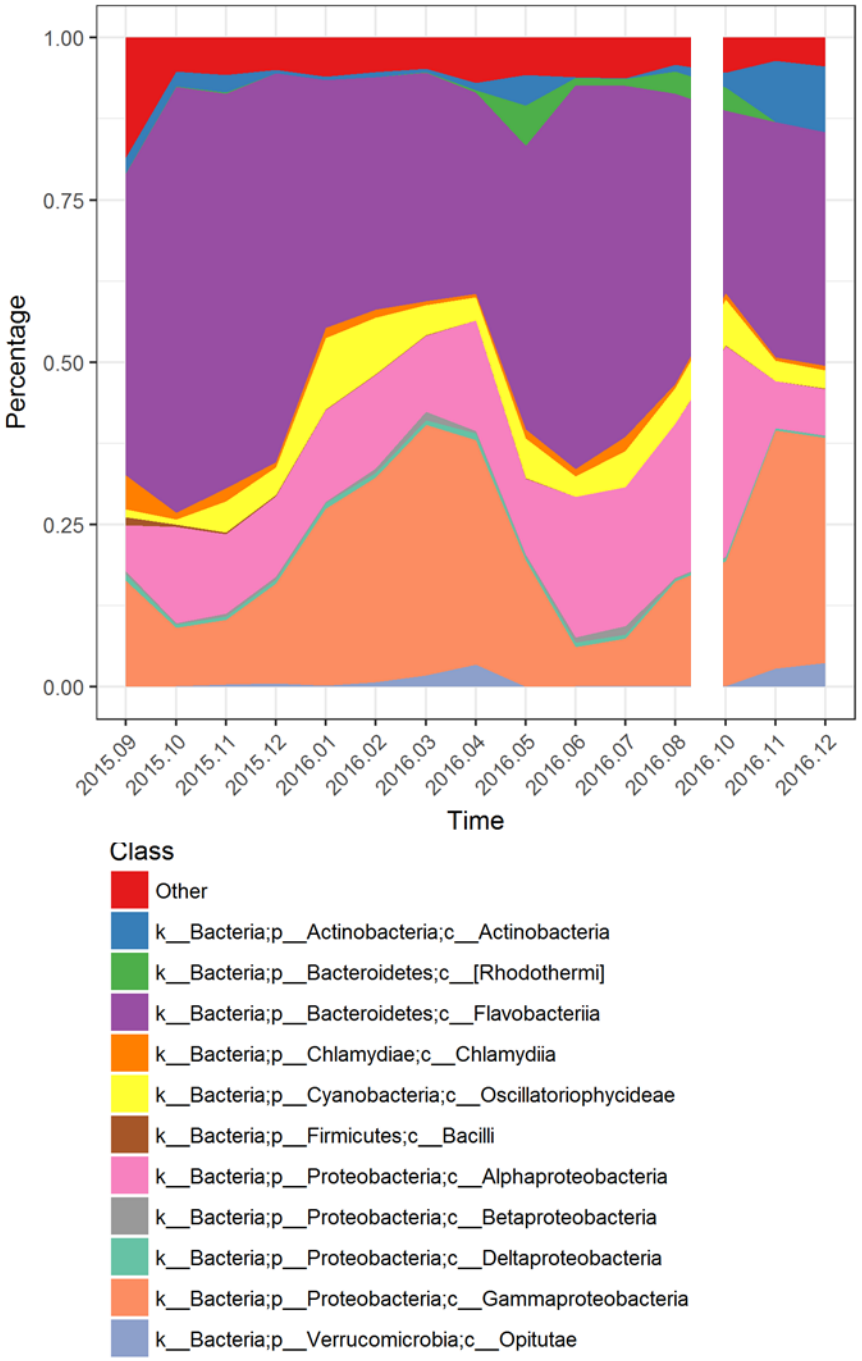

Figure 25. Class-level taxonomy of bacterial community in the Biosphere 2 Ocean.

("k__": kingdom, "p__": phylum, "c__": class)

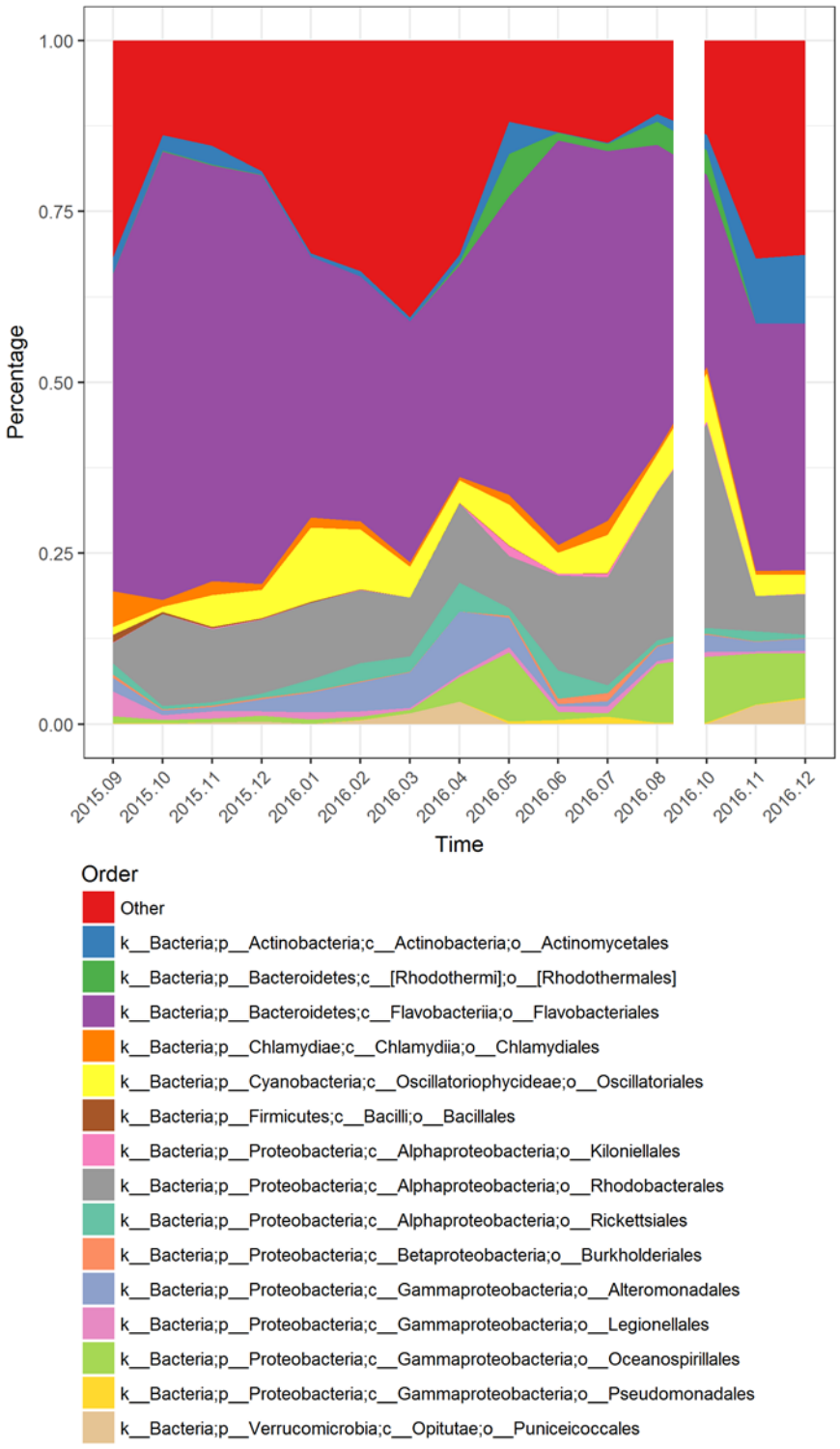

Figure 26. Order-level taxonomy of bacterial community in the Biosphere 2 Ocean.

("k__": kingdom, "p__": phylum, "c__": class, "o__": order)

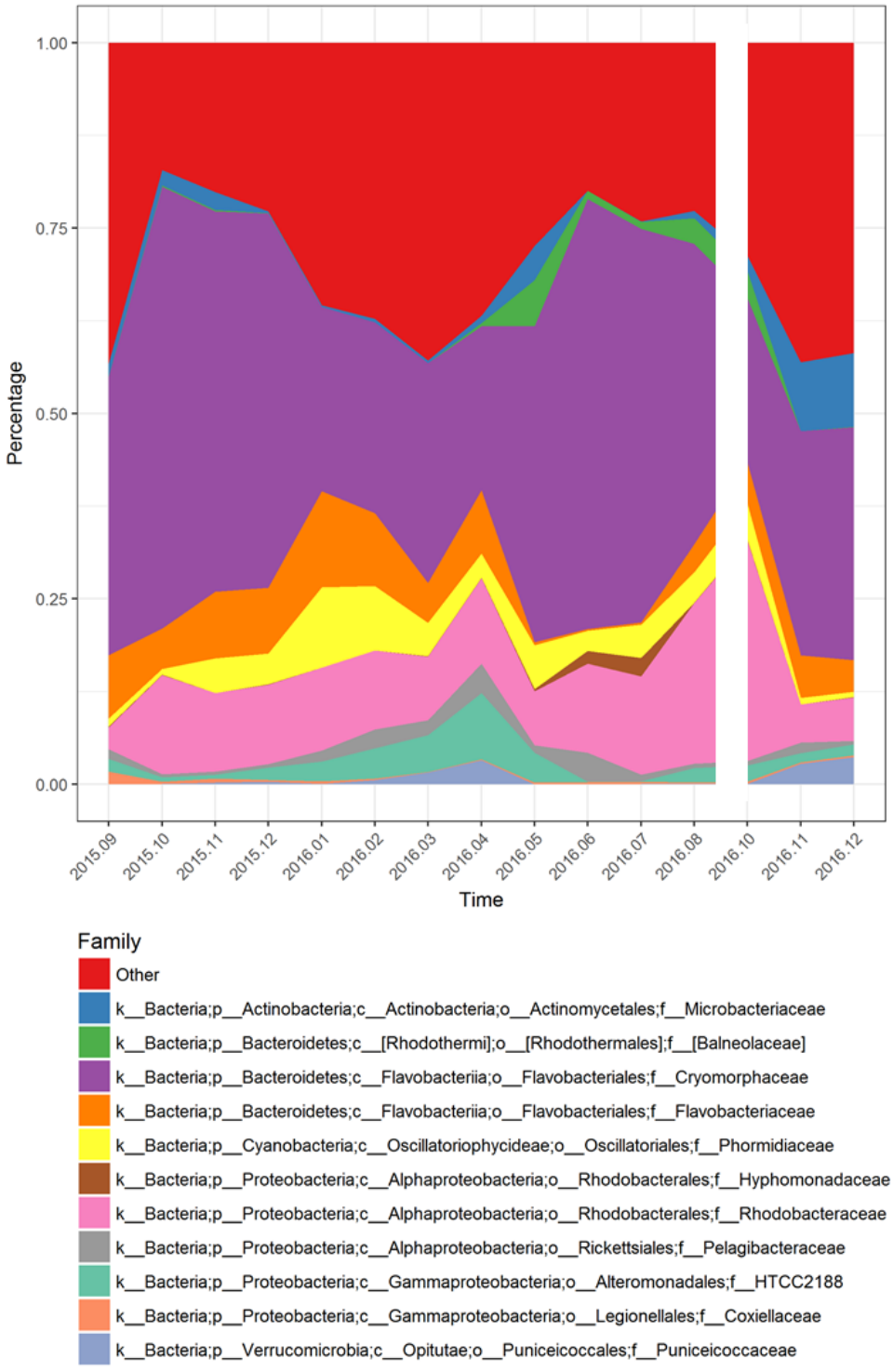

Figure 27. Family-level taxonomy of bacterial community in the Biosphere 2 Ocean.

("k__": kingdom, "p__": phylum, "c__": class, "o__": order, "f__": family)

8.3.3 Bacterial community diversity and seasonality

The species richness has been characterized. The sequencing reads have been re-sampled with a subsampling depth 35,434 sequences. The observed numbers of taxa in the normalized samples were randomly distributed around the mean species richness (**Figure 28A**) 3570, and the phylogenetic diversity (**Figure 28B**) around 190. There were no obvious patterns regarding the species richness and phylogenetic diversity throughout the year. One-way analysis of variance suggested that the species richness did not exhibit significant difference ($p = 0.8986$, F test) during four seasons, neither did phylogenetic diversity ($p = 0.9618$, F test). Different from previous reports showing that the bacterial diversity reached a highest value in winter at a temperate coast (Gilbert et al., 2010), or peaked at summer in a drinking water treatment plant (Pinto et al., 2014), no strong patterns of species richness between different seasons were observed in the Biosphere 2 Ocean. This is reasonable because the Biosphere 2 Ocean is a better-controlled environment. The temperature, salinity, and pH in this ocean have been real-time regulated.

The relative abundance of the populations has been evaluated by calculating two diversity indices (Shannon index and Simpson's diversity index). The Shannon index indicated the diversity of the bacterial community, which was determined by the species richness and evenness. A population with high equitability and more species tends to exhibit high Shannon index. The Simpson's diversity index suggested dominancy of the common species. Similarly, a high Simpson's diversity index showed a high species diversity in a population. In both **Figure 28C** and **28D**, the diversity and evenness of the

bacterial community in the Biosphere 2 Ocean showed similar patterns. Statistical results confirmed that the bacterial community compositions were not significantly different (Shannon index: $p = 0.4883$, F test; Simpson's diversity index: $p = 0.0611$, F test; $\alpha = 0.05$) among four seasons. These results indicate that the bacterial community in the Biosphere 2 Ocean is stable. The community composition and diversity remained constant during four seasons.

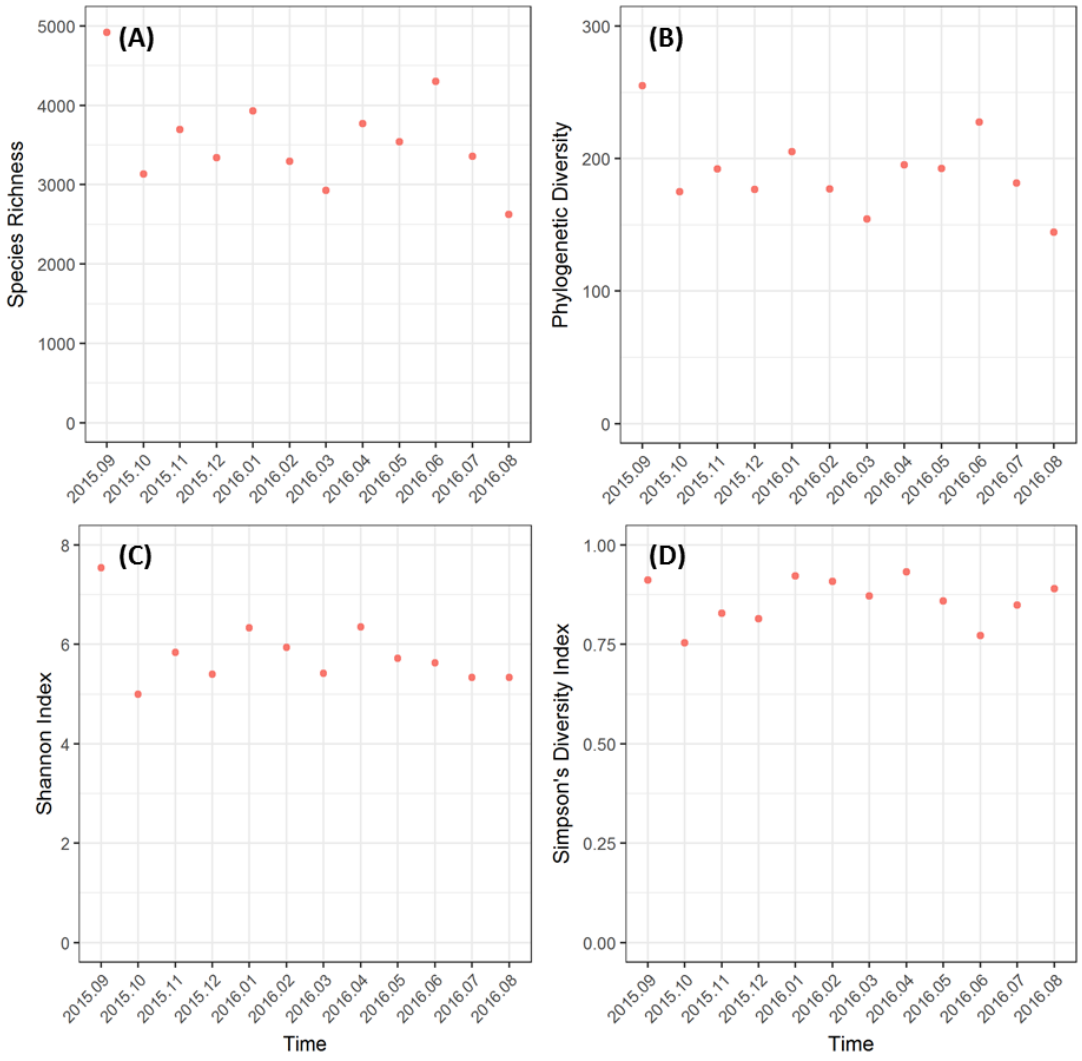

Figure 28. Alpha diversity trends in the Biosphere 2 Ocean bacterial community

The sequencing results were rarefied and the number of observed OTUs was plotted versus the number of reads (**Figure 29**). Based on 97% similarity, the figure suggested the rarefaction curves were approaching the maximum plateaus, meaning the majority of the bacterial communities can be represented. Sample 2015.09 appeared to have high abundant OTUs, while sample 2016.08 has the low abundant OTUs.

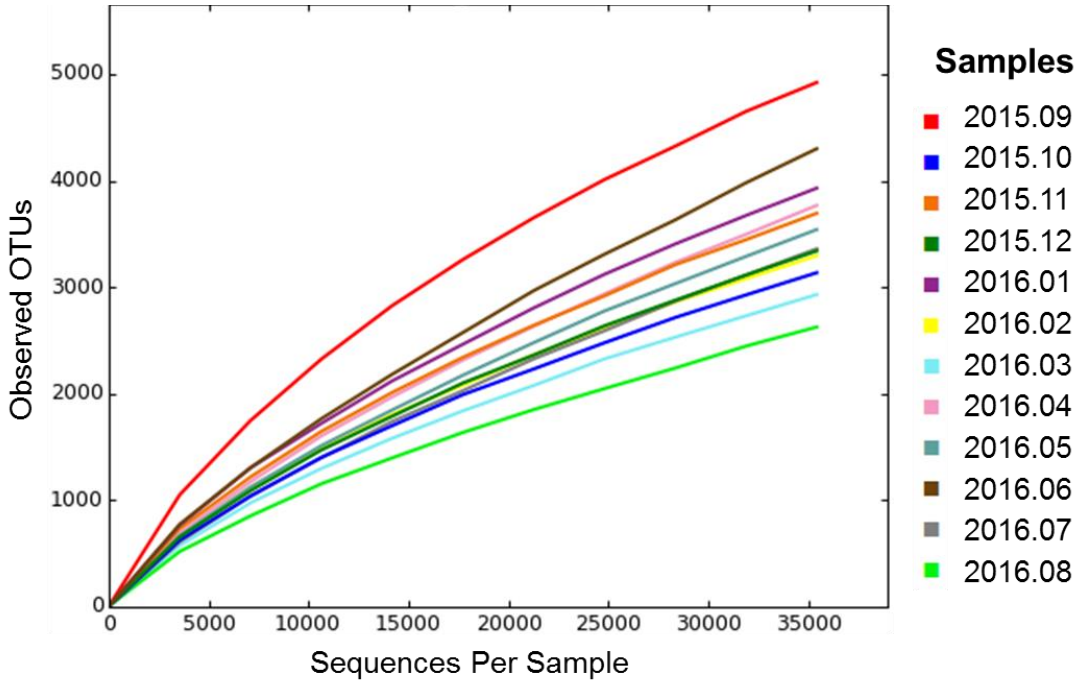

Figure 29. Rarefaction curves of the Biosphere 2 Ocean samples

The evenness of the samples was displayed in **Figure 30**, which showed that the rank-abundance curve from sample 2015.09 lay above the others. The lower slope in sample 2015.09 suggested greater evenness within the community. Except sample 2015.09, the other samples produced approximately similar steepness of rank-abundance curves, indicating the evenness within the community was similar.

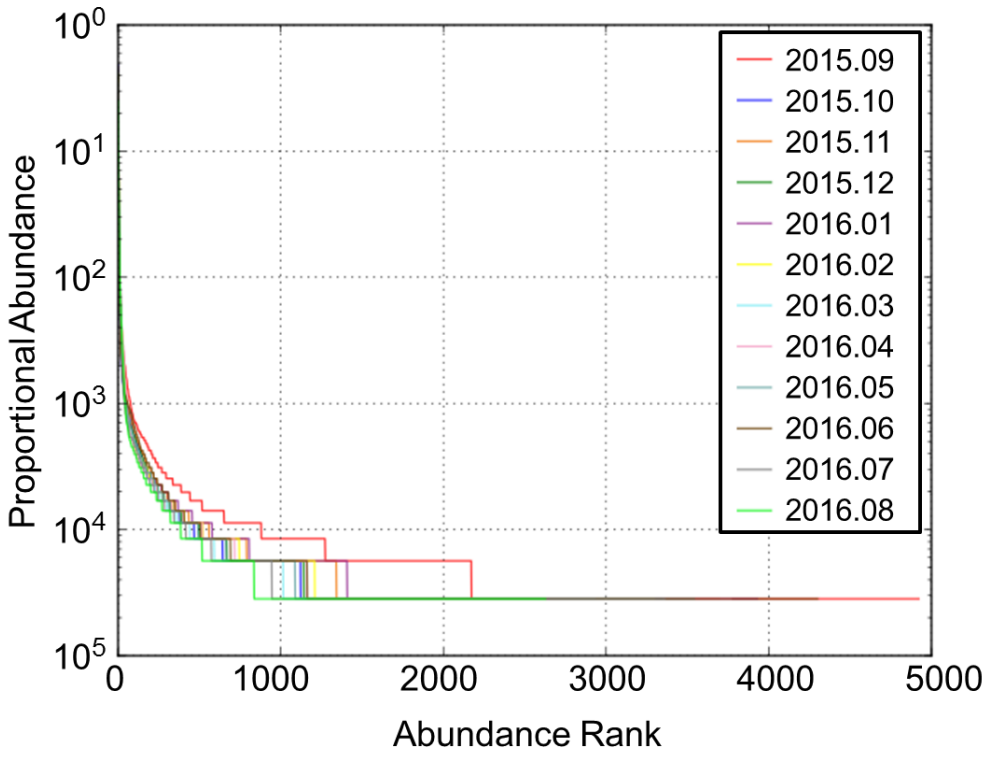

Figure 30. Rank-abundance curves of the Biosphere 2 Ocean samples

8.3.4 Biosphere 2 and real open oceans

In the previous sections, the Biosphere 2 Ocean has been characterized. Its bacterial community seems to be diverse and stable during the investigation period. However, it should not be denied that Biosphere 2 is an artificial environment. Even though the microbial community of this small ocean was collected from the Pacific Ocean, with almost 20 years' cultivation in the desert, its bacterial community structure is likely to have changed significantly. Therefore, the bacterial communities in the Biosphere 2 Ocean were compared with the bacterial communities in real open oceans.

The bacterial community structures in real open oceans were plotted in **Figure 31-34**. **Figure 31, 32** showed the time series observations at the station ALOHA

(22°45'N 158°W) at the North Pacific Ocean. "ALOHA130201" represented by the date (Feb 01, 2013) that the seawater samples were collected. Data collected from the station ALOHA from March to May in 2013 showed that the most abundant phylum was Cyanobacteria (average: 57.7%) during the early spring. Synechococcophycideae (55.9%) was the dominant class in Cyanobacteria. There were sudden increases of Verrrucomicrobia (Feb to Apr average: 1.6%, May average: 23.0%) and Planctomycetes (Feb to Apr average: 3.0%, May average: 21.2%) in May. The second dominant phylum was Proteobacteria (average: 13.0%), while Bacteroidetes only accounted for 2.7% of the bacteria community in spring. The data collected from the TARA Ocean project indicated that the dominant phylum was Proteobacteria (average: 66.3%) in the Pacific Ocean, Atlantic Ocean, Indian Ocean, and the Southern Ocean (**Figure 33, 34**). 70.1% of the Proteobacteria were in the class Alphaproteobacteria, and 27.4% belonged to Gammaproteobacteria. Cyanobacteria accounted for an average of 13.9%. Similar with the structure observed from the station ALOHA, Cyanobacteria were dominated by Synechococcophycideae. Bacteroidetes consisted 8.2% of the community of the open ocean based on the TARA Ocean.

These results from real open oceans showed different patterns compared with the community structures in the Biosphere 2 Ocean. First, the Biosphere 2 Ocean possessed a relatively lower percentage of Cyanobacteria, while a higher percentage of Bacteroidetes. Second, the major player of Cyanobacteria was Oscillatoriophycideae in the Biosphere 2 Ocean, instead of Synechococcophycideae from the open ocean. The reason for the

alternations in the community composition remains to be investigated. It is likely to be the result of the lighting/temperature controlling system in the Biosphere 2 facilities.

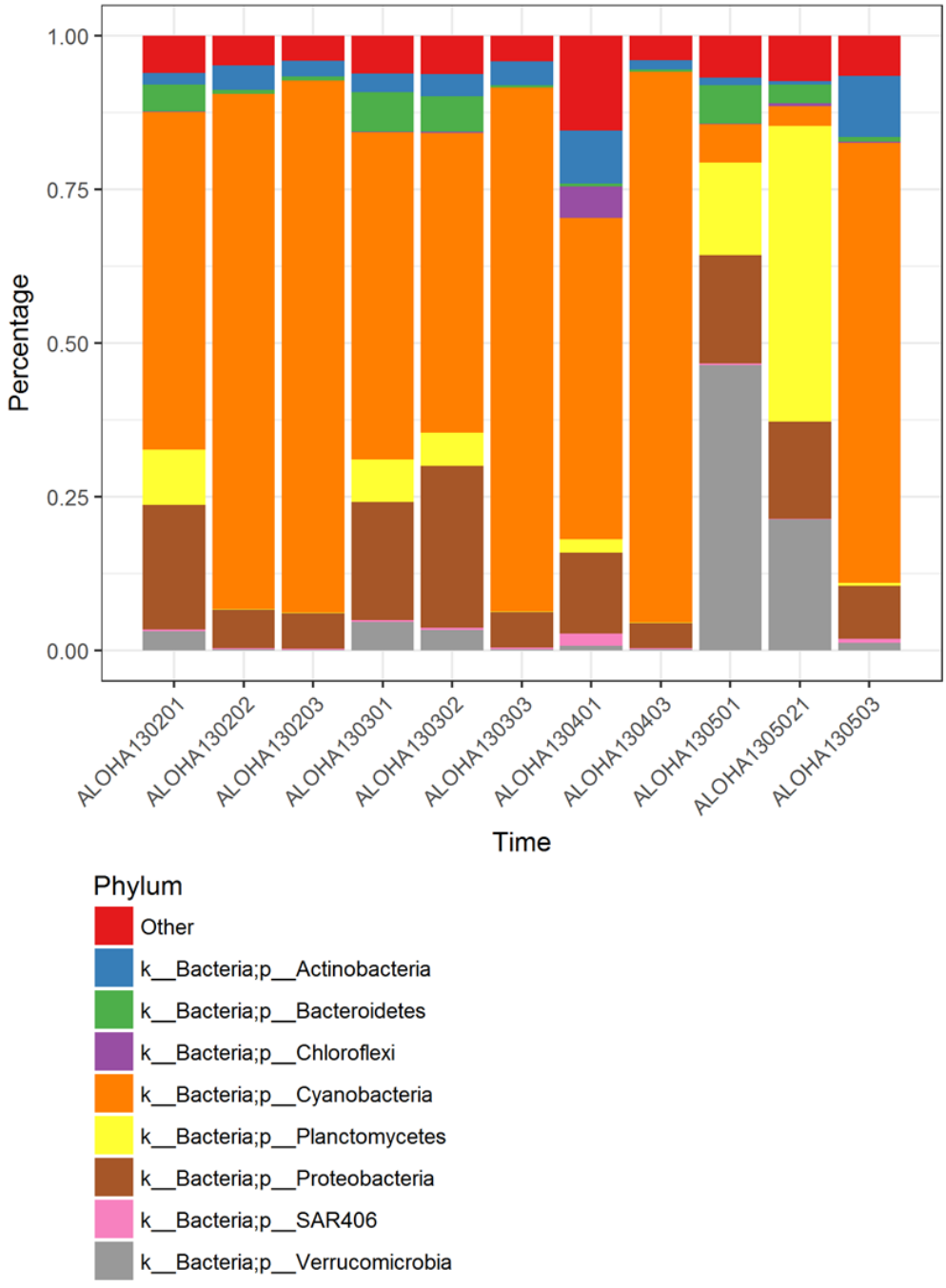

Figure 31. Phylum-level taxonomy of bacterial community from ALOHA station.

("k__": kingdom, "p__": phylum)

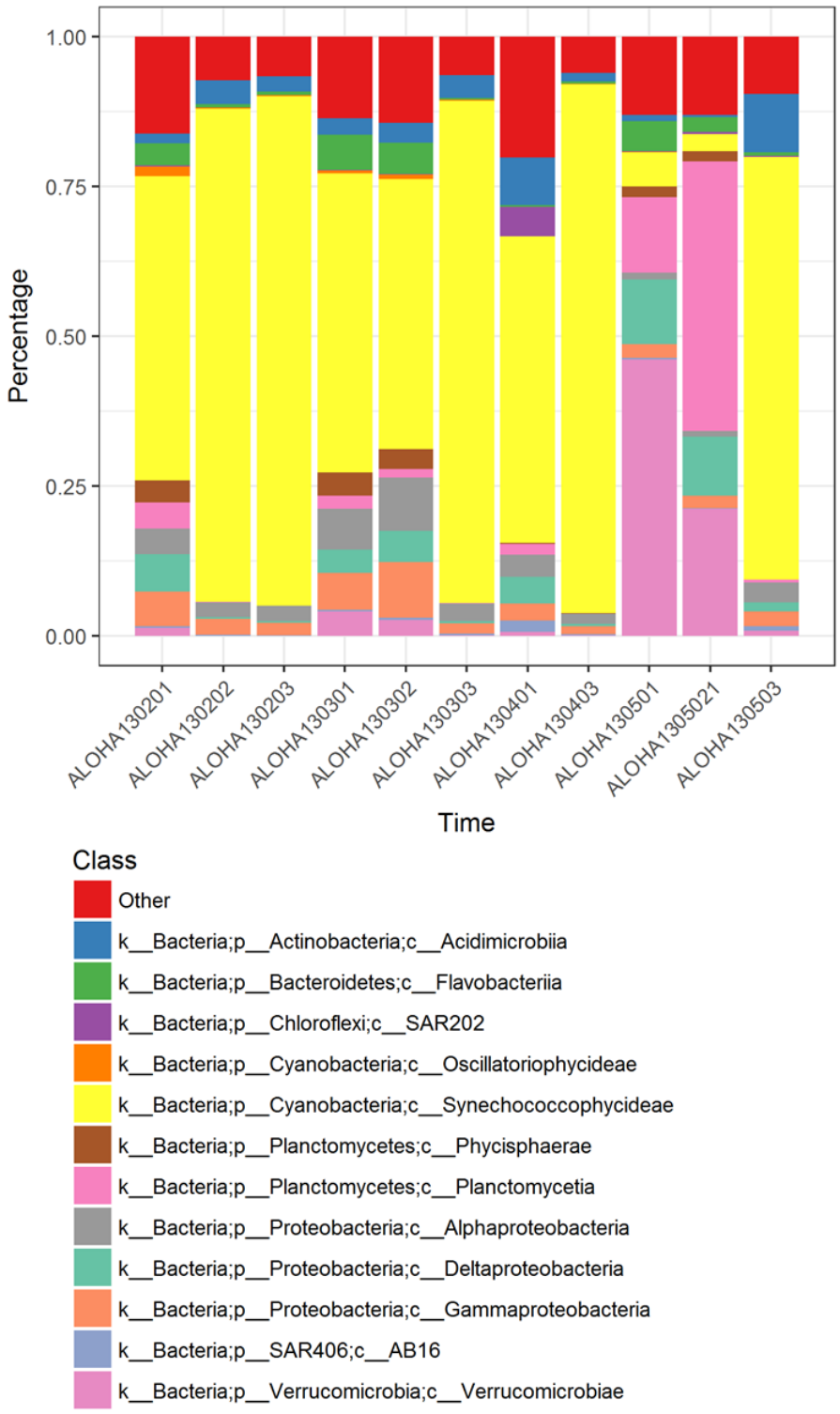

Figure 32. Class-level taxonomy of bacterial community from ALOHA station.

(“k__”: kingdom, “p__”: phylum, “c__”: class)

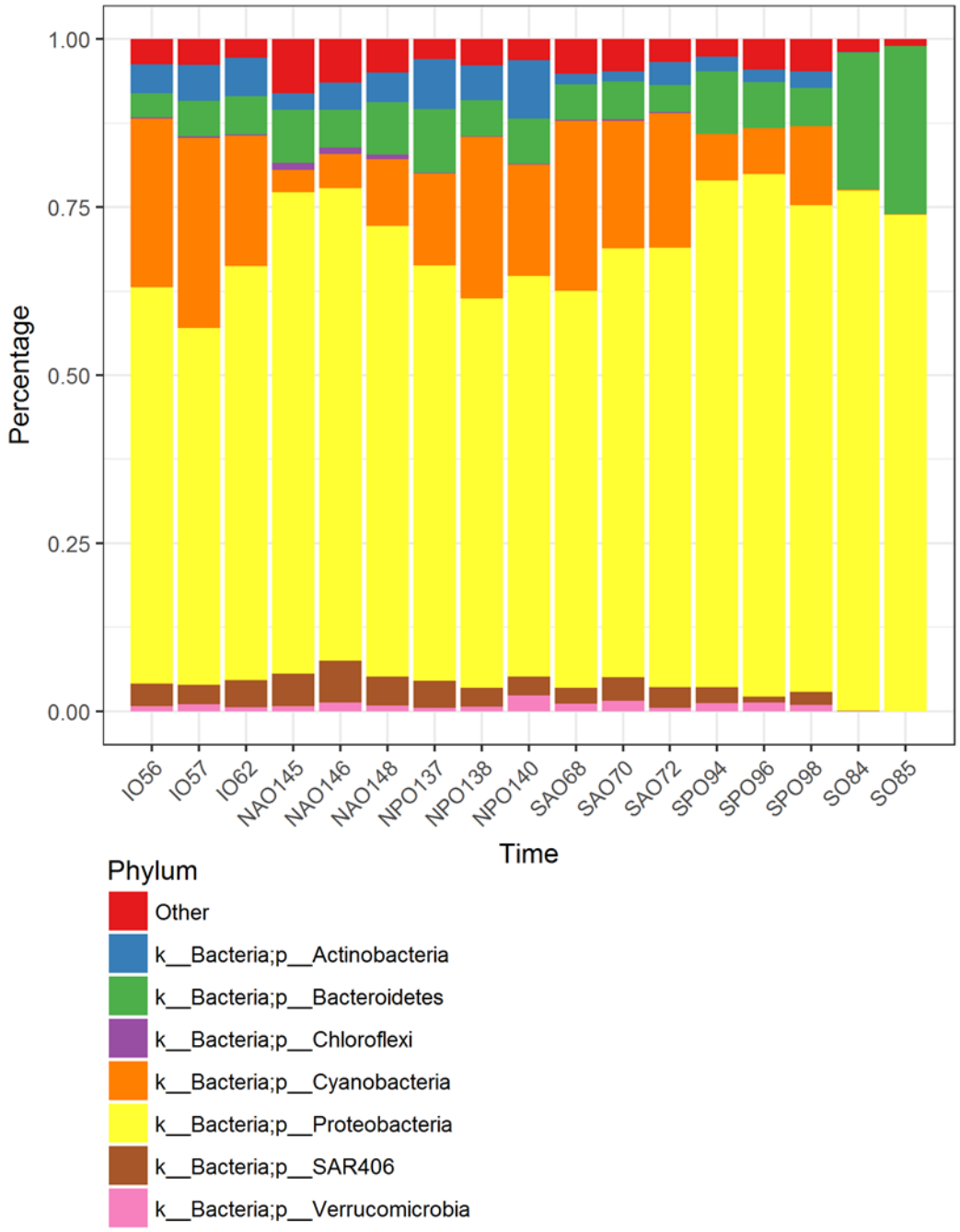

Figure 33. Phylum-level taxonomy of bacterial community from the TARA Ocean.

("k__": kingdom, "p__": phylum)

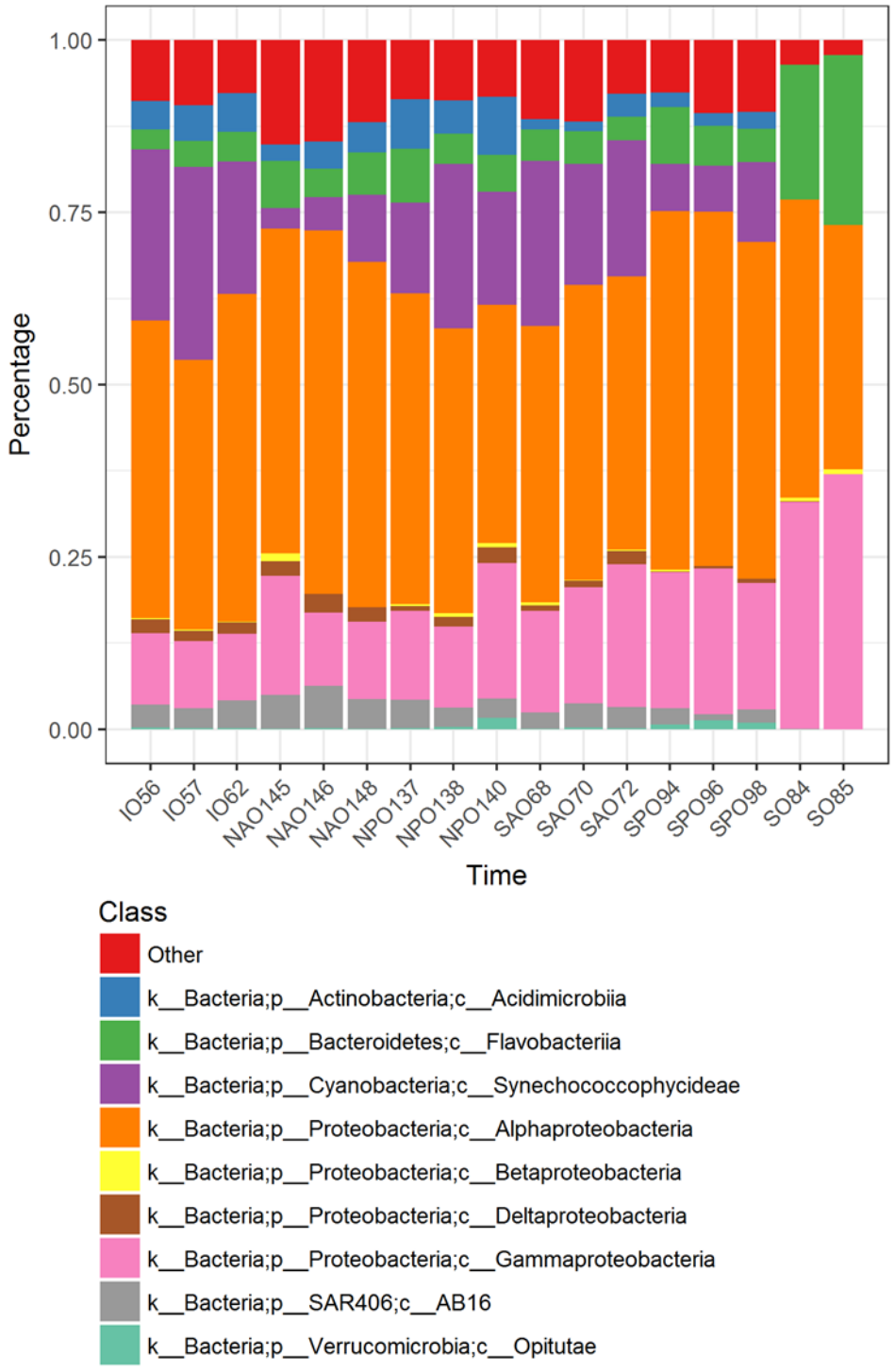

Figure 34. Class-level taxonomy of bacterial community from the TARA Ocean.

("k__": kingdom, "p__": phylum, "c__": class)

In this study, the alpha diversity of the real open ocean has been investigated as well. Shannon index and phylogenetic diversity have been evaluated.

Most of the environmental samples from the real open oceans had a Shannon index between 9 and 12. Among eight sampling locations, the North Atlantic Ocean has the highest species richness with Shannon index higher than 12, while the Shannon index from the majority of the Biosphere 2 Ocean samples was less than 6 (**Figure 35**). This suggested that with around 20 years' cultivation in a closed environment, the species richness in the Biosphere 2 Ocean has decreased, even though the environmental factors were highly controlled. Both of the ALOHA time series and Biosphere 2 time series suggested that the Shannon index varied during the sampling period.

Similar pattern were observed in the phylogenetic diversity plot (**Figure 36**). The phylogenetic diversity was represented by the PD whole-tree index, meaning the sum of the branch lengths in the phylogenetic trees. The North Atlantic Ocean showed the highest phylogenetic diversity, while the phylogenetic diversity in the Biosphere 2 Ocean was lower than in the open oceans.

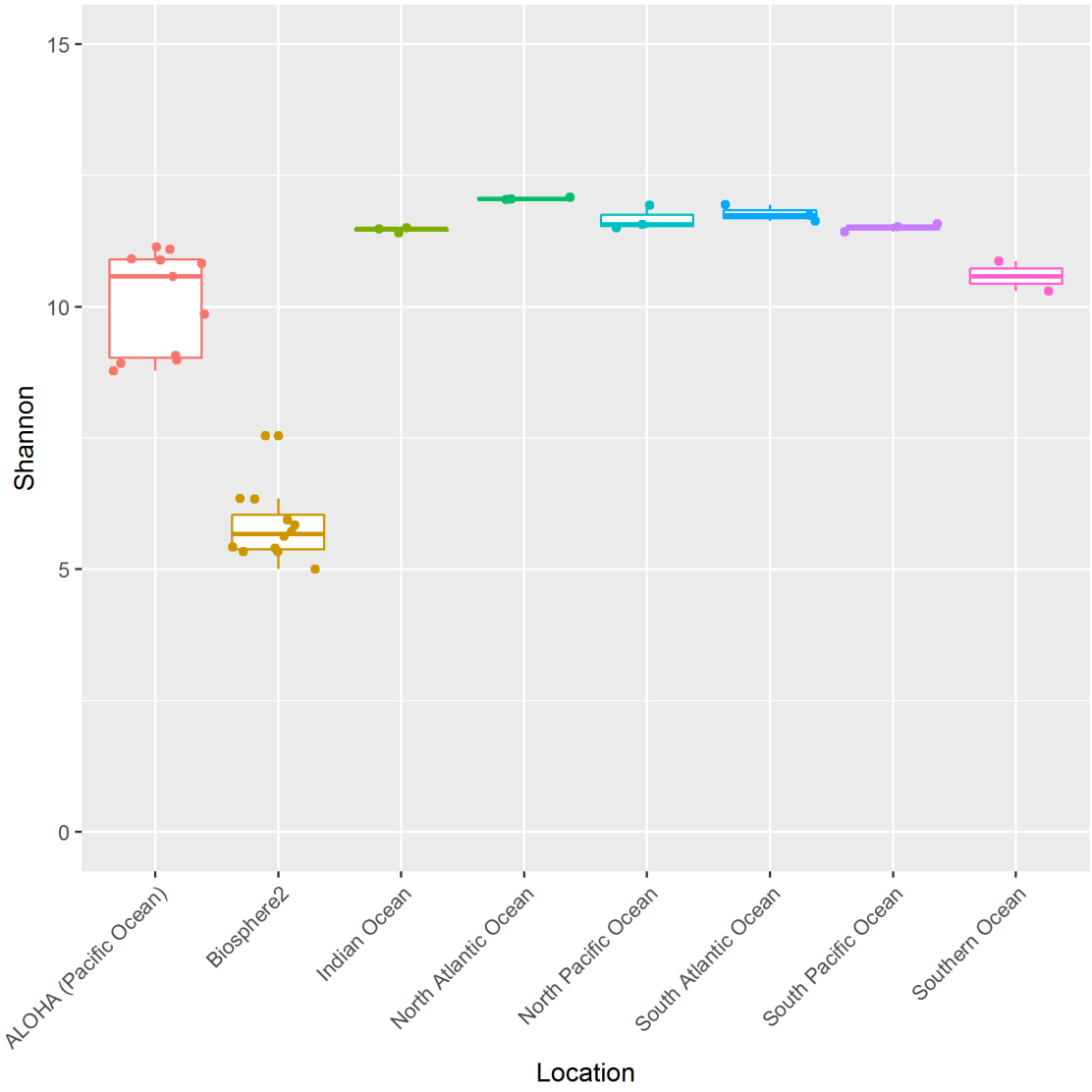

Figure 35. Shannon index from the Biosphere 2 Ocean and real open oceans.

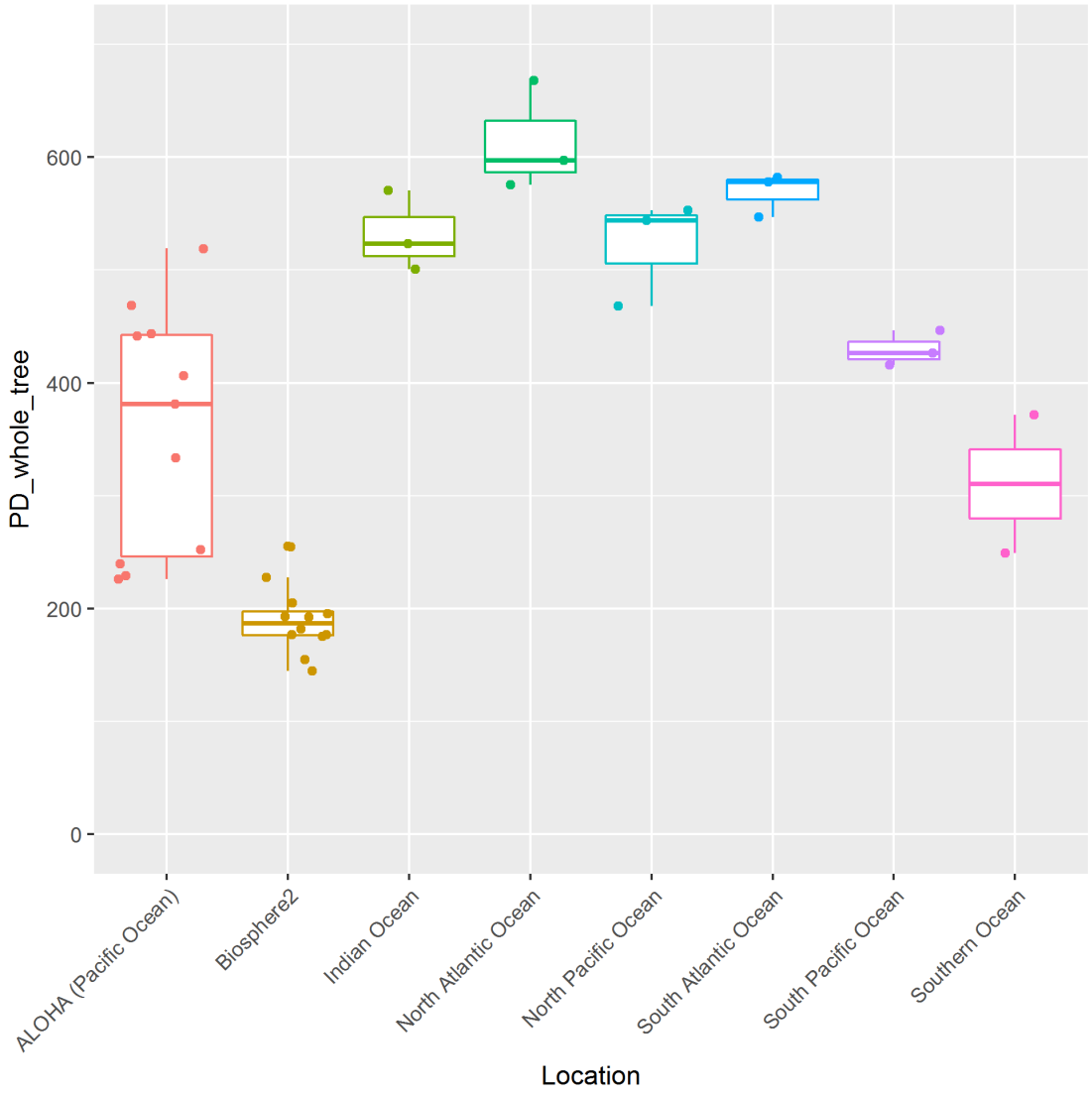

Figure 36. Phylogenetic diversity from the Biosphere 2 Ocean and real open oceans.

8.4 Discussion

The 16S rDNA sequencing profiles suggested temporal patterns of Bacteroidetes and Proteobacteria relative abundance. However, it is interesting to know that the overall evenness and diversity in the Biosphere 2 Ocean bacterial community have not changed significantly within the one year window (**Figure 28**), and did not suggest clear seasonal

trends. This is not surprising, as the environmental factors in the Biosphere 2 Ocean were real-time monitored and regulated.

Comparisons between the Biosphere 2 Ocean and the real open oceans suggest that the species richness and phylogenetic diversity in the Biosphere 2 Ocean bacterial community were lower than the communities in the natural ocean. It seems the ecosystem in an artificial environment is likely to lose certain evenness of species, especially with years' cultivation. Nevertheless, being away from the real ocean for years, the alteration of the bacterial communities implied that the Biosphere 2 Ocean is becoming a unique environment. A stable ecosystem potentially reduced the need of real-time characterization of the bacterial community during *in situ* instrument validation. This information could potentially reduce the cost of testing *in situ* devices. Additionally, the interesting ecosystem in the Biosphere 2 is a promising candidate to be treated as a miniature of a real ecosystem for future ecological investigations.

9. CONCLUSION AND FUTURE WORK

9.1 Conclusion

In environmental and biomedical research, qPCR is a critical tool used widely in laboratory settings. However, it is relatively limited for field applications because it requires a complicated detection platform and large energy storage. In this dissertation project, a novel quantitative DNA analyses system using colorimetric loop mediated isothermal amplification (LAMP) has been demonstrated. The conclusions of this project include:

(1) A novel real-time colorimetric quantification approach has been established. Algorithms and analysis tools have been built that automatically rejects pixels of bubbles, extracts the hues of individual wells, and fits the amplification curves using a sigmoidal function. Threshold time—similar to the threshold cycle number for qPCR—has been defined to represent the relative abundance of the template. These tools enabled automatic and rapid image acquisition, image processing, and data analysis, which are convenient and timesaving. Notably, these tools are user friendly and do not require professional training to operate. This novel quantification idea opened a new path for rapid nucleic acid quantification and the construction of the related analysis tools is a critical step to popularize this technology for routine laboratory use.

(2) The corresponding hardware platform has been built for real-time colorimetric LAMP reactions. The quantification requires only a chip, an inexpensive camera and a heater. A chip with deep wells has been designed to increase the optical paths, thus enhancing the contrast of the color changes. The combination of chip design, protocol,

and algorithm enable better field-operable or *in situ* quantitative DNA analysis measurements. The advantage of this colorimetric approach is that an end point qualitative LAMP measurement can be easily transformed into a real-time quantitative system by adding a camera to record the reaction. Additionally, this real-time reaction can be performed in ambient lighting conditions. Conventional PCR systems require fluorescence measurements while this real-time colorimetric LAMP system can be easily set up in a laboratory and health care facilities without purchasing delicate qPCR thermocyclers. The easy operation makes this system also suitable for institutions without microfabrication specialists. The hardware platform, as well as the analysis software, serve as a generalized product of the quantification system. The innovative quantification device can also be modified for novel commercial instruments manufacturing.

(3) The qLAMP reactions of serially diluted *Synechocystis* sp. PCC 6803 genomic DNA templates showed linear standard curves down to10^3 copies/µL. The RT-qLAMP reactions with serially diluted *Synechocystis* sp. PCC 6803 total RNA templates have a quantitative limit up to 1 pg/µL. The highly quantitative trait paved the way for promoting the colorimetric quantification technology to the research community. The results proved that the quantification approach was robust and sensitive, suggesting that this technology is a promising candidate for *in situ* device development.

(4) The colorimetric RT-qLAMP could be promising not only for microbial gene expression level characterization, but also for viral RNA load quantification. The RT-qLAMP reactions with serially diluted ZIKV RNA suggest that the technology is highly quantitative for viral RNA detection. The detection limit can be as low as 10 copies/µL.

In addition to environmental monitoring, this colorimetric quantification platform will be of immediate use to health care professionals for rapid and low-cost infectious disease diagnosis.

(5) As the Biosphere 2 Ocean showed relatively stable bacterial community structure, and seasonal community composition changes, the Biosphere 2 Ocean could be used to validate our future *in situ* instruments. Before deploying the instrument in real oceans, the instrument can be deployed in the Biosphere 2 Ocean for performance validation and optimization. This will significantly reduce the cost of instrumentation development. The bacterial community structure information will provide background biological knowledge of a promising test site for the researchers who are planning to build *in situ* devices. This information will accelerate environmental observing instrument development, benefit oceanographers, and lead to unprecedented ocean discoveries.

9.2 Future work

Even though this dissertation project provides fundamental concepts and set a solid foundation for *in situ* instrument development, there are still issues that remain to be solved before implementing field-operable devices. For example, regular webcams are low-cost and easily accessible, but they are huge regarding field operation. To save space, a tiny image acquisition element needs to be inserted into the *in situ* instrument to replace the webcam. This image acquisition element might need to be tuned further for optimal performance.

In this dissertation project, for proof-of-concept, only five groups of reactions were performed on a single chip. The throughput can be increased by rearranging the

layout of the reaction chambers or increasing the overall area of the chip. Moreover, in this project, only a single type of nucleic acid was analyzed each time. For future field operations, depending on specific research topics, multiple primer sets can be deposited into the reaction chambers to allow multiple target analysis capability. After integrating the platform with other important components (e.g. sampling unit, power system), the device can be deployed in the Biosphere 2 Ocean to characterize the performance.

REFERENCES

Abbaszadegan, M. (2004). Microbial detection methodologies. Southwest Hydrol. 19–34.

Ahmad, F., and Hashsham, S.A. (2012). Miniaturized nucleic acid amplification systems for rapid and point-of-care diagnostics: A review. Anal. Chim. Acta *733*, 1–15.

Akduman, D., Ehret, J.M., Messina, K., Ragsdale, S., and Judson, F.N. (2002). Evaluation of a Strand Displacement Amplification Assay (BD ProbeTec-SDA) for Detection of Neisseria gonorrhoeae in Urine Specimens. J. Clin. Microbiol. *40*, 281–283.

Allen, J., and Nelson, M. (1999). Overview and Design Biospherics and Biosphere 2, mission one (1991–1993). Ecol. Eng. *13*, 15–29.

Atkinson, M.J., Barnett, H., Aceves, H., Langdon, C., Carpenter, S.J., McConnaughey, T., Hochberg, E., Smith, M., and Marino, B.D.V. (1999). The Biosphere 2 coral reef biome. Ecol. Eng. *13*, 147–172.

Auroux, P.-A., Koc, Y., deMello, A., Manz, A., and Day, P.J.R. (2004). Miniaturised nucleic acid analysis. Lab. Chip *4*, 534.

Aylward, F.O., Eppley, J.M., Smith, J.M., Chavez, F.P., Scholin, C.A., and DeLong, E.F. (2015). Microbial community transcriptional networks are conserved in three domains at ocean basin scales. Proc. Natl. Acad. Sci. *112*, 5443–5448.

Balagaddé, F.K., You, L., Hansen, C.L., Arnold, F.H., and Quake, S.R. (2005). Long-Term Monitoring of Bacteria Undergoing Programmed Population Control in a Microchemostat. Science *309*, 137–140.

Bardgett, R.D., Freeman, C., and Ostle, N.J. (2008). Microbial contributions to climate change through carbon cycle feedbacks. ISME J. *2*, 805–814.

Beier, J.C., Perkins, P.V., Wirtz, R.A., Koros, J., Diggs, D., Gargan, T.P., and Koech, D.K. (1988). Bloodmeal Identification by Direct Enzyme-Linked Immunosorbent Assay (Elisa), Tested on Anopheles (Diptera: Culicidae) in Kenya. J. Med. Entomol. *25*, 9–16.

Bell, D.C., Thomas, W.K., Murtagh, K.M., Dionne, C.A., Graham, A.C., Anderson, J.E., and Glover, W.R. (2012). DNA base identification by electron microscopy. Microsc. Microanal. Off. J. Microsc. Soc. Am. Microbeam Anal. Soc. Microsc. Soc. Can. *18*, 1049–1053.

Besnard, M., Lastère, S., Teissier, A., Cao-Lormeau, V., and Musso, D. (2014). Evidence of perinatal transmission of Zika virus, French Polynesia, December 2013 and February 2014. Eurosurveillance *19*, 20751.

Branton, D., Deamer, D.W., Marziali, A., Bayley, H., Benner, S.A., Butler, T., Di Ventra, M., Garaj, S., Hibbs, A., Huang, X., Jovanovich, S.B., Krstic, P.S., Lindsay, S., Ling, X.S., Mastrangelo, C.H., Meller, A., Olier, J.S., Pershin, Y.V., Ramsey, J.M., Riehn, R., Soni, G.V., Tabard-Cossa, V., Wanunu, M., Wiggin, M., and Schloss, J.A. (2008). The potential and challenges of nanopore sequencing. Nat. Biotechnol. *26*, 1146–1153.

Bridle, H., Miller, B., and Desmulliez, M.P.Y. (2014). Application of microfluidics in waterborne pathogen monitoring: A review. Water Res. *55*, 256–271.

Buffle, J., and Horvai, G. (2000). In-situ monitoring of aquatic systems: chemical analysis and speciation (Chichester; New York: Wiley).

Burgos, J.S., Ramírez, C., Tenorio, R., Sastre, I., and Bullido, M.J. (2002). Influence of reagents formulation on real-time PCR parameters. Mol. Cell. Probes *16*, 257–260.

Calvet, G., Aguiar, R.S., Melo, A.S.O., Sampaio, S.A., de Filippis, I., Fabri, A., Araujo, E.S.M., de Sequeira, P.C., de Mendonça, M.C.L., de Oliveira, L. (2016). Detection and sequencing of Zika virus from amniotic fluid of fetuses with microcephaly in Brazil: a case study. Lancet Infect. Dis. *16*, 653–660.

Cao-Lormeau, V.-M., Roche, C., Teissier, A., Robin, E., Berry, A.-L., Mallet, H.-P., Sall, A.A., and Musso, D. (2014). Zika virus, French polynesia, South pacific, 2013. Emerg. Infect. Dis. *20*, 1085–1086.

Caporaso, J.G., Bittinger, K., Bushman, F.D., DeSantis, T.Z., Andersen, G.L., and Knight, R. (2010). PyNAST: a flexible tool for aligning sequences to a template alignment. Bioinformatics *26*, 266–267.

Caporaso, J.G., Lauber, C.L., Walters, W.A., Berg-Lyons, D., Huntley, J., Fierer, N., Owens, S.M., Betley, J., Fraser, L., Bauer, M., Gormley, N., Gilber, J.A., Smith, G., and Knight, R. (2012). Ultra-high-throughput microbial community analysis on the Illumina HiSeq and MiSeq platforms. ISME J. *6*, 1621–1624.

Cebula, T.A., Payne, W.L., and Feng, P. (1995). Simultaneous identification of strains of Escherichia coli serotype O157:H7 and their Shiga-like toxin type by mismatch amplification mutation assay-multiplex PCR. J. Clin. Microbiol. *33*, 248–250.

Cobbs, G. (2012). Stepwise kinetic equilibrium models of quantitative polymerase chain reaction. BMC Bioinformatics *13*, 203.

Compton, J. (1991). Nucleic acid sequence-based amplification. Nature *350*, 91–92.

Cook, N. (2003). The use of NASBA for the detection of microbial pathogens in food and environmental samples. J. Microbiol. Methods *53*, 165–174.

Crowther, J. (2008). Enzyme Linked Immunosorbent Assay (ELISA). In Molecular Biomethods Handbook, J. Walker, and R. Rapley, eds. (Humana Press), pp. 657–682.

Cunha, M.S., Esposito, D.L.A., Rocco, I.M., Maeda, A.Y., Vasami, F.G.S., Nogueira, J.S., Souza, R.P. de, Suzuki, A., Addas-Carvalho, M., Barjas-Castro, M. de L. (2016). First Complete Genome Sequence of Zika Virus (Flaviviridae, Flavivirus) from an Autochthonous Transmission in Brazil. Genome Announc. *4*, e00032-16.

Curtis Saunders, D., Holst, G.L., Phaneuf, C.R., Pak, N., Marchese, M., Sondej, N., McKinnon, M., and Forest, C.R. (2013). Rapid, quantitative, reverse transcription PCR in a polymer microfluidicchip. Biosens. Bioelectron. *44*, 222–228.

Czerkinsky, C.C., Nilsson, L.-Å., Nygren, H., Ouchterlony, Ö., and Tarkowski, A. (1983). A solid-phase enzyme-linked immunospot (ELISPOT) assay for enumeration of specific antibody-secreting cells. J. Immunol. Methods *65*, 109–121.

Deiman, B., van Aarle, P., and Sillekens, P. (2002). Characteristics and applications of nucleic acid sequence-based amplification (NASBA). Mol. Biotechnol. *20*, 163–179.

DeLong, E.F. (2006). Community Genomics Among Stratified Microbial Assemblages in the Ocean's Interior. Science *311*, 496–503.

Dick, G.W.A., Kitchen, S.F., and Haddow, A.J. (1952). Zika Virus (I). Isolations and serological specificity. Trans. R. Soc. Trop. Med. Hyg. *46*, 509–520.

Doucette, G.J., Mikulski, C.M., Jones, K.L., King, K.L., Greenfield, D.I., Marin III, R., Jensen, S., Roman, B., Elliott, C.T., and Scholin, C.A. (2009). Remote, subsurface detection of the algal toxin domoic acid onboard the Environmental Sample Processor: Assay development and field trials. Harmful Algae *8*, 880–888.

Duffy, M.R., Chen, T.-H., Hancock, W.T., Powers, A.M., Kool, J.L., Lanciotti, R.S., Pretrick, M., Marfel, M., Holzbauer, S., Dubray, C., Guillaumot, L., Griggs, A., Bel, M., Lambert, A.J., Laven, J., Kosoy, O., Panella, A., Biggerstaff, B.J., Fischer, M., and Hayes, E.B. (2009). Zika virus outbreak on Yap Island, federated states of Micronesia. N. Engl. J. Med. *360*, 2536–2543.

En, F.-X., Wei, X., Jian, L., and Qin, C. (2008). Loop-mediated isothermal amplification establishment for detection of pseudorabies virus. J. Virol. Methods *151*, 35–39.

Epstein, J.S., and Vostal, J.G. (2003). FDA approach to evaluation of pathogen reduction technology. Transfusion (Paris) *43*, 1347–1350.

Evans, T.G., and Hofmann, G.E. (2012). Defining the limits of physiological plasticity: how gene expression can assess and predict the consequences of ocean change. Philos. Trans. R. Soc. B Biol. Sci. *367*, 1733–1745.

Falcón, L.I., Carpenter, E.J., Cipriano, F., Bergman, B., and Capone, D.G. (2004). N2 Fixation by Unicellular Bacterioplankton from the Atlantic and Pacific Oceans: Phylogeny and In Situ Rates. Appl. Environ. Microbiol. *70*, 765–770.

Falkowski, P.G., Barber, R.T., and Smetacek, V. (1998). Biogeochemical Controls and Feedbacks on Ocean Primary Production. Science *281*, 200–206.

Fang, X., Liu, Y., Kong, J., and Jiang, X. (2010). Loop-Mediated Isothermal Amplification Integrated on Microfluidic Chips for Point-of-Care Quantitative Detection of Pathogens. Anal. Chem. *82*, 3002–3006.

Fang, X., Chen, H., Xu, L., Jiang, X., Wu, W., and Kong, J. (2012). A portable and integrated nucleic acid amplification microfluidic chip for identifying bacteria. Lab. Chip *12*, 1495.

Faye, O., Faye, O., Dupressoir, A., Weidmann, M., Ndiaye, M., and Alpha Sall, A. (2008). One-step RT-PCR for detection of Zika virus. J. Clin. Virol. *43*, 96–101.

Feng, P., and Lampel, K.A. (1994). Genetic analysis of uidA expression in enterohaemorrhagic Escherichia coli serotype 0157:H7. Microbiology *140*, 2101–2107.

Field, C.B., Behrenfeld, M.J., Randerson, J.T., and Falkowski, P. (1998). Primary Production of the Biosphere: Integrating Terrestrial and Oceanic Components. Science *281*, 237–240.

Finn, M. (1996). The mangrove mesocosm of Biosphere 2: Design, establishment and preliminary results. Ecol. Eng. *6*, 21–56.

Fiorentino, G., Ronca, R., and Bartolucci, S. (2008). A novel E. coli biosensor for detecting aromatic aldehydes based on a responsive inducible archaeal promoter fused to the green fluorescent protein. Appl. Microbiol. Biotechnol. *82*, 67–77.

Fischbach, J., Xander, N.C., Frohme, M., and Glökler, J.F. (2015). Shining a light on LAMP assays--a comparison of LAMP visualization methods including the novel use of berberine. BioTechniques *58*, 189–194.

Follows, M.J., Dutkiewicz, S., Grant, S., and Chisholm, S.W. (2007). Emergent Biogeography of Microbial Communities in a Model Ocean. Science *315*, 1843–1846.

Franks, A.H., Harmsen, H.J.M., Raangs, G.C., Jansen, G.J., Schut, F., and Welling, G.W. (1998). Variations of Bacterial Populations in Human Feces Measured by Fluorescent In Situ Hybridization with Group-Specific 16S rRNA-Targeted Oligonucleotide Probes. Appl. Environ. Microbiol. *64*, 3336–3345.

Fredricks, D.N. (2011). Molecular methods to describe the spectrum and dynamics of the vaginal microbiota. Anaerobe *17*, 191–195.

Friguet, B., Chaffotte, A.F., Djavadi-Ohaniance, L., and Goldberg, M.E. (1985). Measurements of the true affinity constant in solution of antigen-antibody complexes by enzyme-linked immunosorbent assay. J. Immunol. Methods *77*, 305–319.

Fukuba, T., and Fujii, T. (2012). Microfabricated Flow-Through Device for In Situ Gene Analysis. In Molecular Biological Technologies for Ocean Sensing, S.M. Tiquia-Arashiro, ed. (Humana Press), pp. 59–72.

Fukuba, T., Miyaji, A., Okamoto, T., Yamamoto, T., Kaneda, S., and Fujii, T. (2011). Integrated in situ genetic analyzer for microbiology in extreme environments. RSC Adv. *1*, 1567.

Fulop, L., Barrett, A.D.T., Phillpotts, R., Martin, K., Leslie, D., and Titball, R.W. (1993). Rapid identification of flaviviruses based on conserved NS5 gene sequences. J. Virol. Methods *44*, 179–188.

Gan, S.D., and Patel, K.R. (2013). Enzyme Immunoassay and Enzyme-Linked Immunosorbent Assay. J. Invest. Dermatol. *133*, 1–3.

Gandelman, O.A., Church, V.L., Moore, C.A., Kiddle, G., Carne, C.A., Parmar, S., Jalal, H., Tisi, L.C., and Murray, J.A.H. (2010). Novel Bioluminescent Quantitative Detection of Nucleic Acid Amplification in Real-Time. PLOS ONE *5*, e14155.

Gao, W., Zhang, W., and Meldrum, D.R. (2011). RT-qPCR based quantitative analysis of gene expression in single bacterial cells. J. Microbiol. Methods *85*, 221–227.

Giezen, M. van der (2011). Mitochondria and the Rise of Eukaryotes. BioScience *61*, 594–601.

Gilbert, J.A., Field, D., Swift, P., Thomas, S., Cummings, D., Temperton, B., Weynberg, K., Huse, S., Hughes, M., Joint, I., Somefield, P.J., and Mühling, M. (2010). The Taxonomic and Functional Diversity of Microbes at a Temperate Coastal Site: A "Multi-Omic" Study of Seasonal and Diel Temporal Variation. PLoS ONE *5*, e15545.

Goffredi, S.K., Jones, W.J., Scholin, C.A., Marin, R., and Vrijenhoek, R.C. (2006). Molecular Detection of Marine Invertebrate Larvae. Mar. Biotechnol. *8*, 149–160.

Goto, M., Honda, E., Ogura, A., Nomoto, A., and Hanaki, K.-I. (2009). Colorimetric detection of loop-mediated isothermal amplification reaction by using hydroxy naphthol blue. BioTechniques *46*, 167–172.

Gourinat, A.-C., O'Connor, O., Calvez, E., Goarant, C., and Dupont-Rouzeyrol, M. (2015). Detection of Zika Virus in Urine. Emerg. Infect. Dis. *21*, 84–86.

Greenfield, D.I., Marin, R., Jensen, S., Massion, E., Roman, B., Feldman, J., and Scholin, C.A. (2006). Application of environmental sample processor (ESP) methodology for

quantifying Pseudo-nitzschia australis using ribosomal RNA-targeted probes in sandwich and fluorescent in situ hybridization formats. Limnol. Oceanogr. Methods *4*, 426–435.

Greenfield, D.I., Marin, R., Doucette, G.J., Mikulski, C., Jones, K., Jensen, S., Roman, B., Alvarado, N., Feldman, J., and Scholin, C. (2008). Field applications of the second-generation Environmental Sample Processor (ESP) for remote detection of harmful algae: 2006-2007: Field applications of the ESP: 2006-2007. Limnol. Oceanogr. Methods *6*, 667–679.

Griffiths, H.J. (2010). Antarctic Marine Biodiversity – What Do We Know About the Distribution of Life in the Southern Ocean? PLOS ONE *5*, e11683.

Hatch, A.C., Ray, T., Lintecum, K., and Youngbull, C. (2014). Continuous flow real-time PCR device using multi-channel fluorescence excitation and detection. Lab Chip *14*, 562–568.

Ho, C.-M., and Tai, Y.-C. (1998). Micro-Electro-Mechanical-Systems (mems) and Fluid Flows. Annu. Rev. Fluid Mech. *30*, 579–612.

Horisaka, T., Fujita, K., Iwata, T., Nakadai, A., Okatani, A.T., Horikita, T., Taniguchi, T., Honda, E., Yokomizo, Y., and Hayashidani, H. (2004). Sensitive and Specific Detection of Yersinia pseudotuberculosis by Loop-Mediated Isothermal Amplification. J. Clin. Microbiol. *42*, 5349–5352.

Hsieh, K., Patterson, A.S., Ferguson, B.S., Plaxco, K.W., and Soh, H.T. (2012). Rapid, Sensitive, and Quantitative Detection of Pathogenic DNA at the Point of Care through Microfluidic Electrochemical Quantitative Loop-Mediated Isothermal Amplification. Angew. Chem. *124*, 4980–4984.

Huang, L., McCluskey, M.P., Ni, H., and LaRossa, R.A. (2002). Global Gene Expression Profiles of the Cyanobacterium Synechocystis sp. Strain PCC 6803 in Response to Irradiation with UV-B and White Light. J. Bacteriol. *184*, 6845–6858.

Huet, A.-C., Delahaut, P., Fodey, T., Haughey, S.A., Elliott, C., and Weigel, S. (2010). Advances in biosensor-based analysis for antimicrobial residues in foods. TrAC Trends Anal. Chem. *29*, 1281–1294.

Im, J., Biswas, S., Liu, H., Zhao, Y., Sen, S., Biswas, S., Ashcroft, B., Borges, C., Wang, X., Lindsay, S., and Zhang, P. (2016). Electronic single-molecule identification of carbohydrate isomers by recognition tunnelling. Nat. Commun. *7*.

Jaroenram, W., Kiatpathomchai, W., and Flegel, T.W. (2009). Rapid and sensitive detection of white spot syndrome virus by loop-mediated isothermal amplification combined with a lateral flow dipstick. Mol. Cell. Probes *23*, 65–70.

Jones, W.J., Preston, C.M., Marin Iii, R., Scholin, C.A., and Vrijenhoek, R.C. (2008). A robotic molecular method for in situ detection of marine invertebrate larvae. Mol. Ecol. Resour. *8*, 540–550.

Kaneko, T., and Tabata, S. (1997). Complete Genome Structure of the Unicellular Cyanobacterium Synechocystis sp. PCC6803. Plant Cell Physiol. *38*, 1171–1176.

Kaneko, H., Kawana, T., Fukushima, E., and Suzutani, T. (2007). Tolerance of loop-mediated isothermal amplification to a culture medium and biological substances. J. Biochem. Biophys. Methods *70*, 499–501.

Kang, J.H., Kim, Y.C., and Park, J.-K. (2008). Analysis of pressure-driven air bubble elimination in a microfluidic device. Lab Chip *8*, 176–178.

Kelbauskas, L., Glenn, H., Anderson, C., Messner, J., Lee, K.B., Song, G., Houkal, J., Su, F., Zhang, L., Tian, Y., Wang, H., Bussey, K., Johnson, R., and Meldrum, D.R. (2017). A platform for high-throughput bioenergy production phenotype characterization in single cells. Sci. Rep. *7*.

Kell, D.B., and Young, M. (2000). Bacterial dormancy and culturability: the role of autocrine growth factors: commentary. Curr. Opin. Microbiol. *3*, 238–243.

Klein, D. (2002). Quantification using real-time PCR technology: applications and limitations. Trends Mol. Med. *8*, 257–260.

Koh, C.G., Tan, W., Zhao, M., Ricco, A.J., and Fan, Z.H. (2003). Integrating Polymerase Chain Reaction, Valving, and Electrophoresis in a Plastic Device for Bacterial Detection. Anal. Chem. *75*, 4591–4598.

Kokkinos, P.A., Ziros, P.G., Bellou, M., and Vantarakis, A. (2013). Loop-Mediated Isothermal Amplification (LAMP) for the Detection of Salmonella in Food. Food Anal. Methods *7*, 512–526.

Kotiaho, T. (1996). On-site environmental and in situ process analysis by mass spectrometry. J. Mass Spectrom. *31*, 1–15.

Kubo, T., Agoh, M., Mai, L.Q., Fukushima, K., Nishimura, H., Yamaguchi, A., Hirano, M., Yoshikawa, A., Hasebe, F., Kohno, S., and Morita, K. (2010). Development of a Reverse Transcription-Loop-Mediated Isothermal Amplification Assay for Detection of Pandemic (H1N1) 2009 Virus as a Novel Molecular Method for Diagnosis of Pandemic Influenza in Resource-Limited Settings. J. Clin. Microbiol. *48*, 728–735.

Kuboniwa, M., Amano, A., Kimura, K.R., Sekine, S., Kato, S., Yamamoto, Y., Okahashi, N., Iida, T., and Shizukuishi, S. (2004). Quantitative detection of periodontal pathogens using real-time polymerase chain reaction with TaqMan probes. Oral Microbiol. Immunol. *19*, 168–176.

Laiz, L., Piñar, G., Lubitz, W., and Saiz-Jimenez, C. (2003). Monitoring the colonization of monuments by bacteria: cultivation versus molecular methods. Environ. Microbiol. *5*, 72–74.

Lanciotti, R.S., and Kerst, A.J. (2001). Nucleic Acid Sequence-Based Amplification Assays for Rapid Detection of West Nile and St. Louis Encephalitis Viruses. J. Clin. Microbiol. *39*, 4506–4513.

Lanciotti, R.S., Kosoy, O.L., Laven, J.J., Velez, J.O., Lambert, A.J., Johnson, A.J., Stanfield, S.M., and Duffy, M.R. (2008). Genetic and Serologic Properties of Zika Virus Associated with an Epidemic, Yap State, Micronesia, 2007. Emerg. Infect. Dis. *14*, 1232–1239.

Le Chatelier, E., Nielsen, T., Qin, J., Prifti, E., Hildebrand, F., Falony, G., Almeida, M., Arumugam, M., Batto, J.-M., Kennedy, S., Leonard, P., Li, J., Burgdorf, K., Grarup N., Jørgensen, T., Brandslund, I., Nielsen, H.B., Juncker, A.S., Bertalan, M., Levenez, F., Pons, N., Rasmussen, S., Sunagawa, S., Tap, J., and Tims, S. (2013). Richness of human gut microbiome correlates with metabolic markers. Nature *500*, 541–546.

Lee, M.-S., Lin, Y.-C., Lai, G.-H., Lai, S.-Y., Chen, H.-J., and Wang, M.-Y. (2011). One-step reverse-transcription loop-mediated isothermal amplification for detection of infectious bursal disease virus. Can. J. Vet. Res. *75*, 122–127.

Lehmann, U., and Kreipe, H. (2001). Real-Time PCR Analysis of DNA and RNA Extracted from Formalin-Fixed and Paraffin-Embedded Biopsies. Methods *25*, 409–418.

Leigh, L.S., Burgess, T., Marino, B.D.V., and Wei, Y.D. (1999). Tropical rainforest biome of Biosphere 2: Structure, composition and results of the first 2 years of operation. Ecol. Eng. *13*, 65–93.

Leone, G., Gemen, B. van, Schoen, C.D., Schijndel, H. van, and Kramer, F.R. (1998). Molecular beacon probes combined with amplification by NASBA enable homogeneous, real-time detection of RNA. Nucleic Acids Res. *26*, 2150–2155.

Li, W., and Godzik, A. (2006). Cd-hit: a fast program for clustering and comparing large sets of protein or nucleotide sequences. Bioinforma. Oxf. Engl. *22*, 1658–1659.

Lindsay, S., Zhang, P., and Zhao, Y. (2013). Systems, apparatuses and methods for reading an amino acid sequence (Google Patents).

Liu, J., Weinbauer, M.G., Maier, C., Dai, M., and Gattuso, J. (2010). Effect of ocean acidification on microbial diversity and on microbe-driven biogeochemistry and ecosystem functioning. Aquat. Microb. Ecol. *61*, 291–305.

Livak, K.J., and Schmittgen, T.D. (2001). Analysis of Relative Gene Expression Data Using Real-Time Quantitative PCR and the $2^{-\Delta\Delta CT}$ Method. Methods *25*, 402–408.

Lizardi, P.M., Huang, X., Zhu, Z., Bray-Ward, P., Thomas, D.C., and Ward, D.C. (1998). Mutation detection and single-molecule counting using isothermal rolling-circle amplification. Nat. Genet. *19*, 225–232.

Loeffler, J., Hebart, H., Cox, P., Flues, N., Schumacher, U., and Einsele, H. (2001). Nucleic Acid Sequence-Based Amplification ofAspergillus RNA in Blood Samples. J. Clin. Microbiol. *39*, 1626–1629.

Ma, X., Shu, Y., Nie, K., Qin, M., Wang, D., Gao, R., Wang, M., Wen, L., Han, F., Zhou, S., Zhao, X., Cheng, Y., Li, D., and Dong, X. (2010). Visual detection of pandemic influenza A H1N1 Virus 2009 by reverse-transcription loop-mediated isothermal amplification with hydroxynaphthol blue dye. J. Virol. Methods *167*, 214–217.

Maher-Sturgess, S.L., Forrester, N.L., Wayper, P.J., Gould, E.A., Hall, R.A., Barnard, R.T., and Gibbs, M.J. (2008). Universal primers that amplify RNA from all three flavivirus subgroups. Virol. J. *5*, 16.

Martineau, R.L., Ci, S., Houkal, J., Gao, W., Chao, S.-H., and Meldrum, D.R. (2014). DEEP-well microfluidics for arrayed colorimetric LAMP analysis. pp. 1009–1011.

Martineau, R.L., Murray, S.A., Ci, S., Gao, W., Chao, S., and Meldrum, D.R. (2017). Improved Performance of Loop-Mediated Isothermal Amplification Assays via Swarm Priming. Anal. Chem. *89*, 625–632.

Matsuda, K., Tsuji, H., Asahara, T., Kado, Y., and Nomoto, K. (2007). Sensitive Quantitative Detection of Commensal Bacteria by rRNA-Targeted Reverse Transcription-PCR. Appl. Environ. Microbiol. *73*, 32–39.

Mora, C., Tittensor, D.P., Adl, S., Simpson, A.G.B., and Worm, B. (2011). How Many Species Are There on Earth and in the Ocean? PLOS Biol *9*, e1001127.

Morgan, X.C., Tickle, T.L., Sokol, H., Gevers, D., Devaney, K.L., Ward, D.V., Reyes, J.A., Shah, S.A., LeLeiko, N., Snapper, S.B., Bousvaros, A., Korzenik, J., Sands, B.E., Xavier, R.J., and Huttenhower, C. (2012). Dysfunction of the intestinal microbiome in inflammatory bowel disease and treatment. Genome Biol. *13*, R79.

Mori, Y., and Notomi, T. (2009). Loop-mediated isothermal amplification (LAMP): a rapid, accurate, and cost-effective diagnostic method for infectious diseases. J. Infect. Chemother. *15*, 62–69.

Mori, Y., Nagamine, K., Tomita, N., and Notomi, T. (2001). Detection of Loop-Mediated Isothermal Amplification Reaction by Turbidity Derived from Magnesium Pyrophosphate Formation. Biochem. Biophys. Res. Commun. *289*, 150–154.

Mori, Y., Kitao, M., Tomita, N., and Notomi, T. (2004). Real-time turbidimetry of LAMP reaction for quantifying template DNA. J. Biochem. Biophys. Methods *59*, 145–157.

Mulcahy, H., Charron-Mazenod, L., and Lewenza, S. (2008). Extracellular DNA Chelates Cations and Induces Antibiotic Resistance in Pseudomonas aeruginosa Biofilms. PLoS Pathog *4*, e1000213.

Muller, P.Y., Janovjak, H., Miserez, A.R., and Dobbie, Z. (2002). Short technical report processing of gene expression data generated by quantitative Real-Time RT-PCR. Biotechniques *32*, 1372–1379.

Musso, D., and Gubler, D.J. (2016). Zika Virus. Clin. Microbiol. Rev. *29*, 487–524.

Musso, D., Nilles, E.J., and Cao-Lormeau, V.-M. (2014). Rapid spread of emerging Zika virus in the Pacific area. Clin. Microbiol. Infect. *20*, O595–O596.

Musso, D., Cao-Lormeau, V.M., and Gubler, D.J. (2015). Zika virus: following the path of dengue and chikungunya? The Lancet *386*, 243–244.

Nagamine, K., Hase, T., and Notomi, T. (2002). Accelerated reaction by loop-mediated isothermal amplification using loop primers. Mol. Cell. Probes *16*, 223–229.

Nakamura, K. (2012). Ultrasonic Transducers: Materials and Design for Sensors, Actuators and Medical Applications (Elsevier).

Njiru, Z.K. (2011). Rapid and sensitive detection of human African trypanosomiasis by loop-mediated isothermal amplification combined with a lateral-flow dipstick. Diagn. Microbiol. Infect. Dis. *69*, 205–209.

Nolan, T., and Bustin, S.A. (2013). PCR Technology: Current Innovations, Third Edition (CRC Press).

Notomi, T., Okayama, H., Masubuchi, H., Yonekawa, T., Watanabe, K., Amino, N., and Hase, T. (2000). Loop-mediated isothermal amplification of DNA. Nucleic Acids Res. *28*, e63–e63.

Oehler, E., Watrin, L., Larre, P., Leparc-Goffart, I., Lastere, S., Valour, F., Baudouin, L., Mallet, H., Musso, D., and Ghawche, F. (2014). Zika virus infection complicated by Guillain-Barre syndrome–case report, French Polynesia, December 2013. Euro Surveill *19*, 20720.

Oliveira, D.C., and Lencastre, H. de (2002). Multiplex PCR Strategy for Rapid Identification of Structural Types and Variants of the mec Element in Methicillin-Resistant Staphylococcus aureus. Antimicrob. Agents Chemother. *46*, 2155–2161.

Ottesen, E.A., Young, C.R., Gifford, S.M., Eppley, J.M., Marin, R., Schuster, S.C., Scholin, C.A., and DeLong, E.F. (2014). Multispecies diel transcriptional oscillations in open ocean heterotrophic bacterial assemblages. Science *345*, 207–212.

Pardee, K., Green, A.A., Takahashi, M.K., Braff, D., Lambert, G., Lee, J.W., Ferrante, T., Ma, D., Donghia, N., Fan, M., Daringer, N.M., Bosch, I., Dudley, D.M., O'Connor, D.H., Gehrke, L., and Collins, J.J. (2016). Rapid, Low-Cost Detection of Zika Virus Using Programmable Biomolecular Components. Cell *165*, 1255–1266.

Parida, M., Horioke, K., Ishida, H., Dash, P.K., Saxena, P., Jana, A.M., Islam, M.A., Inoue, S., Hosaka, N., and Morita, K. (2005). Rapid Detection and Differentiation of Dengue Virus Serotypes by a Real-Time Reverse Transcription-Loop-Mediated Isothermal Amplification Assay. J. Clin. Microbiol. *43*, 2895–2903.

Parida, M.M., Santhosh, S.R., Dash, P.K., Tripathi, N.K., Lakshmi, V., Mamidi, N., Shrivastva, A., Gupta, N., Saxena, P., Babu, J.P., Rao, P.V.L., and Morita, K. (2007). Rapid and Real-Time Detection of Chikungunya Virus by Reverse Transcription Loop-Mediated Isothermal Amplification Assay. J. Clin. Microbiol. *45*, 351–357.

Park, S.-J., Taton, T.A., and Mirkin, C.A. (2002). Array-based electrical detection of DNA with nanoparticle probes. Science *295*, 1503–1506.

Paul, J., SCholIN, C., VaN deN eNGh, G., and Perry, M.J. (2007). In situ instrumentation. Oceanography *20*, 70.

Pflughoeft, K.J., and Versalovic, J. (2012). Human Microbiome in Health and Disease. Annu. Rev. Pathol. Mech. Dis. *7*, 99–122.

Piepenburg, O., Williams, C.H., Stemple, D.L., and Armes, N.A. (2006). DNA Detection Using Recombination Proteins. PLOS Biol *4*, e204.

Pinto, A.J., and Raskin, L. (2012). PCR Biases Distort Bacterial and Archaeal Community Structure in Pyrosequencing Datasets. PLOS ONE *7*, e43093.

Pinto, A.J., Schroeder, J., Lunn, M., Sloan, W., and Raskin, L. (2014). Spatial-Temporal Survey and Occupancy-Abundance Modeling To Predict Bacterial Community Dynamics in the Drinking Water Microbiome. mBio *5*, e01135-14.

Preston, C.M., Harris, A., Ryan, J.P., Roman, B., Iii, R.M., Jensen, S., Everlove, C., Birch, J., Dzenitis, J.M., Pargett, D., Adachi, M., Turk, K., Zehr, J.P., and Scholin, C.A. (2011). Underwater Application of Quantitative PCR on an Ocean Mooring. PLOS ONE *6*, e22522.

Price, M.N., Dehal, P.S., and Arkin, A.P. (2009). FastTree: computing large minimum evolution trees with profiles instead of a distance matrix. Mol. Biol. Evol. *26*, 1641–1650.

Punter-Villagrasa, J., Cid, J., Páez-Avilés, C., Rodríguez-Villarreal, I., Juanola-Feliu, E., Colomer-Farrarons, J., and Miribel-Català, P.L. (2015). An instantaneous low-cost point-of-care anemia detection device. Sensors *15*, 4564–4577.

Qiao, Y.-M., Guo, Y.-C., Zhang, X.-E., Zhou, Y.-F., Zhang, Z.-P., Wei, H.-P., Yang, R.-F., and Wang, D.-B. (2007). Loop-mediated isothermal amplification for rapid detection of Bacillus anthracis spores. Biotechnol. Lett. *29*, 1939–1946.

Rasmussen, S.A., Jamieson, D.J., Honein, M.A., and Petersen, L.R. (2016). Zika Virus and Birth Defects — Reviewing the Evidence for Causality. N. Engl. J. Med. *374*, 1981–1987.

Rippka, R., Deruelles, J., Waterbury, J.B., Herdman, M., and Stanier, R.Y. (1979). Generic Assignments, Strain Histories and Properties of Pure Cultures of Cyanobacteria. Microbiology *111*, 1–61.

Rivkin, R.B., and Legendre, L. (2001). Biogenic Carbon Cycling in the Upper Ocean: Effects of Microbial Respiration. Science *291*, 2398–2400.

Roszak, D.B., and Colwell, R.R. (1987). Survival strategies of bacteria in the natural environment. Microbiol. Rev. *51*, 365–379.

Rusch, D.B., Halpern, A.L., Sutton, G., Heidelberg, K.B., Williamson, S., Yooseph, S., Wu, D., Eisen, J.A., Hoffman, J.M., and Remington, K. (2007). The Sorcerer II Global Ocean Sampling Expedition: Northwest Atlantic through Eastern Tropical Pacific. PLOS Biol *5*, e77.

Russell, H., Sampson, J.S., Schmid, G.P., Wilkinson, H.W., and Plikaytis, B. (1984). Enzyme-Linked Immunosorbent Assay and Indirect Immunofluorescence Assay for Lyme Disease. J. Infect. Dis. *149*, 465–470.

Rutledge, R.G., and Stewart, D. (2008). A kinetic-based sigmoidal model for the polymerase chain reaction and its application to high-capacity absolute quantitative real-time PCR. BMC Biotechnol. *8*, 47.

Safavieh, M., Ahmed, M.U., Sokullu, E., Ng, A., Braescu, L., and Zourob, M. (2014). A simple cassette as point-of-care diagnostic device for naked-eye colorimetric bacteria detection. The Analyst *139*, 482–487.

Schneider, P., Wolters, L., Schoone, G., Schallig, H., Sillekens, P., Hermsen, R., and Sauerwein, R. (2005). Real-Time Nucleic Acid Sequence-Based Amplification Is More Convenient than Real-Time PCR for Quantification of Plasmodium falciparum. J. Clin. Microbiol. *43*, 402–405.

Scholin, C., Jensen, S., Roman, B., Massion, E., Marin, R., Preston, C., Greenfield, D., Jones, W., and Wheeler, K. (2006). The Environmental Sample Processor (ESP) - An

Autonomous Robotic Device for Detecting Microorganisms Remotely using Molecular Probe Technology. In OCEANS 2006, pp. 1–4.

Scholin, C., Doucette, G., Jensen, S., Roman, B., Pargett, D., Iii, R.M., Preston, C., Jones, W., Feldman, J., Everlove, C., Harris, A., Alvarado, N., Massion, E., Birch, J., Greenfield, D., Vrijenhoek, R., Mikulski, C., and Jones, K. (2009). Remote Detection of Marine Microbes, Small Invertebrates, Harmful Algae, and Biotoxins using the Environmental Sample Processor (ESP). Oceanography.

Shan, C., Xie, X., Barrett, A.D.T., Garcia-Blanco, M.A., Tesh, R.B., Vasconcelos, P.F. da C., Vasilakis, N., Weaver, S.C., and Shi, P.-Y. (2016). Zika Virus: Diagnosis, Therapeutics, and Vaccine. ACS Infect. Dis. *2*, 170–172.

Shendure, J., and Ji, H. (2008). Next-generation DNA sequencing. Nat. Biotechnol. *26*, 1135–1145.

Shi, X., Lin, L.-I., Chen, S., Chao, S., Zhang, W., and Meldrum, D.R. (2011). Real-time PCR of single bacterial cells on an array of adhering droplets. Lab. Chip *11*, 2276.

Shi, X., Gao, W., Chao, S., Zhang, W., and Meldrum, D.R. (2013). Monitoring the Single-Cell Stress Response of the Diatom Thalassiosira pseudonana by Quantitative Real-Time Reverse Transcription-PCR. Appl. Environ. Microbiol. *79*, 1850–1858.

Shoemark, D.K., and Allen, S.J. (2015). The microbiome and disease: reviewing the links between the oral microbiome, aging, and Alzheimer's disease. J. Alzheimers Dis. *43*, 725–738.

Sirohi, D., Chen, Z., Sun, L., Klose, T., Pierson, T.C., Rossmann, M.G., and Kuhn, R.J. (2016). The 3.8 Å resolution cryo-EM structure of Zika virus. Science *352*, 467–470.

Smith, A.R. (1978). Color Gamut Transform Pairs. In Proceedings of the 5th Annual Conference on Computer Graphics and Interactive Techniques, (New York, NY, USA: ACM), pp. 12–19.

Solomon, C., and Breckon, T. (2011). Fundamentals of Digital Image Processing: A Practical Approach with Examples in Matlab (John Wiley & Sons).

Song, G., Shetty, R.M., Zhu, H., Ashili, S., Zhang, L., Kim, G., Shabilla, A., Teller, W., Mei, Q., Kelbauskas, L., Tian, Y., Wang, H., Johnson, R.H., and Meldrum, D.R. (2013). Multiple sensor arrays for single cell metabolic analysis. In 2013 IEEE SENSORS, pp. 1–4.

Song, J., Mauk, M.G., Hackett, B.A., Cherry, S., Bau, H.H., and Liu, C. (2016). Instrument-Free Point-of-Care Molecular Detection of Zika Virus. Anal. Chem. *88*, 7289–7294.

Sooknanan, R., and Malek, L.T. (1995). Nasba: A Detection and Amplification System Uniquely Suited for Rna. Bio/Technology *13*.

Spiess, A.-N., Feig, C., and Ritz, C. (2008). Highly accurate sigmoidal fitting of real-time PCR data by introducing a parameter for asymmetry. BMC Bioinformatics *9*, 221.

Squires, T.M., and Quake, S.R. (2005). Microfluidics: Fluid physics at the nanoliter scale. Rev. Mod. Phys. *77*, 977–1026.

Stocker, R. (2012). Marine Microbes See a Sea of Gradients. Science *338*, 628–633.

Streit, W.R., and Schmitz, R.A. (2004). Metagenomics – the key to the uncultured microbes. Curr. Opin. Microbiol. *7*, 492–498.

Strockbine, N.A., Jackson, M.P., Sung, L.M., Holmes, R.K., and O'Brien, A.D. (1988). Cloning and sequencing of the genes for Shiga toxin from Shigella dysenteriae type 1. J. Bacteriol. *170*, 1116–1122.

Strovas, T.J., and Lidstrom, M.E. (2009). Population heterogeneity in Methylobacterium extorquens AM1. Microbiology *155*, 2040–2048.

Su, L., Jia, W., Hou, C., and Lei, Y. (2011). Microbial biosensors: A review. Biosens. Bioelectron. *26*, 1788–1799.

Sunagawa, S., Coelho, L.P., Chaffron, S., Kultima, J.R., Labadie, K., Salazar, G., Djahanschiri, B., Zeller, G., Mende, D.R., Alberti, A. (2015). Structure and function of the global ocean microbiome. Science *348*, 1261359.

Tanner, N.A., Zhang, Y., and Evans, T.C. (2015). Visual detection of isothermal nucleic acid amplification using pH-sensitive dyes. BioTechniques *58*.

Templeton, K.E., Scheltinga, S.A., Graffelman, A.W., Schie, J.M. van, Crielaard, J.W., Sillekens, P., Broek, P.J. van den, Goossens, H., Beersma, M.F.C., and Claas, E.C.J. (2003). Comparison and Evaluation of Real-Time PCR, Real-Time Nucleic Acid Sequence-Based Amplification, Conventional PCR, and Serology for Diagnosis of Mycoplasma pneumoniae. J. Clin. Microbiol. *41*, 4366–4371.

Thielicke, E., and Obermeier, E. (2000). Microactuators and their technologies. Mechatronics *10*, 431–455.

Thomson, D.A.C., and Cooper, M.A. (2013). A paramagnetic-reporter two-particle system for amplification-free detection of DNA in serum. Biosens. Bioelectron. *50*, 499–501.

Tomita, N., Mori, Y., Kanda, H., and Notomi, T. (2008). Loop-mediated isothermal amplification (LAMP) of gene sequences and simple visual detection of products. Nat. Protoc. *3*, 877–882.

Tront, J.M., Fortner, J.D., Plötze, M., Hughes, J.B., and Puzrin, A.M. (2008). Microbial fuel cell biosensor for in situ assessment of microbial activity. Biosens. Bioelectron. *24*, 586–590.

Tsai, S.-M., Chan, K.-W., Hsu, W.-L., Chang, T.-J., Wong, M.-L., and Wang, C.-Y. (2009). Development of a loop-mediated isothermal amplification for rapid detection of orf virus. J. Virol. Methods *157*, 200–204.

Turnbaugh, P.J., and Gordon, J.I. (2009). The core gut microbiome, energy balance and obesity. J. Physiol. *587*, 4153–4158.

Turnbaugh, P.J., Ley, R.E., Mahowald, M.A., Magrini, V., Mardis, E.R., and Gordon, J.I. (2006). An obesity-associated gut microbiome with increased capacity for energy harvest. Nature *444*, 1027–1131.

Ussler, W., Preston, C., Tavormina, P., Pargett, D., Jensen, S., Roman, B., Marin, R., Shah, S.R., Girguis, P.R., Birch, J.M., Orphan, V., and Scholin, C. (2013). Autonomous Application of Quantitative PCR in the Deep Sea: In Situ Surveys of Aerobic Methanotrophs Using the Deep-Sea Environmental Sample Processor. Environ. Sci. Technol. *47*, 9339–9346.

Vartoukian, S.R., Palmer, R.M., and Wade, W.G. (2010). Strategies for culture of "unculturable" bacteria. FEMS Microbiol. Lett. *309*, 1–7.

Vincent, M., Xu, Y., and Kong, H. (2004). Helicase-dependent isothermal DNA amplification. EMBO Rep. *5*, 795–800.

Wade, W. (2002). Unculturable bacteria—the uncharacterized organisms that cause oral infections. J. R. Soc. Med. *95*, 81–83.

Wagner, M., Amann, R., Lemmer, H., and Schleifer, K.H. (1993). Probing activated sludge with oligonucleotides specific for proteobacteria: inadequacy of culture-dependent methods for describing microbial community structure. Appl. Environ. Microbiol. *59*, 1520–1525.

Walker, G.T., Fraiser, M.S., Schram, J.L., Little, M.C., Nadeau, J.G., and Malinowski, D.P. (1992). Strand displacement amplification--an isothermal, in vitro DNA amplification technique. Nucleic Acids Res. *20*, 1691–1696.

Walker, G.T., Nadeau, J.G., Spears, P.A., Schram, J.L., Nycz, C.M., and Shank, D.D. (1994). Multiplex strand displacement amplification (SDA) and detection of DNA

sequences from Mycobacterium tuberculosis and other mycobacteria. Nucleic Acids Res. *22*, 2670–2677.

Walker, G.T., Nadeau, J.G., Linn, C.P., Devlin, R.F., and Dandliker, W.B. (1996). Strand displacement amplification (SDA) and transient-state fluorescence polarization detection of Mycobacterium tuberculosis DNA. Clin. Chem. *42*, 9–13.

Wang, B., Wang, J., Zhang, W., and Meldrum, D.R. (2012). Application of synthetic biology in cyanobacteria and algae. Front. Microbiol. *3*.

Wang, C., Yan, Q., Liu, H.-B., Zhou, X.-H., and Xiao, S.-J. (2011). Different EDC/NHS Activation Mechanisms between PAA and PMAA Brushes and the Following Amidation Reactions. Langmuir *27*, 12058–12068.

Wang, Q., Garrity, G.M., Tiedje, J.M., and Cole, J.R. (2007). Naïve Bayesian Classifier for Rapid Assignment of rRNA Sequences into the New Bacterial Taxonomy. Appl. Environ. Microbiol. *73*, 5261–5267.

Wang, S., Lifson, M.A., Inci, F., Liang, L.-G., Sheng, Y.-F., and Demirci, U. (2016). Advances in addressing technical challenges of point-of-care diagnostics in resource-limited settings. Expert Rev. Mol. Diagn. *16*, 449–459.

Wang, Y., Yang, Q., and Wang, Z. (2015). The evolution of nanopore sequencing. Front. Genet. *5*.

Wharam, S.D., Marsh, P., Lloyd, J.S., Ray, T.D., Mock, G.A., Assenberg, R., McPhee, J.E., Brown, P., Weston, A., and Cardy, D.L.N. (2001). Specific detection of DNA and RNA targets using a novel isothermal nucleic acid amplification assay based on the formation of a three-way junction structure. Nucleic Acids Res. *29*, e54–e54.

Whitesides, G.M. (2006). The origins and the future of microfluidics. Nature *442*, 368–373.

Whitman, W.B., Coleman, D.C., and Wiebe, W.J. (1998). Prokaryotes: The unseen majority. Proc. Natl. Acad. Sci. *95*, 6578–6583.

Wu, F., and Dekker, C. (2016). Nanofabricated structures and microfluidic devices for bacteria: from techniques to biology. Chem Soc Rev *45*, 268–280.

Wu, Q., Jin, W., Zhou, C., Han, S., Yang, W., Zhu, Q., Jin, Q., and Mu, Y. (2011). Integrated Glass Microdevice for Nucleic Acid Purification, Loop-Mediated Isothermal Amplification, and Online Detection. Anal. Chem. *83*, 3336–3342.

Wu, S.-J.L., Lee, E.M., Putvatana, R., Shurtliff, R.N., Porter, K.R., Suharyono, W., Watts, D.M., King, C.-C., Murphy, G.S., Hayes, C.G., and Romano, J.W. (2001). Detection of

Dengue Viral RNA Using a Nucleic Acid Sequence-Based Amplification Assay. J. Clin. Microbiol. *39*, 2794–2798.

Wu, Z., Willing, B., Bjerketorp, J., Jansson, J.K., and Hjort, K. (2009). Soft inertial microfluidics for high throughput separation of bacteria from human blood cells. Lab. Chip *9*, 1193.

Yamazaki, W., Seto, K., Taguchi, M., Ishibashi, M., and Inoue, K. (2008). Sensitive and rapid detection of cholera toxin-producing Vibrio cholerae using a loop-mediated isothermal amplification. BMC Microbiol. *8*, 94.

Yan, L., Zhou, J., Zheng, Y., Gamson, A.S., Roembke, B.T., Nakayama, S., and Sintim, H.O. (2014). Isothermal amplified detection of DNA and RNA. Mol. Biosyst. *10*, 970.

Yeo, B.-S., Stadler, J., Schmid, T., Zenobi, R., and Zhang, W. (2009). Tip-enhanced Raman Spectroscopy – Its status, challenges and future directions. Chem. Phys. Lett. *472*, 1–13.

Yu, Y., Lee, C., Kim, J., and Hwang, S. (2005). Group-specific primer and probe sets to detect methanogenic communities using quantitative real-time polymerase chain reaction. Biotechnol. Bioeng. *89*, 670–679.

Zhang, J., Feng, Y., Hu, D., Lv, H., Zhu, J., Cao, M., Zheng, F., Zhu, J., Gong, X., Hao, L., Srinivas, S., Ren, H., Qi, Z., Li, B., and Wang, C. (2013). Rapid and Sensitive Detection of H7N9 Avian Influenza Virus by Use of Reverse Transcription–Loop-Mediated Isothermal Amplification. J. Clin. Microbiol. *51*, 3760–3764.

Zhao, X., Li, Y., Wang, L., You, L., Xu, Z., Li, L., He, X., Liu, Y., Wang, J., and Yang, L. (2009). Development and application of a loop-mediated isothermal amplification method on rapid detection Escherichia coli O157 strains from food samples. Mol. Biol. Rep. *37*, 2183–2188.

Zhao, Y., Lindsay, S., Jeon, S., Kim, H.-J., Su, L., Lim, B., and Koo, S. (2013). Combined effect of polar substituents on the electronic flows in the carotenoid molecular wires. Chem. Eur. J. *19*, 10832–10835.

Zhao, Y., Ashcroft, B., Zhang, P., Liu, H., Sen, S., Song, W., Im, J., Gyarfas, B., Manna, S., Biswas, S., Borges, C., and Lindsay, S. (2014). Single-molecule spectroscopy of amino acids and peptides by recognition tunnelling. Nat. Nanotechnol. *9*, 466–473.

APPENDIX A

MATLAB CODE FOR COLORIMETRIC QLAMP IMAGE PROCESSING

```
function varargout = analysis(varargin)
% ANALYSIS MATLAB code for analysis.fig
%      ANALYSIS, by itself, creates a new ANALYSIS or raises the existing
%      singleton*.
%
%      H = ANALYSIS returns the handle to a new ANALYSIS or the handle to
%      the existing singleton*.
%
%      ANALYSIS('CALLBACK',hObject,eventData,handles,...) calls the local
%      function named CALLBACK in ANALYSIS.M with the given input arguments.
%
%      ANALYSIS('Property','Value',...) creates a new ANALYSIS or raises the
%      existing singleton*.  Starting from the left, property value pairs are
%      applied to the GUI before analysis_OpeningFcn gets called.  An
%      unrecognized property name or invalid value makes property application
%      stop.  All inputs are passed to analysis_OpeningFcn via varargin.
%
%      *See GUI Options on GUIDE's Tools menu.  Choose "GUI allows only one
%      instance to run (singleton)".
%
% See also: GUIDE, GUIDATA, GUIHANDLES

% Edit the above text to modify the response to help analysis

% Last Modified by GUIDE v2.5 25-Nov-2014 22:50:14

% Begin initialization code - DO NOT EDIT
gui_Singleton = 1;
gui_State = struct('gui_Name',       mfilename, ...
                   'gui_Singleton',  gui_Singleton, ...
                   'gui_OpeningFcn', @analysis_OpeningFcn, ...
                   'gui_OutputFcn',  @analysis_OutputFcn, ...
                   'gui_LayoutFcn',  [] , ...
                   'gui_Callback',   []);
if nargin && ischar(varargin{1})
    gui_State.gui_Callback = str2func(varargin{1});
end

if nargout
    [varargout{1:nargout}] = gui_mainfcn(gui_State, varargin{:});
else
    gui_mainfcn(gui_State, varargin{:});
end
% End initialization code - DO NOT EDIT


% --- Executes just before analysis is made visible.
function analysis_OpeningFcn(hObject, eventdata, handles, varargin)
% This function has no output args, see OutputFcn.
% hObject    handle to figure
% eventdata  reserved - to be defined in a future version of MATLAB
% handles    structure with handles and user data (see GUIDATA)
% varargin   command line arguments to analysis (see VARARGIN)

% Choose default command line output for analysis
handles.output = hObject;

% Update handles structure
guidata(hObject, handles);
```

```
% UIWAIT makes analysis wait for user response (see UIRESUME)
% uiwait(handles.figure1);


% --- Outputs from this function are returned to the command line.
function varargout = analysis_OutputFcn(hObject, eventdata, handles)
% varargout  cell array for returning output args (see VARARGOUT);
% hObject    handle to figure
% eventdata  reserved - to be defined in a future version of MATLAB
% handles    structure with handles and user data (see GUIDATA)

% Get default command line output from handles structure
varargout{1} = handles.output;


% --- Executes on button press in Open_button.
function Open_button_Callback(hObject, eventdata, handles)
% hObject    handle to Open_button (see GCBO)
% eventdata  reserved - to be defined in a future version of MATLAB
% handles    structure with handles and user data (see GUIDATA)
global directory_name;
global fileIndex;
global current_file_index;
global files;
directory_name = uigetdir;
files = dir(directory_name);
fileIndex = find(~[files.isdir]);
if ~isempty(fileIndex)
    current_file_index = fileIndex(1);
    axes(handles.Raw_image);
    imshow(strcat(directory_name,'\',files(current_file_index).name));
    set(handles.Raw_image_label,'String',files(current_file_index).name);

set(handles.image_name,'String',strcat(num2str(1),'/',num2str(length(fileIndex)
)));
end


% --- Executes on button press in Save_button.
function Save_button_Callback(hObject, eventdata, handles)
% hObject    handle to Save_button (see GCBO)
% eventdata  reserved - to be defined in a future version of MATLAB
% handles    structure with handles and user data (see GUIDATA)

global files;
global fileIndex;
global directory_name;
global Total_channel_number;
global channel_info;
global side_length;
global H_color;
global S_color;
global V_color;
format long;
%set(handles.Processed_image_label,'String','Saving Channels');
axes(handles.Processed_image);
```

```
currentFolder = pwd;
for k=1:length(fileIndex)
    rgb=imread(strcat(directory_name,'\',files(fileIndex(k)).name));
    [pathstr,name,ext]=fileparts(files(fileIndex(k)).name);
    axes(handles.Raw_image);
    imshow(rgb);
    set(handles.Raw_image_label,'String',name);
    H_color(k,1) = str2double(name(10:15));
    S_color(k,1) = H_color(k,1);
    V_color(k,1) = H_color(k,1);
    H_color_temp = zeros(1,Total_channel_number);
    S_color_temp = zeros(1,Total_channel_number);
    V_color_temp = zeros(1,Total_channel_number);
    parfor d=1:Total_channel_number
        channel_name_num = num2str(d);
        rgb_temp = imcrop(rgb,[channel_info(d,1) channel_info(d,2) side_length
side_length]);
        hsv_image = rgb2hsv(rgb_temp);
        h_image = hsv_image(:,:,1);
        s_image = hsv_image(:,:,2);
        v_image = hsv_image(:,:,3);
        threshold = hsv_image(:,:,2) > 0.1;
        h_ave = mean(h_image(threshold));
        s_ave = mean(s_image(threshold));
        v_ave = mean(v_image(threshold));

        H_color_temp(d) = h_ave*360;
        S_color_temp(d) = s_ave*360;
        V_color_temp(d) = v_ave*360;
        if(~exist(channel_name_num,'dir'))
            mkdir(channel_name_num);
        end
        savewheel(hsv_image,fullfile(currentFolder,channel_name_num),name);
    end
    H_color(k,2:Total_channel_number+1) = H_color_temp;
    S_color(k,2:Total_channel_number+1) = S_color_temp;
    V_color(k,2:Total_channel_number+1) = V_color_temp;
    cla(handles.Raw_image,'reset');

set(handles.image_name,'String',strcat(num2str(k),'/',num2str(length(fileIndex)
)));
end
csvwrite('H_Channel.csv',H_color);
csvwrite('S_Channel.csv',S_color);
csvwrite('V_Channel.csv',V_color);


% --- Executes on button press in Previous_button.
function Previous_button_Callback(hObject, eventdata, handles)
% hObject    handle to Previous_button (see GCBO)
% eventdata  reserved - to be defined in a future version of MATLAB
% handles    structure with handles and user data (see GUIDATA)
global current_file_index;
global fileIndex;
global directory_name;
global files;

cla(handles.Raw_image,'reset');
if (current_file_index > fileIndex(1))
```

```
    current_file_index = fileIndex(find(fileIndex ==current_file_index)-1);
    axes(handles.Raw_image);
    imshow(strcat(directory_name,'\',files(current_file_index).name));
    set(handles.Raw_image_label,'String',files(current_file_index).name);
end


% --- Executes on button press in Next_button.
function Next_button_Callback(hObject, eventdata, handles)
% hObject    handle to Next_button (see GCBO)
% eventdata  reserved - to be defined in a future version of MATLAB
% handles    structure with handles and user data (see GUIDATA)
global current_file_index;
global fileIndex;
global directory_name;
global files;

cla(handles.Raw_image,'reset');
if (current_file_index <= fileIndex(end-1))
    current_file_index = fileIndex(find(fileIndex == current_file_index)+1);
    axes(handles.Raw_image);
    imshow(strcat(directory_name,'\',files(current_file_index).name));
    set(handles.Raw_image_label,'String',files(current_file_index).name);
%    set(handles.image_name,'String',files(current_file_index).name);
end


function Total_CH_Callback(hObject, eventdata, handles)
% hObject    handle to Total_CH (see GCBO)
% eventdata  reserved - to be defined in a future version of MATLAB
% handles    structure with handles and user data (see GUIDATA)

% Hints: get(hObject,'String') returns contents of Total_CH as text
%        str2double(get(hObject,'String')) returns contents of Total_CH as a
double


% --- Executes during object creation, after setting all properties.
function Total_CH_CreateFcn(hObject, eventdata, handles)
% hObject    handle to Total_CH (see GCBO)
% eventdata  reserved - to be defined in a future version of MATLAB
% handles    empty - handles not created until after all CreateFcns called

% Hint: edit controls usually have a white background on Windows.
%       See ISPC and COMPUTER.
if ispc && isequal(get(hObject,'BackgroundColor'),
get(0,'defaultUicontrolBackgroundColor'))
    set(hObject,'BackgroundColor','white');
end


% --- Executes on button press in Est_radii_set.
function Est_radii_set_Callback(hObject, eventdata, handles)
% hObject    handle to Est_radii_set (see GCBO)
% eventdata  reserved - to be defined in a future version of MATLAB
% handles    structure with handles and user data (see GUIDATA)
global d
axes(handles.Raw_image);
```

```
if(strcmp(get(handles.Est_radii_set,'String'),'Est Radii'))
    d = imdistline;
    set(handles.Est_radii_set,'String','Set');
else
    set(handles.Est_radii_set,'String','Est Radii');
    api = iptgetapi(d);
    api.delete();
end


function Radius_Callback(hObject, eventdata, handles)
% hObject    handle to Radius (see GCBO)
% eventdata  reserved - to be defined in a future version of MATLAB
% handles    structure with handles and user data (see GUIDATA)

% Hints: get(hObject,'String') returns contents of Radius as text
%        str2double(get(hObject,'String')) returns contents of Radius as a
double


% --- Executes during object creation, after setting all properties.
function Radius_CreateFcn(hObject, eventdata, handles)
% hObject    handle to Radius (see GCBO)
% eventdata  reserved - to be defined in a future version of MATLAB
% handles    empty - handles not created until after all CreateFcns called

% Hint: edit controls usually have a white background on Windows.
%       See ISPC and COMPUTER.
if ispc && isequal(get(hObject,'BackgroundColor'),
get(0,'defaultUicontrolBackgroundColor'))
    set(hObject,'BackgroundColor','white');
end


% --- Executes on button press in Select_CH.
function Select_CH_Callback(hObject, eventdata, handles)
% hObject    handle to Select_CH (see GCBO)
% eventdata  reserved - to be defined in a future version of MATLAB
% handles    structure with handles and user data (see GUIDATA)
global h_rec;
global side_length;
%h_rec = rectangle('Position',[250 250 side_length side_length]);
%ini_rec = [250 250 side_length side_length];
%[h_rec] = dragrect(ini_rec);
%axes(handles.Raw_image);
%waitforbuttonpress;
%point1 = get(handles.Raw_image,'CurrentPoint'); % button down detected
h_rec = impositionrect(handles.Raw_image,[250 250 side_length side_length]);


function CH_Callback(hObject, eventdata, handles)
% hObject    handle to CH (see GCBO)
% eventdata  reserved - to be defined in a future version of MATLAB
% handles    structure with handles and user data (see GUIDATA)

% Hints: get(hObject,'String') returns contents of CH as text
%        str2double(get(hObject,'String')) returns contents of CH as a double
```

```
% --- Executes during object creation, after setting all properties.
function CH_CreateFcn(hObject, eventdata, handles)
% hObject    handle to CH (see GCBO)
% eventdata  reserved - to be defined in a future version of MATLAB
% handles    empty - handles not created until after all CreateFcns called

% Hint: edit controls usually have a white background on Windows.
%       See ISPC and COMPUTER.
if ispc && isequal(get(hObject,'BackgroundColor'),
get(0,'defaultUicontrolBackgroundColor'))
    set(hObject,'BackgroundColor','white');
end



% --- Executes on button press in Set_CH.
function Set_CH_Callback(hObject, eventdata, handles)
% hObject    handle to Set_CH (see GCBO)
% eventdata  reserved - to be defined in a future version of MATLAB
% handles    structure with handles and user data (see GUIDATA)

Current_channel_number = floor(str2double(get(handles.CH,'String')));

global channel_info;
global h_rec;

api = iptgetapi(h_rec);
pos = api.getPosition();
channel_info(Current_channel_number,1)=pos(1);
channel_info(Current_channel_number,2)=pos(2);



% --- Executes on button press in Test_all_CH.
function Test_all_CH_Callback(hObject, eventdata, handles)
% hObject    handle to Test_all_CH (see GCBO)
% eventdata  reserved - to be defined in a future version of MATLAB
% handles    structure with handles and user data (see GUIDATA)
global channel_info;
global side_length;
for i=1:length(channel_info(:,1))
    rectangle('Position',[channel_info(i,1) channel_info(i,2) side_length
side_length]);

text(floor(channel_info(i,1)+side_length/2),floor(channel_info(i,2)+side_length
/2),num2str(i));
end



% --- Executes on button press in Start.
function Start_Callback(hObject, eventdata, handles)
% hObject    handle to Start (see GCBO)
% eventdata  reserved - to be defined in a future version of MATLAB
% handles    structure with handles and user data (see GUIDATA)
global Total_channel_number;
global channel_info;
global side_length;
global H_color;
global S_color;
```

```
global V_color;
global fileIndex;

Total_channel_number = floor(str2double(get(handles.Total_CH,'String')));
channel_info = zeros(Total_channel_number,2);
side_length = floor(str2double(get(handles.Radius,'String'))*1.4);
H_color = zeros(length(fileIndex),Total_channel_number+1);
S_color = zeros(length(fileIndex),Total_channel_number+1);
V_color = zeros(length(fileIndex),Total_channel_number+1);


function savewheel(hsv_image_temp, path, save_file_name)

format long g;
format compact;
fontSize = 20;

% Let's compute and display the histogram.
figure('Visible','off');
numberOfBins = 120;
step = 360/numberOfBins;
h = hsv_image_temp(:,:,1);
% Display the original color image.
scaledHue = 360*h;
[pixelCount, grayLevels] = hist(scaledHue(:), 1:step:360);
subplot(2, 1, 1);
bar(grayLevels, pixelCount);
grid on;
title('Histogram of Hue Channel', 'FontSize', fontSize);
xlim([0 360]); % Scale x axis manually.

subplot(2, 1, 2);
cmap = hsv(length(1:step:360));
r = pixelCount / max(pixelCount(:));
drawWheel(r,cmap);
saveas(gcf,fullfile(path,save_file_name),'png');
%figure('Visible','on')



function drawWheel(r, cmap)
if (any(r > 1) || any(r < 0))
    error('R must be a vector of values between 0 and 1')
end

if numel(r) ~= size(cmap,1)
    error('Length of r and cmap must be the same')
end

n = numel(r);
innerRadius =  250;
outerRadius = 300;

angles = linspace(0,2*pi,n+1);
newR = innerRadius*(1-r);
% Draw the hue in the annulus.
for k = 1:n
%   newR(k);
```

```
    drawSpoke(innerRadius, outerRadius, angles(k), angles(k+1), cmap(k,:));
    drawSpoke(newR(k), innerRadius, angles(k), angles(k+1), cmap(k,:));
end

% Draw circle at the center.
line(0,0,'marker','o');
% Draw outer black ring.
line(cos(angles)*outerRadius, sin(angles)*outerRadius, 'LineWidth', 2, 'Color',
'k');
% Draw inner black ring.
line(cos(angles)*innerRadius, sin(angles)*innerRadius, 'LineWidth', 2, 'Color',
'k');
axis equal;


function h = drawSpoke(ri,ro,thetaStart,thetaEnd,c)
xInnerLeft  = cos(thetaStart) * ri;
xInnerRight = cos(thetaEnd)   * ri;
xOuterLeft  = cos(thetaStart) * ro;
xOuterRight = cos(thetaEnd)   * ro;
yInnerLeft  = sin(thetaStart) * ri;
yInnerRight = sin(thetaEnd)   * ri;
yOuterLeft  = sin(thetaStart) * ro;
yOuterRight = sin(thetaEnd)   * ro;

X = [xInnerLeft, xInnerRight, xOuterRight xOuterLeft];
Y = [yInnerLeft, yInnerRight, yOuterRight yOuterLeft];

h = patch(X,Y,c);
set(h,'edgeColor', 'none');
```

APPENDIX B

R CODE FOR COLORIMETRIC QLAMP HUE DATA ANALYSIS

```
Sigmoid <- function(params, x) {
    # Four-parameter sigmoidal function.
    params[1] + (params[2] - params[1]) / (1 + 10 ^ ((params[3] - x) *
params[4]))
}


SigmoidFit <- function(x, y) {
    # Fit the data with four-parameter sigmoidal function.
    #
    # Args:
    #   x: predictive variable in Sigmoid function. e.g. time.
    #   y: response variable in Sigmoid funtion. e.g. Hue of a specific group.
    #
    # Returns:
    #   If a Sigmoid function can be applied to the provided y, return 4 coefs.
    #   Four params: Max, Min, Tt, Slope.
    #   Otherwise, return 4 "NA"s.

    library(nls2)
    coefs <- c()
    tryCatch({
        start.df <- data.frame(a = c(232, 230, 228),
                               b = c(210, 215, 220),
                               c = c(20, 30, 50),
                               d = c(0.07, 0.08, 0.15))
        # calculate starting value for nls optimization
        start.value <- nls2(y ~ a + (b - a) / (1 + 10 ^ ((c - x) * d)),
                            start     = start.df,
                            algorithm = "brute-force",
                            control   = list(maxiter = 500))
        coefs <- coef(nls2(y ~ a + (b - a) / (1 + 10 ^ ((c - x) * d)),
                            start   = start.value,
                            control = list(maxiter = 500)))

    }, error = function(p) {
        coefs <- c(NA, NA, NA, NA)
    })
    return(coefs)
}


FindParams <- function(hue, groups = 2 : ncol(hue),
                       save2file = "threshold") {
    # Find four parameters of the sigmoidal function for multiple groups.
    #
    # Args:
    #   hue: an input data frame that contains real time hue data.
    #       (Format: first column is time, following columns are reaction
groups;
    #                colnames:"time", "R0.1"(Reaction
logConcentration.Replicate), "R2.1": first replicate in 100 copies reaction.)
    #   groups: a list contains column numbers that need to be analyzed.
    #   save2file: types of data that need to be saved to csv files. Three
choices available:
    #              "all": a data frame containing four parameters of all
analyzed groups;
    #              "reacted": a data frame containing four parameters of all
reacted groups (max > min + 3);
```

```
    #             "tt": a data frame containing the threshold times for all
reacted groups.
    # Returns:
    #   --

    library(nls2)
    params <- c()
    coefs <- c()
    for (i in groups) {
        x <- hue[, 1]
        y <- hue[, i]
        coefs      <- SigmoidFit(x, y)
        params.new <- as.data.frame(matrix(c(colnames(hue)[i], coefs), ncol =
5))
        params     <- rbind(params, params.new)
    }
    params[, 2:5]    <- as.numeric(as.character(unlist(params[, 2:5])))
    colnames(params) <- c("groups", "Max", "Min", "Tt", "Slope")
    params.reacted    <- params[which(params$Max > params$Min + 3), ]
    result <- list("all"       = params,
                   "reacted"   = params.reacted,
                   "threshold" = data.frame("groups"    = params.reacted[, 1],
                                            "threshold" = params.reacted[, 4]))
    if ("threshold" %in% save2file) {
        write.csv(result$threshold, "tt.csv")
    }
    if ("all" %in% save2file) {
        write.csv(result$all, "parameters_all.csv")
    }
    if ("reacted" %in% save2file) {
        write.csv(result$reacted, "parameters_reacted.csv")
    }
}


SummariseTt <- function(filedir = "tt.csv", save2file = T) {
    # Summarise the threshold time (Tt) by calculating the mean and standard
error of Tts in each group
    #
    # Args:
    #   filedir: the directory of a csv file containing a data frame of the
threshold times for all reacted groups;
    #            this file could be generated by FindParams().
    #   save2file: if TRUE, save the summarized data frame (mean and ste of
each group) in "summarisedTt.csv"; if not, not. Default is TRUE.
    # Returns:
    #   --

    library(dplyr)
    library(tidyr)
    threshold.time <- tbl_df(read.csv(filedir)) %>%
        separate(groups, c("concentrations", "replicates")) %>%
        mutate(concentrations = extract_numeric(concentrations)) %>%
        group_by(concentrations) %>%
        select(concentrations, replicates, threshold)
    summarise.tt <- summarise(threshold.time,
                              means = mean(threshold),
                              se = sd(threshold)/sqrt(length(threshold)))
    if (save2file) {
        write.csv(summarise.tt, "summarizedTt.csv")
```

```
    }
}


PlotStdCurve <- function(filedir = "summarizedTt.csv",
                         xlabel = expression("log"[10]*"concentraion"~
"("*"Copies /" ~ mu*L*")"), ylabel= "Tt (min)",
                         trend.start.row = 1, trend.end.row = nrow(tt),
                         points.col = "blue", line.col = "red",
                         legendx = "topright", legendy = NULL,
                         img.save = F, img.width = 300, img.height = 250) {
    # Plot a standard curve using the Tt values.
    #
    # Args:
    #   filedir: the directory of a csv file containing the mean and standard
error of Tts in each group;
    #            this file can be generated by SummariseTt().
    #   xlabel: x axis label of the standard curve.
    #   ylabel: y axis label of the standard curve.
    #   trend.start.row: from which row the Tt values will be plotted on the
standard curve.
    #   trend.end.row: to which row the Tt values will be plotted on the
standard curve.
    #   points.col: the color of points on the standard curve.
    #   line.col: the color of the fitted line on the standard curve.
    #   legendx: the x location to put the legend. Default is topright.
    #   legendy: the y location to put the legend.
    #   img.save: if TRUE, save the standard curve to a png file; if not, not.
Default is FALSE.
    #   img.width: if img.save, what is the width of the image.
    #   img.height: if img.save, what is the height of the image.
    #
    # Returns:
    #   r.square: r^2 of the fitted line.
    #   adj.r.square: adjucted r^2 of the fitted line.
    #   beta0: intercept of the regression line.
    #   beta1: slope of the regression line.

    tt <- read.csv(filedir)
    lm.fit <- lm(tt$means[trend.start.row:trend.end.row] ~
tt$concentrations[trend.start.row:trend.end.row])
    r.square     <- round(summary(lm.fit)$r.squared, 3)
    adj.r.square <- round(summary(lm.fit)$adj.r.squared, 3)
    beta0        <- round(summary(lm.fit)$coef[1], 2)
    beta1        <- round(summary(lm.fit)$coef[2], 2)

    # Plotting
    plot(x = tt$concentrations, y = tt$means,
         type = "n", ylim = c(0, 60),
         xlab = xlabel, ylab = ylabel)
    points(x = tt$concentrations, y = tt$means,
           pch = 19, col = points.col)
    abline(lm.fit,
           col = adjustcolor(line.col, alpha = 0.5), lwd = 2)
    legend(x = legendx, y = legendy, bty = "n", legend = bquote(R^2
== .(r.square)))
    arrows(tt$concentrations, tt$means - tt$se,
           tt$concentrations, tt$means + tt$se,
           length = 0.05, angle = 90, code = 3)
```

```
    # Saving image
    if (img.save) {
        dev.copy(png, file = "standcurve.png",
                 width = img.width, height = img.height)
        dev.off()
    }
    result <- list("r.square"     = r.square,
                   "adj.r.square" = adj.r.square,
                   "beta0"        = beta0,
                   "beta1"        = beta1)
    return(result)
}


PlotAmpCurve <- function(hue.start.column, hue.end.column,
                         xlabel= "Time (min)", ylabel= "Hue",
                         xlim = c(1, 60), ylim = c(210, 240),
                         legendx = "topright", legendy = NULL, legend = NULL) {
    # Plot amplification curves using the real-time hue data.
    #
    # Args:
    #   hue.start.column: from which column the hue data needs to be plotted on
the amplification curve.
    #   hue.end.column: to which column the hue data needs to be plotted on the
amplification curve.
    #   xlabel: x axis label of the amplification curve.
    #   ylabel: y axis label of the amplification curve.
    #   xlim: range of x axis.
    #   ylim: range of y axis.
    #   legendx: the x location to put the legend. Default is topright.
    #   legendy: the y location to put the legend.
    #   legend: text in the legend.
    # Returns:
    #   --

    library(RColorBrewer)
    colpal <- brewer.pal(5, "Set1")
    set.seed(123)
    plot(x = hue$time, y = hue[, 2],
         type = "n",
         xlim = xlim, ylim = ylim,
         xlab = xlabel, ylab = ylabel)
    legend(x = legendx, y = legendy, legend = legend, bty = "n")
    for (i in hue.start.column : hue.end.column) {
        x <- hue$time
        y <- hue[, i]
        tryCatch({
            params <- SigmoidFit(x, y)
            if (params[1] < params[2] + 3) {
                points(x = hue$time, y = hue[, i], pch = 20,
                       col = adjustcolor(sample(colpal, 1), alpha = 0.5))
            }
            else {
                color <- sample(colpal, 1)
                y2 <- Sigmoid(params, x)
                lines(x = hue$time, y = y2,
                      col = adjustcolor(color, alpha = 0.7), lwd = 2)
                points(x = hue$time, y,
                       pch = 20, col = adjustcolor(color, alpha = 0.5))
            }
```

```
        }, error = function(p) {
            points(x = hue$time, y = hue[, i],
                   pch = 20,
                   col = adjustcolor(sample(colpal, 1), alpha = 0.5))
        })
    }
}


# processing example
hue <- read.csv("Hue.csv")
FindParams(hue)
SummariseTt()
par(mfrow = c(2, 3), mar = c(4, 4, 1, 1))
PlotAmpCurve(22, 26, legend = "A")
PlotAmpCurve(17, 21, legend = "B")
PlotAmpCurve(12, 16, legend = "C")
PlotAmpCurve(7, 11, legend = "D")
PlotAmpCurve(2, 6, legend = "E")
PlotStdCurve()
```